ulm university universität
uulm

Multi-Objective Optimization of Simple and Multiple Dividing Wall Columns and their Operational Flexibility Close to the Optimum

Dissertation

to obtain the academic title of

Doktor-Ingenieur
(Dr.-Ing.)

at the Faculty of Engineering,
Computer Science and Psychology at the University of Ulm

by

Lena-Marie Ränger
from Hamburg

First Examiner:	Prof. Dr.-Ing. Thomas Grützner
Second Examiner:	Prof. Dr.-Ing. Hans Hasse
Acting Dean:	Prof. Dr.-Ing. Maurits Ortmanns

Ulm, November 16, 2021

Parts of the dissertation have already been published in scientific journal articles. More information can be found in the Appendix in Section C.1.

2nd corrected edition

Preface

This thesis was written during my work at the Laboratory for Thermal Process Engineering, part of the Institute of Chemical Engineering at Ulm University, Germany, from February 2018 to July 2021. The working group was founded in November 2017, so there were still many bureaucratic and organizational hurdles to overcome in addition to the actual research work. Also, the Covid-19 pandemic made the work more difficult. Nevertheless, I received support from many people, so I would like to take this opportunity to acknowledge the efforts of some of those involved.

First of all, I would like to thank my supervisor Prof. Dr.-Ing. Thomas Grützner. Despite that fact that he made it possible for me to work at the institute and to write this doctoral thesis, he always assisted with advice and support. At the same time, he gave me a lot of freedom to work on my own ideas and always supported me extensively in my scientific development, also in other research fields. Additionally, I would like to thank Prof. Dr.-Ing. Hans Hasse for being the second examiner of my thesis.

Very special thanks also goes to the staff of the Fraunhofer Institute for Industrial Mathematics in Kaiserslautern. In particular I would like to mention the support and scientific contributions of PD Dr. Michael Bortz, Dr. Martin von Kurnatowski and Dr. Tobias Seidel. They not only provided a large part of the algorithms used in my work and gave me inspiration for problem solutions, but also supported me in the preparation of a couple of publications. In several research visits, they taught me the great importance of optimization and assisted me with any questions regarding the topic.

On a work-related level, I would also like to thank the head of the institute, Prof. Güttel and my numerous colleagues. Even though all of them work on quite different research areas, there was always a suitable contact person for organizational questions. In particular, I would like to mention our secretary Katrin Sauter, who was for most of the time one of only two other female supporters in the entire group and always had an open ear. In addition, coffee breaks, institute excursions and events provided a good balance to the normal everyday university life.

On a private level, I first want to thank my friends. They stood by me in good and bad times and provided a lot of variety during my leisure time. I would especially like to mention my boyfriend Johannes Neukäufer. Thank you for always being there for me and supporting me in finding solutions in every situation. Finally, of course, a big thank you to my family. Despite the great distance between Ulm and Hamburg, you have always been a strong mental support for me. Even before my doctorate, you supported and encouraged me unconditionally in all my requests and decisions.

In summary, there is only one thing to say: Thank you all!

Abstract

This work aims to investigate the high-dimensional optimal space of simple and multiple dividing wall columns, clarify the impact of included variables and identify when this type of intensified column is more advantageous than conventional distillation sequences. Although this knowledge is highly relevant to the understanding of these complex devices, this topic has not been sufficiently explored in the literature. In order to fill this gap this work presents theoretical calculations performed based on automated flow sheet simulations in Aspen Plus with an external optimizer. An additional objective of this contribution is to apply the findings on a flexible designed simplified multiple dividing wall column pilot plant which should be build at Ulm University. Last, the operational flexibility of the liquid and vapor splits close to the found optimum, which allows conclusions to be drawn about its robustness, is studied in detail.
A new kind of multi-objective optimization procedure is introduced which includes, additionally to the total stage number N and energy demand $\dot{Q}$, also the product purities as objectives. Consequently, an *a posteriori* analysis of the objective space is realizable which enables the human decision maker to analyze the data for several cases without the need of a new calculation run. An in depth study on the impact of the included variables on the optimal output indicates that the ratio of product flows divided by the feed flow of the corresponding component can significantly affect the minimum energy demand of the column. Consequently, the product flows should not be assumed constant but rather be included as optimization variables. On the other hand, it is proven that the number of theoretical stages in the column sections can simply be determined with the shortcut Fenske equation. Based on the obtained optimization data a simple empirical method is presented to estimate Pareto-optimal compromises between energy demand and total stage number of dividing wall or simple distillation columns and sequences of those. This approach can also be included into a calculation to evaluate which distillation option is better suited over the whole $N\dot{Q}$ optimal range. As a general rule it is found that column sequences require a lower minimum stage number while dividing wall columns show a lower minimum energy demand. Consequently in certain regions of the optimal space dividing wall columns are better suitable and in another column sequences. The new introduced Decision Number helps to evaluate which option is more beneficial over the whole feasible operating range. The results show that the dividing wall column is superior over the direct split sequence for systems requiring significantly more stages for the low boiling components, while the benefit decreases for increasing stage requirements for the high boiling components. A reversed effect is found in comparison to the indirect split sequence. However, there is no case in which the column sequences are overall superior over the dividing wall column. Additionally, no impact of the fraction of the middle boiling component in the feed stream on the energy saving potential of dividing wall columns is observed. This refutes a widespread statement in the literature. For the multiple dividing wall column pilot plant at Ulm University it is found that high energy savings between 25 and 45 % can

be expected for a broad set of systems. Thus, this work makes an essential contribution to answering the question under which circumstances dividing wall columns can be used profitably.
Additionally, the robustness of a dividing wall column operation close to the corresponding energetic optimum in the context of multiple steady states of the internal vapor and liquid splits is evaluated. The results show that the location of suitable vapor and liquid split ranges is not only determined by the system itself, but also by the total stage number and their allocation in the column sections. To understand this behavior an extended version of the minimum vapor ($\dot{V}_{min}$) diagram is developed witch also includes the dimension $n_i = \frac{N_i}{N_{min,i}}$ and thus the distance to the minimum stage number of the column and column sections. This extended diagram can also be applied to estimate suited vapor and liquid split ranges in multiple dividing wall columns with finite and non-optimal stages. These estimations can be used to initialize flow-sheet simulations. Additionally, the flexibility of several systems separated in the pilot plant at Ulm University is evaluated. It is found that the vapor splits in such a column should be adjustable to values different to 0.5 in order to maintain demanded product specifications. Thus, it requires an internal tool to roughly adjust the vapor splits, like for example a pinhole sheet. Otherwise it cannot be guaranteed that the column can split a broad set of mixtures. However, if the vapor split is set to a value suited for the system, also feed stream disturbances can be handled without problems and deviation of the vapor split can be compensated by the liquid splits.
All in all it can be concluded that simple and multiple dividing wall columns are a superior technique to reduce the energy demand of distillation processes, also as multi-purpose apparatus. However, a deep process understanding is required in order to design such columns in a robust way. The required knowledge is provided in this work.

Contents

Symbols and abbreviations

Latin Symbols (Chemical engineering context)

a_{ij} to f_{ij}	NRTL parameters of components i and j
$A_{j,i}$	Antoine parameters for component i
$B_{j,i}$	Parameters for DIPPR eq. 106 for component i
$C_{j,i}$	Parameters for DIPPR eq. 107 for component i
CPIG	Ideal gas heat capacity (Aspen Plus internal variable name)
$\dot{D}$	Molar distillate flow
DHFORM	Heat of formation of an ideal gas (Aspen Plus internal variable name)
DN	Decision Number
DHRSWT	Heat of vaporization (Aspen Plus internal variable name)
E	Energy savings
ESI	Ease of Separation Index
$\dot{F}$	Molar feed flow
GAMMA	Activity coefficient (Aspen Plus internal variable name)
$HETP$	Height equivalent to one theoretical plate
K_i	Distribution coefficient of component i
m_i	Ratio of theoretical stage number divided by total one
N	Number of theoretical stages
n	Number of components
$\dot{n}$	Molar flow
N_i	Number of theoretical stages in section/region i
n_i	Ratio of th. stage number divided by minimum one
p	Pressure
PC	Critical Pressure (Aspen Plus internal variable name)
q	Liquid fraction/thermal state of feed stream
$\dot{Q}$	Reboiler duty
R_L	Liquid split ratio
R_V	Vapor split ratio
R_R	Reflux ratio
$\dot{S}$	Molar side draw flow
T	Temperature
TAC	Total Annual Costs

TC	Critical Temperature (Aspen Plus internal variable name)
$\dot{V}$	Molar vapor flow
VC	Critical volume (Aspen Plus internal variable name)
X	Standardized stage number (Molokanov [1])
x_i^j	Molar fraction of component i in stream j
Y	Standardized reflux ratio (Molokanov [1])
y_i^j	Molar fraction of component i in vapor stream j
z_i	Molar fraction of component i in feed stream

Latin Symbols (Mathematical context)

F	Objective function
g	Inequality constraint
h	Equality constraint
j	Loop variable describing index on single-objective problem
m	Number of equality constraints
n	Number of objective functions
p	Number of inequality constraints
$\boldsymbol{w}$	Vector of weighting factors
$\boldsymbol{x}$	Vector of continuous optimization variables
$\boldsymbol{y}$	Vector of discrete optimization variables

Subscriptions and superscriptions

$*$	Pure Component
$approx$	Approximation
HK	High boiling key component
is	intersection
L	Liquid phase
l	Left
LK	Low boiling key component
$main$	Main column C1
min	Minimum
opt	Optimal or optimization
r	Right
R	Reflux
rel	Relative
V	Vapor phase

Greek Symbols

α_i	Relative volatility of component i
σ	Standard deviation

Abbreviations

A - D	Components sorted according to boiling point (A light boiler)
BMU	Best matching unit
DSS	Direct split sequence
DWC	Dividing wall columns
EH	Error handler
ISS	Indirect split sequence
MISQP	Mixed-integer sequential quadratic programming
MS	Microsoft
MultiFrac	Rigorous column model in Aspen Plus
NRTL	Non-Random-Two-Liquid
PP	Pilot plant
RadFrac	Rigorous column model in Aspen Plus
SOM	Self-organizing map
SOPP	Self-organizing patch plot
VBA	Visual Basic for Applications

1 Introduction

The reduction of CO_2 emissions is an important issue in order to slow down global warming. One sector with a high saving potential due to its significant energy consumption is the chemical industry. Especially commonly used separation and purification steps are highly energy-intensive. The most frequently applied separation step is distillation, for which in 2001 approximately 2.5 % of the totally consumed energy were used [2–4], another reference reports 10 % in 2016 [5]. Accordingly, the search for distillation options being more efficient is an important research topic.
In this context a very promising approach are so called intensified columns. Their objective is to combine several unit operations into one column shell in order to increase the process efficiency [6]. A well-known representative of this group in the field of distillation are dividing wall columns [7–12]. For ternary product splits literature reports a reduction in energy consumption of approximately 30 % compared to conventional distillation sequences like the direct split sequence [13–17]. However, due to an increased complexity they are still a niche application in chemical industry. The principle was patented in 1946 [18] and first applied in chemical industry in 1985 [19]. Since then the number of columns constantly increases. In 2011 around 125 columns were reported and for 2015 approximately 350 were predicted [10]. Accordingly, nowadays it can be expected that at least 500 - 1000 columns are in use.
The advancement of simple dividing wall columns are multiple dividing wall columns offering energy savings up to 55 % for quaternary product splits [20, 21]. However, these columns are much more complex in comparison to conventional sequences. This is probably the main reason why, to the best of the authors knowledge, no real plant of this kind has been build yet. The working group in Ulm is taking up this challenge and is building the first multiple dividing wall column pilot plant worldwide in 2021 [22]. The author of the latter cited paper, working in the same group as the author does, is responsible for the design of the plant, while the author of this work aims to optimize this and other dividing wall columns and evaluate their saving potential on a theoretical basis. The saving potential is to be evaluated in comparison to conventional column sequences, which has not yet been studied in detail in the multi-objective space. For a fair comparison of the configurations, optimizations have to be performed. At this point it should clearly be distinguished between optimization in a mathematical context and a simple enhancement of an existing process which is often also referred to colloquially as optimization. This work focuses on optimization on a mathematical basis which requires sophisticated algorithms to find a solution. However, as already mentioned simple and multiple dividing wall columns are comparably complex, which makes the mathematical optimization computationally extensive.
The complexity of the optimization problem does not only result from the high number of optimization variables but also from its multi-objective nature. In other words, there is not only one, but a large number of so-called Pareto-optimal solutions, for each of which it is true that one objective cannot be enhanced further without compromising

another [23]. However, only one optimal solution is required for the design of a column. The methods available to chose only one optimal point out of the Pareto-optimal set can be classified as *a priori* and *a posteriori* [24]. *A priori* approaches perform assumptions prior to the optimization with the goal to simplify its calculation and usually reduce the optimal solutions to (in most cases) only one. A commonly applied *a priori* method combines actual objective functions as energy demand and number of theoretical stages to one economic function as for example the total annualized costs (TAC) [25]. This transforms the multi-objective problem to a simple single-objective one. Nevertheless, it is obvious that potential other candidates for the operating point are neglected in advance. Additionally, often empirically developed factors are included in the calculation [25, 26] resulting in problem-specific results. This leads to a leak of knowledge about the connection between the real objectives and the corresponding variables even though it is indispensable for an extensive process comprehension. Accordingly, *a posteriori* methods offer a suitable alternative to prevent the stated loss of knowledge. In this approach a large part of the solution space is calculated and the decision maker can choose the best suited option after the optimization itself [27]. Even though this method requires more calculation time, the advantage of a multi-use solution predominates. Accordingly, several scientific publications focus on a bi-objective optimization of columns [28–32]. The objectives are then for example the total number of theoretical stages, the energy input or one of the product purities. Nevertheless, to the best of the authors knowledge no higher dimensional optimizations of distillation columns considering all candidates simultaneously as objectives have been performed yet. Also, a deep understanding about variable correlations and their impact on the optimum is missing, because often only the objectives are visualized and not the corresponding optimal variables.

Based on the stated facts the first pillar of this work are multi-objective optimizations. On the one hand, an *a posteriori* optimization and evaluation approach is developed and presented for two kinds of dividing wall columns. In order to visualize the high-dimensional solution space and also the corresponding optimal variables, unique visualization techniques are applied. For a reliable result interpretation, the solution space including all variable correlations has to be fully understood. This goal is reached by performing simpler bi-objective optimizations, which aim to calculate an easier understandable subspace of the full solution set. Then, also the impact of different optimization problem definitions and simplifications can be studied in depth. On the other hand, it should be clarified for which cases dividing wall columns are a suited alternative to conventional column sequences. Based on literature data the dividing wall column is always more beneficial, however it should be investigated whether this fact is actually true in the multi-objective space. For this purpose also easy heuristics are needed to allow a simple estimation of the results without extensive optimizations. Each of the optima can only be reached in combination with the optimal variables. However, in some cases variables have some flexibility and can be changed within a certain range without worsening the objective function. In other words, several inputs can result in the same optimal output. In the context of distillation, this input multiplicity is also denoted as multiple steady states [33, 34]. As a rule of thumb one

can assume that the probability of such a behavior increases with the degree of process intensification. Thus, this phenomenon also occurs in dividing wall columns, where the flexible variables are mainly the vapor and liquid splits at the dividing wall [35–37]. Especially for the operation of a dividing wall column close to one of its energetic optima this behavior is of interest. Usually the vapor split below the dividing wall is not actively regulated during operation [38]. This is often classified as disadvantage using the argumentation that a deviation of the vapor split might lead to losses in product purities [39]. However, multiple steady states occur and thus the vapor split can actually be operated in a certain range. Then, the prerequisite for maintaining the product purities is that the liquid split is adjusted correspondingly. This behavior results in a flexibility in operation for the liquid and vapor splits which simplifies the operation of a column close to the design specific energetic optimum. However, in literature no extensive studies are available dealing with this flexibility range depending on the design of the column, accordingly several questions are still unanswered and targeted in this work. This includes for example, if the flexibility changes depending on the total stage number and also the stage allocation in the column sections. Also, almost no studies are available dealing extensively with the flexibility of multiple dividing wall columns.
At first glance, it may seem that optimization and multiple steady states are two different topics. However, they should rather be seen as two sides of the same coin. First, from a computational point of view the optimization problem is easier to solve, when several inputs result in the same optimal output. Second, theoretical energy savings are not worth much, if they cannot be reached in a stable manner during the operation of a real plant. Similar to the calculation, also the operation is easier, if multiple steady states occur. Even though some authors mention this connection [28], it is not emphasized enough according to its importance.
This observation leads to the second pillar of this work. The occurrence and extent of multiple steady states in simple and multiple dividing wall columns are studied in detail. Of special interest is the effect of input parameters on suited ranges of the liquid and vapor splits in such columns. An additional focus is to emphasize the connection between an optimal column design and the corresponding split flexibility.
Based on the stated pillars, the work is organized as follows. First, theoretical fundamentals are presented including dividing wall columns, their optimization and the occurrence of multiple steady states. Since part of the results are multi-dimensional, also suited visualization tools are discussed resulting in the use of self-organizing patch plots. After the presentation of the applied methods follows the results section, which is separated into two parts. One focuses on optimization and one on the flexibility ranges of the vapor and liquid splits at the dividing walls. In other words, the second part is relevant in order to evaluate the robustness of optima.
In the optimization section, first a large part of the solution space of a simple and multiple dividing wall column is calculated based on a multi-objective optimizations including five objective functions. With the presented method, an *a posteriori* exploration of the high-dimensional space is enabled. Afterwards, bi-objective optimizations are performed to calculate subspaces of the full solution range with the purpose to understand variable interactions. Additionally, the energy saving potential of dividing wall columns in

comparison to conventional column sequences is studied in detail. A heuristic rule is developed as decision support to evaluate the most beneficial column version considering a bi-objective space without the need of an optimization run. For its calculation only feed properties have to be known.
The following flexibility part focuses on the investigation of design parameters affecting the location of suited vapor and liquid split ranges to operate a column close to the corresponding energetic optimum. This includes among others ranges for different total stage numbers and allocations, feed mixtures and compositions. In this context the connection to the optimum emphasized several times. Additionally, an enhanced approach to estimate the vapor and liquid split ranges for columns with finite stage numbers is suggested. Last, the work is closed with a summary of the key findings.

2 Theoretical background and state-of-the-art

This chapter summarizes the theoretical background and state-of-the-art that are relevant to understand the results of this work. For this, Section 2.1 summarizes fundamentals about multi-component distillation and dividing wall columns. This also includes available shortcut methods to approximate the extreme compromises of the optimization, the minimum energy operation and minimum stage number. Afterwards, the state-of-the-art concerning the flexibility of the liquid and vapor splits (Section 2.2) and optimization (Section 2.3) are presented. Last, Section 2.4 focuses on high-dimensional data visualization techniques.

2.1 Distillation and shortcut design methods

Distillation is a process to separate liquid mixtures into pure components based on partial evaporation and condensation of the mixture. The process can either be performed batch-wise or in a continuous way, which is usually implemented in distillation columns. The process is not limited to the separation of binary mixtures, also multi-component mixtures can be split [40]. In this work the separation of ternary and quaternary mixtures in continuously operated columns is investigated on a theoretical basis.
The following Section 2.1.1 first summarizes distillation options to split multi-component mixtures focusing on dividing wall columns. Also, a pilot plant of a multiple dividing wall column planned to be built at Ulm University is introduced briefly in Section 2.1.2. Afterwards, shortcut design methods which are applied in this work are summarized in Section 2.1.3.

2.1.1 Separation of multi-component mixtures

Ternary or higher mixtures are conventionally separated in a sequence of simple distillation columns which are materially coupled. Two commonly used options for ternary splits are the direct and indirect split sequence (DSS and ISS, respectively) [7, 8, 41]. In a DSS, as shown in Figure 2.1a, the distillate product $\dot{D}$ of the first column is the pure light boiler (denoted as component A), while the bottom stream $\dot{B}$ is a mixture of the middle and heavy boiling components (component B and C, respectively), which is further purified in the second column. Reverse, in the indirect split the bottom stream of the first column is the pure heavy boiler and the distillate stream being a mixture of components A and B is processed in the second column. For the separation of higher mixtures with more than three components one column can be added for each component. Which sequence is the most energy saving one for the split of the feed stream mainly depends on its composition, but also the relative volatilities α_{ij} of the

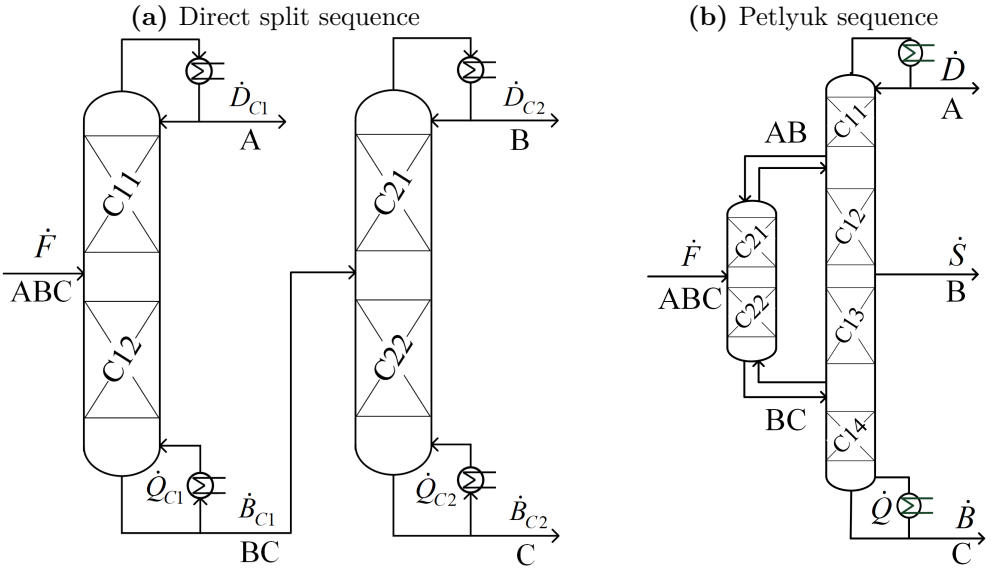

Figure 2.1: Options for ternary product splits in conventional columns.

components [7].

Another alternative for ternary mixtures is to combine not only two but three conventional columns, this sequence is called sloppy sequence [11]. The first column, which is often called prefractionator, performs a split between components A and C while B distributes between both product streams. The distillate product of the first column proceeds to a second one in which A and B are split, the bottom product proceeds to a third column splitting components B and C. Since this options desires relatively high investment costs for three instead of two columns it is rarely used. However, both columns performing the AB and BC split can be combined into one shell. If also the reboiler and evaporator of the first column are saved and replaced by a thermal coupling in addition to the material one, the result is the so called Petlyuk sequence shown in Figure 2.1b [42]. This principle can also be extended for mixtures higher than ternary, for each additional component one more thermally coupled column is required. In any case, the thermal and material coupling avoids a remixing of the intermediate boiling component(s) with the feed stream. As a consequence, energy savings of around 30 % can be expected [43]. It is often stated that this type of column has the lowest energy requirement of all known distillation variants over the entire feed composition range. However, the savings are relatively low with high proportions of light or heavy boilers. Thus, the savings increase with the proportion of middle boilers [7]. Nevertheless, these statements are partly based on the assumption of infinite stages.

The energy savings of Petlyuk sequences come at the cost of more complexity, and also only one operating pressure can be applied. The increased complexity arises from the fact that the theoretical stage number has to be specified for two additional column sections compared to a conventional column sequence. A column section is a segment of a column between incoming and outgoing streams that contains separating internals (indicated by boxes filled with an x and a numbering in Figure 2.1). A column region

consists of two sections which are located above and below a feed stream (rectifying and stripping sections) and is responsible to separate two components. The Petlyuk sequence has a column region to perform the separation between the components A and C (prefractionator, sections C21 and C22 in Figure 2.1) which is not present in the direct or indirect split sequence. Correspondingly, the number of stages for these two column sections has to be defined additionally. Further, the vapor and liquid split ratio between the two columns, R_V and R_L respectively have to be defined [10, 44]. Note that the liquid and vapor splits can either be defined as the flow on the right side of the dividing wall according to Figure 2.2 (index r) related to the total one ($R_{V,r}$ and $R_{L,r}$) or the flow on the left side (index l) ($R_{V,l}$ and $R_{L,l}$). Depending on the point of view either one or the other notation is more useful.
However, even though the energy consumption and thus the operational costs are reduced with a Petlyuk sequence, still two columns are needed. This can be avoided by integration of the Petlyuk sequence into only one column shell with an internal separating wall resulting in the dividing wall column (DWC). A DWC is thermodynamically equivalent to the Petlyuk sequence [11]. The separation of multi-component feeds into pure products in only one column shell results in additional savings of the investment costs and plant footprint [45]. The necessary number of dividing walls depends on the number of components in the feed mixture. For a ternary feed stream only one dividing wall is required as shown in Figure 2.2a. A feed mixture consisting of four components can

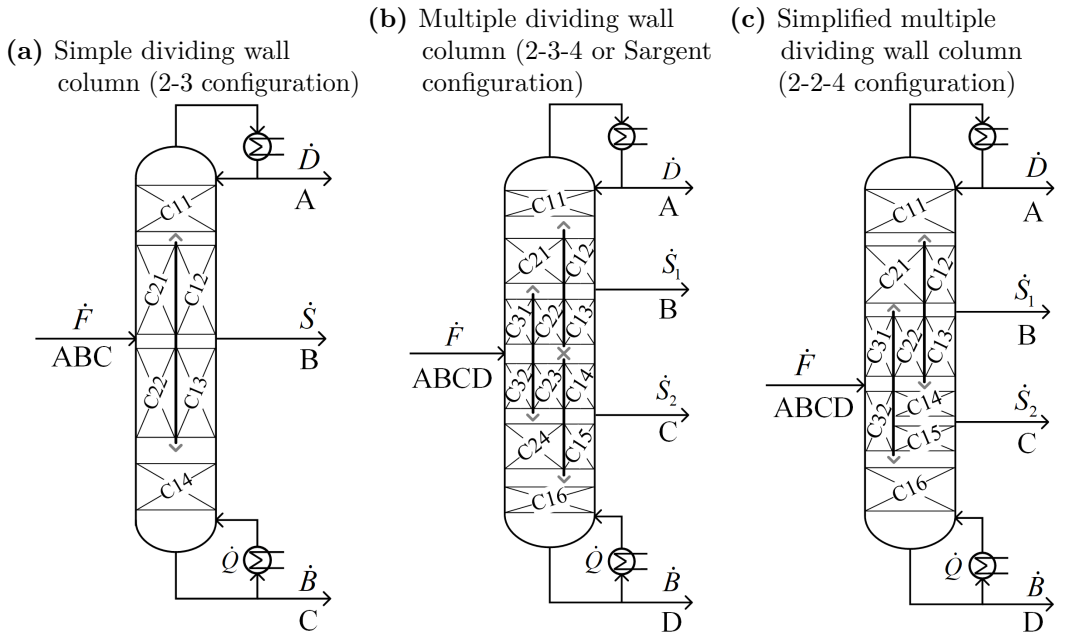

Figure 2.2: Ternary and quaternary versions of dividing wall columns. Gray angles indicate liquid and vapor splits, note also the section numbering.

also be split in a simple dividing wall column, which is then called Kaibel column or 2-4 configuration [46, 47]. However, applying more dividing walls results in higher energy savings [20, 48]. In the multiple dividing wall column (mDWC), which is shown in Figure 2.2b, three dividing walls are used. This column version is sometimes denoted as

2-3-4 configuration [21, 47] or Sargent DWC [49, 50]. The application of three dividing walls leads to a reduction of energy consumption of around 20 % to 55 % [20, 21, 50, 51]. This advantage is again offset by an increased number of degrees of freedom [52]. Correspondingly, several simplified versions of this column are suggested in literature. One method to simplify the mDWC is to assume liquid-only transfers to reduce the number of vapor splits [53, 54]. An additional approach is to reduce the number of dividing walls to two instead of three. This can either be done by merging the two walls at the product side or by totally neglecting one of them. This work focuses on the simplified multiple dividing wall column (smDWC) version shown in Figure 2.2c which neglects the dividing wall in the lower part of the product sections. Another name for the column version is 2-2-4 configuration [21, 47]. It is expected to be suitable for a large quantity of material systems [22]. Thus, this column configuration is chosen to be built at Ulm University [22]. More information about the pilot plant specifications is given in the following Section 2.1.2. Reducing the number of dividing walls by one can actually be done without causing an increase in energy consumption [21, 48]. Whether the column from Figure 2.2c can be operated at the same minimum energy demand as the one with three dividing walls mainly depends on the mixture. This is discussed in more detail in Section 2.1.3.1.

A recurring topic in this work is the theoretical stage allocation or distribution inside dividing wall columns. This expression is intended to describe the number of theoretical stages available in each section in relation to the other sections. In other words, if the stage number in all six sections of a dividing wall column is identical, the theoretical stage allocation is denoted as uniform. If the stages are different in all sections, it is denoted as non-uniform. A uniform stage allocation is for example used for multi-purpose plants in order to be able to split a large set of different mixture. However, usually columns are designed for a certain mixture and correspondingly the optimal stage allocation for this mixture might be rather non-uniform.

Another notable aspect is that the total stage number of dividing wall columns can be counted in two ways. The main difference lies in whether stages operated in parallel, thus on the left and right side of a dividing wall, are counted as one or separately. Counting these stages as only one is often done in industry, as the resulting number of stages allows conclusions about the column height (as performed in [50]). However, from a scientific point of view, these stages, which are operated in parallel, perform different separation tasks and thus should not be merged. Counting them separately also allows different stage numbers on both sides of dividing walls. This is the reason why the second approach is used in this work.

2.1.2 Pilot Plant: Simplified multiple dividing wall column

A simplified multiple dividing wall column pilot plant based on the smDWC version shown in Figure 2.2c is planned to be built at Ulm University in 2021. Thus, this kind of column is investigated in more detail in this work. Preißinger *et al.* summarized all steps

of the column design in a publication [22] and the most important facts are presented here briefly. A scheme of the plant can be found in the Appendix in Figure A.1.
In particular, the main objectives of column is to be suitable for a wide range of different mixtures. Thus, it is chosen to apply the same number of theoretical stages in all column sections despite C32, where twice as many stages are used due to fluid dynamic reasons. For the determination of the required total number of theoretical stages, a set of seven suitable systems is defined fulfilling certain specifications like zeotropic behavior, low price and low toxicity. For all systems an equimolar feed flow with $0.1\,\mathrm{kmol} \cdot \mathrm{h}^{-1}$ at liquid boiling state $q = 1$ is assumed. Several of the presented systems are also investigated in this work which can be found in Section 3.5. For the actual column design the system being most difficult to split is chosen, which is system 4.1 (Section 3.5). Then, a manual hierarchically oriented optimization minimizing the energy demand and total stage number required to reach at least 98 mol % pure product is performed. Finally, the total theoretical stage number is chosen at the strongest curvature of the calculated Pareto-front. At this point, the total stage number inside the column is 220, thus in each section 20 stages are used and 40 in section C32.
Based on these theoretical considerations the translation to the actual design of the pilot plant is done. For this, local conditions at the university are to be respected. These limit the total height of the column to 9.7 m. This height also includes liquid distributers, the evaporator and reboiler, thus the resulting height for the column sections itself is lower. Additionally, it is decided to build the two sections on the left and right side of a dividing wall as separate segments. Thus, the column shell is split into two with an Y-shaped connector. Consequently, the heat transfer across the dividing wall is neglected. These Y-shaped connecting parts above and below the two dividing walls also require a certain height. Consequently, the actual packing height of each section and half of the packing height for section C32 is 1060 mm. In order to reach the specified number of theoretical stages in this actually available section height, a structured wire mesh packing with a height equivalent to one theoretical plate ($HETP$) value of 0.053 m is needed. Thus, the Sulzer DX is chosen. It has $HETP$ values between 0.04 and 0.07 m, where the exact HETP value depends on the gas load (F-factor) inside the column [55]. However, if another kind of packing is chosen in future, a different number of theoretical stages in the column sections could result. Accordingly, for the optimization of the pilot plant in this work, the total number of theoretical stages is chosen as objective while the distribution of the theoretical stages on the column sections is assumed to be set.
Another notable feature of the pilot plant are perforated metal plates below the dividing walls. The wholes inside the plates can either be opened or closed, like this the pressure drop on both sides of the dividing walls can be manipulated prior to the operation. Consequently, the vapor splits are roughly adjustable to values different to 0.5.

2.1.3 Shortcut design methods

For the design of dividing wall columns several shortcut techniques are applicable. Most of them are based on the distribution coefficient of the components between the vapor and liquid phase K_i which is shown in Equation 2.1 [56].

$$K_i = \frac{y_i}{x_i} \tag{2.1}$$

y_i is the molar fraction of component i in the vapor phase and x_i the molar fraction in the liquid phase. Commonly the relative volatility α_i is given instead of K_i, its definition is shown in Equation 2.2.

$$\alpha_{ij} = \frac{K_i}{K_j} \tag{2.2}$$

Two extreme cases limit the operation range of distillation columns. One is the minimum energy operation at an infinite stage number (can practically approximated at $N = 4 \cdot N_{min}$ [20]) which is discussed in Section 2.1.3.1. The second one is the operation at the minimum number of theoretical stages and accordingly at high energy consumption, which is explained in more detail in Section 2.1.3.2.

2.1.3.1 First extreme case: Minimum energy operation and corresponding estimation of vapor and liquid splits

For the estimation of the minimum energy demand $\dot{V}_{min}$ diagrams can be used. Their calculation is based on the Underwood equations [57,58] and were presented by Halvorsen and Skogestad [59–61]. Underlying assumptions are constant molar flows, constant relative volatilities and an infinite stage number. For the calculation of $\dot{V}_{min}$ diagrams only feed stream properties have to be known, which are the molar fraction of all components z_i, their relative volatilities α_i and its thermal state q. Figure 2.3 shows how a $\dot{V}_{min}$ diagram looks like for a ternary system. However, the application is not limited to three components and can thus also be applied for quaternary or higher mixtures [61]. The calculation procedure can be found in the supporting material [62].

The feed stream $\dot{F}$ is assumed to enter a standard two-product distillation column. The $\dot{V}_{min}$ diagram shows the vapor demand at the top of the column related to the feed flow $\frac{\dot{V}_T}{\dot{F}}$ over the corresponding distillate to feed ratio $\frac{\dot{D}}{\dot{F}}$ for different product splits, which are shown at the bottom of Figure 2.3. A product split is defined as the complete separation (sharp split) of a light boiling component from a heavy boiling component, in this case AB, AC or BC where the first component is obtained in the distillate and the second one in the bottom product. If all data points are connected, the result are straight lines which intersect at maxima and minima. The number of maxima is the number of components minus one and between the maxima minima appear. Each maximum denotes the vapor demand for the product split of two close-boiling components, at the minima there are always one or more components with a boiling

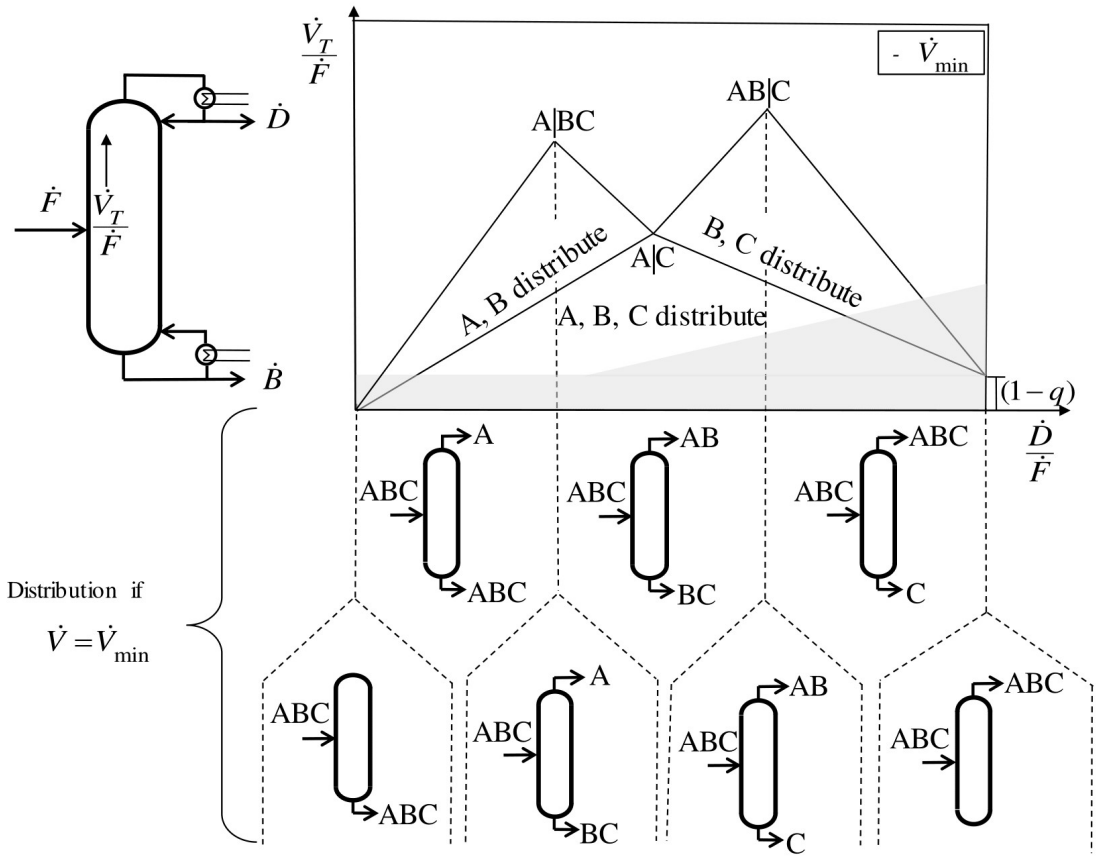

Figure 2.3: Explanation of $\dot{V}_{min}$ diagram for a ternary system.

point in between the components that are split. The intermediate boiling component(s) then distribute between the two product streams. If less vapor than required is used, both components that should be split start to distribute between the product flows and the split is no more called sharp. Using more vapor than needed is basically a waste of energy, since it does not enhance the performance of the column. Note that the fact, which of the peaks is the highest one depends on the system properties. In the shown example the BC peak is the highest one, however there are also systems for which the AB peak is higher.

There are two infeasible regions inside the $\dot{V}_{min}$ diagram which are indicated by gray regions inside Figure 2.3. The first infeasible region is the one below $(1-q)$, as at least the vapor fraction of the feed stream will always leave the column at the top. The second region results from the fact, that the distillate flow has to be at least equal or higher than the vapor flow at the top of the column.

The $\dot{V}_{min}$ diagram can directly be applied to a simple or multiple dividing wall column [61]. In this case the highest peak determines the total energy demand of the column. Additionally, several aspects have to be considered which is first explained for the easier case of a ternary system in a simple dividing wall column. Afterwards, the knowledge is extended on quaternary systems in a (simplified) multiple dividing

wall column. For column sequences, the diagram has to be adapted which is briefly discussed at the end of this section.

Ternary split in simple dividing wall column

As already mentioned the total vapor demand of a dividing wall column is set by the highest peak in the $\dot{V}_{min}$ diagram. The prerequisite for the applicability of the diagram is that all column regions performing a certain product separation work at the predicted flows. This means for a simple dividing wall column with a ternary feed that the sections C21 and C22 perform the AC split, the sections C11 and C12 the AB split and C13 and C14 the BC split as shown in Figure 2.4 on the left and in Equation 2.3. Note that the Petlyuk column is shown in the figure instead of the dividing wall column for clarity.

$$\begin{aligned} N_{AC} &= N_{C21} + N_{C22} \\ N_{AB} &= N_{C11} + N_{C12} \\ N_{BC} &= N_{C13} + N_{C14} \end{aligned} \tag{2.3}$$

Being able to determine the vapor demand in the prefractionator and main column means that also the required vapor and liquid splits at the dividing walls can be calculated based on the $\dot{V}_{min}$ diagram. In Figure 2.4 the corresponding points at which the vapor demand and related distillate streams must be read from the $\dot{V}_{min}$ diagram to determine suited liquid and vapor splits in a simple DWC are marked with horizontal black lines ($\dot{V}_{min}^{Original}$). The vapor split based on the original $\dot{V}_{min}$ diagram can accordingly

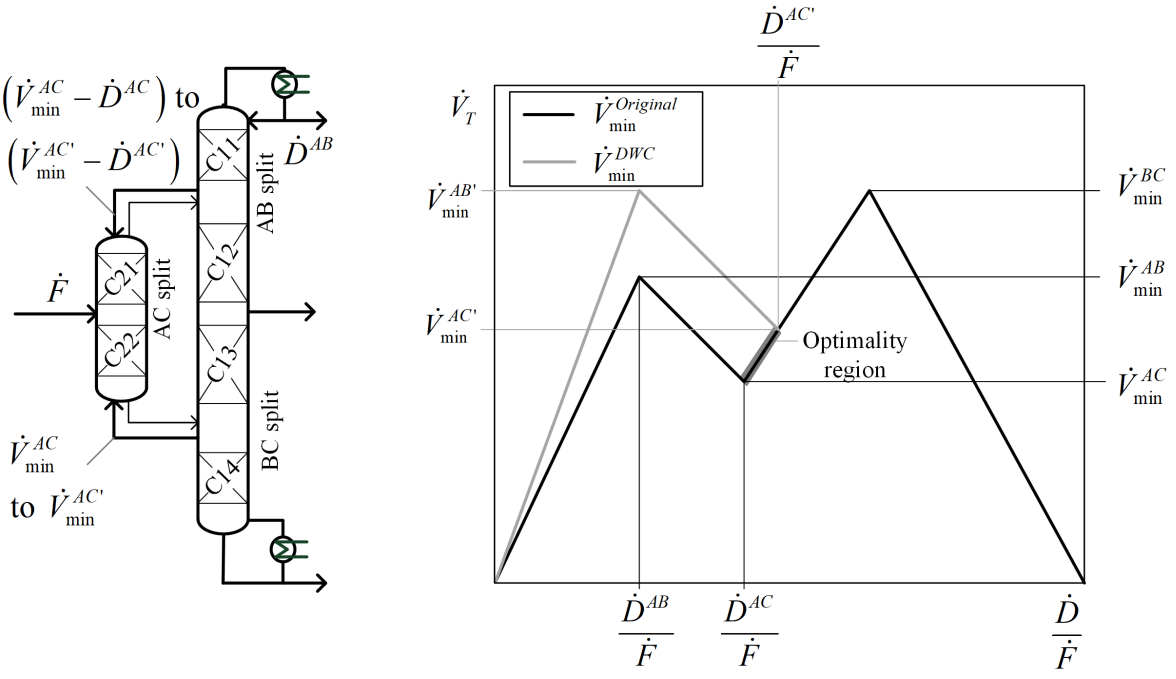

Figure 2.4: Optimality region in $\dot{V}_{min}$ diagram for the ternary case.

be calculated from the vapor demand of the AC split $\dot{V}_{min}^{AC}$ and the maximum one $\dot{V}_{min}^{max} = \max(\dot{V}_{min}^{BC}, \dot{V}_{min}^{AB})$ as shown in Equation 2.4.

$$R_{V,r}^{Original} = \frac{\dot{V}_{min}^{max} - \dot{V}_{min}^{AC}}{\dot{V}_{min}^{max}} \tag{2.4}$$

For the calculation of the liquid split also the distillate flows have to be considered as shown in Equation 2.5.

$$R_{L,r}^{Original} = \frac{(\dot{V}_{min}^{max} - \dot{D}^{AB}) - (\dot{V}_{min}^{AC} - \dot{D}^{AC})}{\dot{V}_{min}^{max} - \dot{D}^{AB}} \tag{2.5}$$

The resulting split fractions are a useful tool to initialize flow-sheet simulations [63]. However, performing a simple mass balance for a dividing wall column results in the conclusion that that the product splits AB and BC and thus all maxima have to be operated at the same vapor amount, assuming that all vapor leaving the evaporator will also be present at the top of the column (for constant molar flows, liquid feed and liquid side draw). In the $\dot{V}_{min}$ diagram this means that all maxima are shifted to the same height. This is shown in Figure 2.4 on the right side with gray lines ($\dot{V}_{min}^{DWC}$). In the original diagram of the system itself (black lines) the BC peak is the highest one and if the product split is performed in a dividing wall column, the AB peak is shifted to the same vapor demand (gray lines). Consequently, also the intermediate minimum AC is increased to $\dot{V}_{min}^{AC'}$. The region between the original position considering only the system and the new position occurring in a dividing wall column is denoted as optimality or flat region. The AC split can be operated anywhere in this region without causing an increase in total energy demand of the column. Accordingly, also the liquid and vapor split can be operated in a certain range, which can be calculated by inserting $\dot{V}_{min}^{AC'}$ and $\dot{D}^{AC'}$ in the equations 2.4 and 2.5, which represent the first limit of the splits. The resulting second limit of the split ranges is shown in Equation 2.6 and 2.7.

$$R_{V,r}^{DWC} = \frac{\dot{V}_{min}^{max} - \dot{V}_{min}^{AC'}}{\dot{V}_{min}^{max}} \tag{2.6}$$

$$R_{L,r}^{DWC} = \frac{(\dot{V}_{min}^{max} - \dot{D}^{AB}) - (\dot{V}_{min}^{AC'} - \dot{D}^{AC'})}{\dot{V}_{min}^{max} - \dot{D}^{AB}} \tag{2.7}$$

All feasible intermediate solutions for the liquid and vapor splits between the first and second limit, in other words between the value of the original diagram and the one inside a DWC, can be plotted. This results in a straight line with a positive slope [36].

Quaternary split in multiple dividing wall columns

For quaternary product splits in a column like the one from Figure 2.2b three additional column regions are required to perform the AD, BD and CD splits as shown in

Equation 2.8. The three regions for the AC, AB and BC split are analogue to the simple DWC from the previously shown Equation 2.3.

$$\begin{aligned} N_{AD} &= N_{C31} + N_{C32} \\ N_{BD} &= N_{C23} + N_{C24} \\ N_{CD} &= N_{C15} + N_{C16} \end{aligned} \tag{2.8}$$

Due to one additional component, the $\dot{V}_{min}$ diagram has three maxima instead of two as observed for the ternary systems. This is shown for one system as an example in Figure 2.5 on the right, indicated by the black lines ($\dot{V}_{min}^{Original}$, corresponding to the column from Figure 2.2b). Again, the highest peak determines the total energy demand of the column. Additionally, all required vapor and liquid splits can be read similar as described in the previous paragraph and be used as initial guess for simulations [63]. However, in this work only the simplified version of the multiple dividing wall column from Figure 2.2c is investigated, thus the $\dot{V}_{min}$diagram of this column version is explained in more detail here.
The considered simplified mDWC has two instead of three dividing walls. Accordingly, the column has two sections less for all product splits. In order to still obtain pure products, the AD split is skipped and the BD split is performed in the prefractionator (sections C31 and C32) instead as shown in Equation 2.9 and Figure 2.5 on the left.

$$N_{BD}^{smDWC} = N_{C31} + N_{C32} \tag{2.9}$$

Performing the BD instead of the preferred AD split results in a changed distillate flow of the prefractionator compared to the energetically optimal operation. This causes a shift of the following AC and AB split in the $\dot{V}_{min}$ diagram as indicated in Figure 2.5 by the dashed black lines ($\dot{V}_{min}^{Original+smDWC}$). However, if the increased AB peak stays below the highest one determining the overall energy demand, the column can still be operated without energy penalty compared to the three dividing wall version in Figure 2.2b. In the case that the peak is increased above the initially highest one, the system is assumed to be not suited for this simplified column version since the minimum energy operation is not feasible. Alternatively, a column with the second dividing wall in the lower part of the main column can be used. For this column option, the prefractionator performs the AC split and consequently the BD and CD splits are increased. However, since this kind of column is not the focus of this work it is not explained in more detail here.
Also analogue to the simple DWC all maxima have to be located at the same height for the real operation due to mass balance reasons. This is indicated in Figure 2.5 on the right by the gray lines ($\dot{V}_{min}^{smDWC}$). Accordingly, again an optimality region results causing flexibility of the vapor and liquid splits [61]. It is indicated by gray shaded areas in Figure 2.5. The behavior of this optimality region is expected to be more complex than for the simple dividing wall column since two peaks are increased instead of just one. Best to the authors knowledge, no extensive studies are available in literature

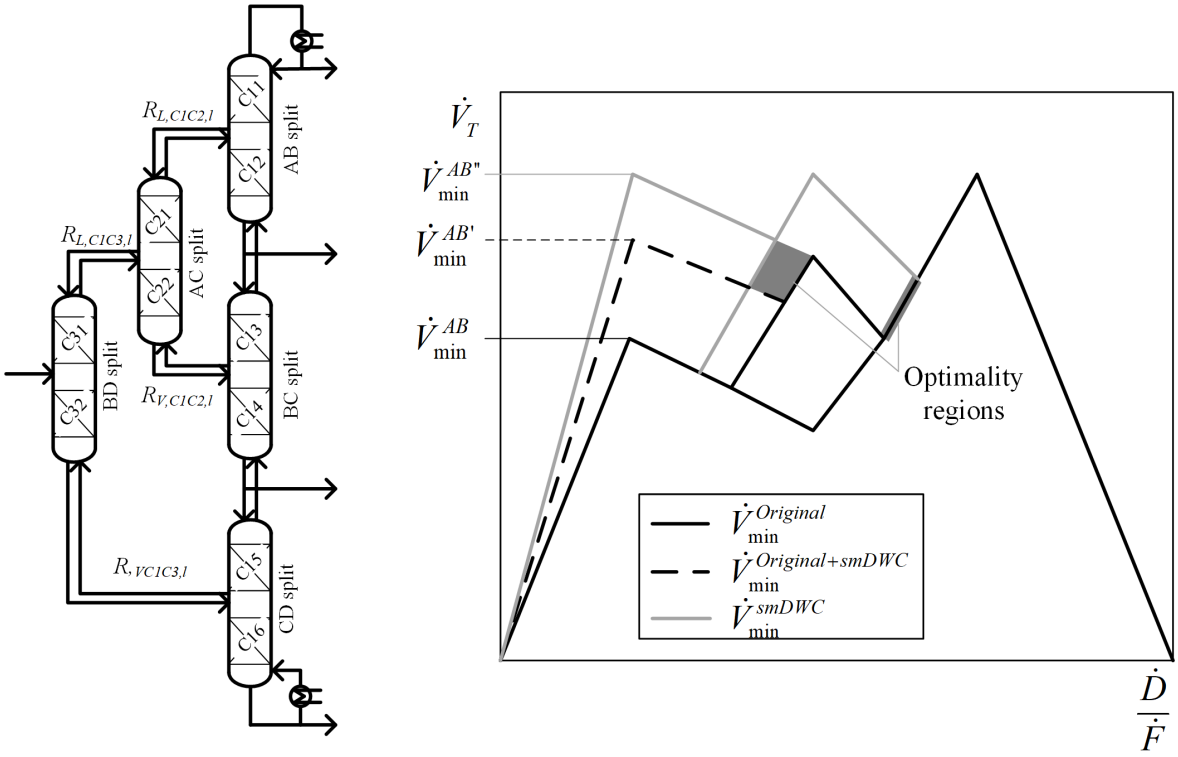

Figure 2.5: $\dot{V}_{min}$ diagram for quaternary systems: Suitability of systems for smDWC and optimality region. Inspired by [61].

about the optimality regions of smDWCs and their calculation with $\dot{V}_{min}$ diagrams. Thus this topic is discussed in more detail in the results Section 5.1.2.

Conventional column sequences

For column sequences as the direct split sequence the $\dot{V}_{min}$ diagram can also be used. However, for each column a new diagram has to be calculated. The reason for this are reboilers or condensers used between the columns, which change the available amount of vapor between two product splits. The properties of the product stream of the first column fed to the second one are used for the calculation of the new diagram.

2.1.3.2 Second extreme case: Minimum number of theoretical stages

The second extreme case for the operation of distillation columns is the operation at the minimum stage number. To determine this number for a simple two-product distillation column the Fenske equation from Equation 2.10 can be applied [64]. The index HK defines the high boiling key component and LK the low boiling key component, where the key components are the ones that are separated inside the column.

$$N_{min} = \frac{\log\left[\frac{x_{LK}^{\dot{D}}}{x_{HK}^{\dot{D}}} \cdot \frac{x_{HK}^{\dot{B}}}{x_{LK}^{\dot{B}}}\right]}{\log \alpha_{LK/HK}} \tag{2.10}$$

The Fenske equation considers only a binary mixture. Whether it is applicable on dividing wall columns or not is frequently discussed in literature. Several authors suggest to split the dividing wall column into regions performing binary product splits according to Equation 2.3 and 2.8, which are then considered as two-product distillation columns [13, 26, 65]. For each of these columns the minimum stage number is estimated with Equation 2.10. The sum of the minimum stage number for all regions performing one product split inside the dividing wall column is then its total minimum stage number. The main argument against this procedure is that the flows entering and leaving the prefractionating column do not have the same compositions [66]. However, best of the authors knowledge no reliable optimization based study is performed to prove or disprove these contradictory hypotheses. Thus, this question should be answered in this work by comparing optimization results with the ones provided from the Fenske equation in Section 4.3.2.
For dimensioning a dividing wall column it is especially important to know, whether the AB or BC split needs a higher number of theoretical stages. A simple procedure to answer this question without solving Fenske's equation is to determine the Ease of Separation Index (ESI) of the system [67]. The ESI of a ternary system results from Equation 2.11.

$$ESI_{ABC} = \frac{K_A \cdot K_C}{K_B^2} = \frac{\alpha_{AB}}{\alpha_{BC}} \tag{2.11}$$

If the ESI is one, the AB split requires approximately the same number of theoretical stages as the BC split. If it is below one, the AB split is harder and requires more stages and the other way around. Accordingly, for an ESI above one, the BC split

needs more stages than AB. Note that the $\dot{V}_{min}$ diagram in Figure 2.3 is for a system with an ESI around one. Also it should be kept in mind that the ESI is only useful for almost sharp product splits.

2.1.3.3 Compromises between minimum energy and minimum stage operation

Usually, distillation columns are not operated at one of the extreme cases presented in the two previous paragraphs. An established method to determine a compromise operating point is the one of Gilliland [68]. He suggests a standardization of the number of stages and the reflux ratio according to Equation 2.12 leading to the dimensionless parameters Y and X. In the corresponding publication it is shown that Pareto-optimal designs of some distillation columns always lie on the same line when plotting X over Y.

$$\begin{aligned} Y &= \frac{N - N_{min}}{N+1} \\ X &= \frac{R_R - R_{R,min}}{R_R + 1} \end{aligned} \tag{2.12}$$

Gilliland's publication was only graphically based. Later, Molokanov extended the method by an equation [1]. The correlation between the two standardized parameters from Equation 2.12 is described with the empirical Equation 2.13.

$$Y = 1 - exp\left[\left(\frac{1 + 54.4 \cdot X}{11 + 117.2 \cdot X}\right)\left(\frac{X-1}{\sqrt{X}}\right)\right] \tag{2.13}$$

Additionally, the Kirkbride equation can be applied in order to estimate the optimum feed stage of the column [69]. N_R are the number of stages in the rectifying and N_S in the stripping section.

$$\frac{N_R}{N_S} = \left[\left(\frac{x_{HK}^{\dot{F}}}{x_{LK}^{\dot{F}}}\right) \cdot \left(\frac{x_{LK}^{\dot{B}}}{x_{HK}^{\dot{D}}}\right)^2 \cdot \frac{\dot{B}}{\dot{D}}\right]^{0.206} \tag{2.14}$$

2.2 Flexibility of liquid and vapor splits

As already stated, the $\dot{V}_{min}$ diagram predicts an operating range for the liquid and vapor splits in dividing wall columns called optimality region. The behavior is also observable from rigorous simulations, which no more rely on strong assumptions like the ones of the $\dot{V}_{min}$ diagram [28, 33]. In the context of optimization this is an important observation, since several variable inputs can result in the same optimal output.
In literature that observation is also called multi or multiple steady states [33, 34, 70]. Note that in this work a flexibility region is determined which includes several multiple steady states. Multiple steady states denote one set of variable ranges corresponding to only one column design with exact product specifications which is often operated

at the Pareto-optimum of the energy input. The flexibility region is a broadened area around this specifically defined column design. This arises from the fact, that inequality constraints are applied on product purities. Thus, several sets of multiple steady states are observable at the same time. Each of these sets broadens further, if a certain increase of energy input is considered in comparison to the Pareto-optimal one. These additional easing of restrictions on the column design result in the occurrence of many multiple steady state at the same time. This behavior is denoted as flexibility of the vapor and liquid splits or flexibility region in this work.
Several publications are available focusing on the split flexibility in simple dividing wall columns. One of the first publications stating this behavior is from 1986 [33] and focuses on the occurrence of multiple steady state solutions of interlinked columns. The behavior is explained visually by several intersections of the isopurity lines of the products and a mathematical approach is presented to predict the existence of multiple solutions. This method is also applied by several other authors in the context of dividing wall columns [34, 35, 37]. Halvorsen *et al.* published an extensive study about the suited splits at the dividing wall resulting in an energetically optimal operation [36]. It is shown that several combinations of R_V and R_L located on a straight line enable a minimum energy operation at infinite stage numbers. If the splits are operated besides this optimal range, the total energy demand increases. Depending on the direction of the deviation of the vapor and liquid splits, either a very steep or a rather smooth increase in energy demand can be observed. Similar observations are stated in several other reports [39, 71, 72]. Additionally, Halvorsen *et al.* [36] show that the shape and location of the split flexibility region is strongly affected by the thermal state of the feed. For higher values of q, the range of suited splits is shifted and broadened in the direction of lower liquid and higher vapor splits. For deviations in the feed stream compositions the flat region also shifts. Similar observations are made for a calculation with finite stage numbers, however the stage numbers in the column sections is not given [36]. Ge *et al.* study the flexibility of a simple dividing wall columns designed for a certain feed stream composition in the event of feed disturbances [73]. They conclude, that the dividing wall column can tolerate feed stream disturbances to a certain extend and that columns designed for a higher content of the light boiling component tend to be more flexible.
For multiple dividing wall columns only few studies are published. Ge *et al.* [74] present the effect of feed composition disturbances on suited vapor split ranges for two versions of multiple dividing wall columns with two partition walls. For this purpose, first a manual optimization approach is applied. Afterwards, suited split ranges to reach 96 mol % pure products 2 % above the optimal energy input is investigated. It is found that suited split ranges are shifted, analogue to the simple dividing wall column. The authors conclude, that liquid splits should be adjusted during the operation of such columns in order to obtain the specified product purities. However, the liquid splits required in combination with the presented vapor splits are not shown and thus their flexibility is excluded from the evaluation [74].
Most presented publications (despite [73]) assume an optimal stage allocation in the column sections and then investigate the split flexibility. To the best of the authors

knowledge, no investigation was performed evaluating the impact of a non-optimal stage allocation inside the column and also of the total stage number. Additionally, a clear compilation summarizing the impact of all column parameters on the flexibility must still be provided to emphasize the significance of this issue. On the other side, also detailed studies about multiple dividing wall column split flexibility are still missing. The stated gaps are closed in this work in Section 5.

2.3 Optimization of distillation processes

Generally, an optimization problem consists of three parts. First, the objective function(s) $\boldsymbol{F}$, which should be minimized or maximized. If only one objective function is considered, the problem is called single-objective, if there are several it is called multi-objective. Second, the optimization variables which define the design space and are either discrete y or continuous x. Third but optionally, equality or inequality constraints, h (total number m) or g (total number p), can be applied to limit variables [75]. Equation 2.15 shows the general definition of an optimization problem [24, 76, 77]. Note that bold variables indicate a vector.

$$\begin{aligned} \underset{\boldsymbol{x},\boldsymbol{y}}{\text{Minimize}} \quad & \boldsymbol{F}(\boldsymbol{x},\boldsymbol{y}) = [F_1(\boldsymbol{x},\boldsymbol{y}),\ldots,F_n(\boldsymbol{x},\boldsymbol{y})] \\ \text{subject to} \quad & g_k(\boldsymbol{x},\boldsymbol{y}) \leq 0,\ k = 1,\ldots,p \\ & h_l(\boldsymbol{x},\boldsymbol{y}) = 0,\ l = 1,\ldots,m \end{aligned} \tag{2.15}$$

This work focuses on multi-objective optimization problems. A solution of the multi-objective optimization problem is a point for which no other point exists that is better in every objective. Such a point is called Pareto-optimal solution. This means that in order to improve a Pareto-optimal solution in one objective, another objective is degraded. The set of all Pareto-optimal solutions are called Pareto-front [24, 78–81].
In the following, two aspects about optimization are summarized in more detail. The first aspect is the computational point of view, which is about how the optimization problem itself is solved (see Section 2.3.1). The second aspect is the engineering aspect, which is about how optimization problem are usually defined for distillation processes (see Section 2.3.2).

2.3.1 Computational point of view

The core of optimization is the computational framework which is used to solve it. Generally, either process simulation and optimization are integrated into one stand-alone model [82, 83] or two separate programs are coupled. The use of separated programs is often applied because commercially available tools can be coupled rather simple. In this context, Aspen Plus [14, 16, 28, 84], Aspen HYSYS [85, 86] or CHEMCAD [31] are used but basically every simulation tool is suited. From here on, the optimization can be performed manually by an iterative approach [8, 74, 87], semi-automated using design

of experiments methods [14, 84, 88] or by a fully automated algorithm [16, 28, 31]. For the latter one, input and output data have to be exchanged between the flow-sheet simulator and an external optimization algorithm.
The algorithms applied to solve the problem can be differentiated into stochastic and deterministic ones [23]. Stochastic algorithms randomly generate parameter sets, evaluate outputs and proceed with the most promising combinations in the next iteration step, accordingly they are also called genetic or evolutionary. These kind of algorithms are very commonly used for the optimization of dividing wall columns [16, 32, 85, 89, 90]. However, if a sequential modular flow-sheet simulator as Aspen Plus is used, the erratic parameter changes can result in convergence problems, especially when it comes to multiple dividing wall columns. Deterministic algorithms use gradients to determine a local approximation of the problem. Based on this approximation, the next iteration is proposed. Common examples for this approach are sequential quadratic programming (SQP) and interior-point methods [91–94]. With this approach there is no guarantee that a global optimum is found [23] and accordingly several starting points should be tested. Also often the derivatives are not accessible, especially if an external flow-sheet simulator is used. Additionally, a strategy how to handle non-convergent runs is required. Thus, a relatively high number of calculation runs are needed in order to determine the derivatives by finite differences. However, less drastic changes in the variables cause less convergence problems in externally operated commercial flow-sheet simulators compared to stochastic approaches. Nevertheless, this kind of optimization is rarely used in the context of distillation, as for example in [31], or applied as a hybrid version in combination with a stochastic approach [83].
An additional aspect that should be mentioned is how constraints are handled during optimization. Of course the procedure is depending on the type of constraints and the algorithm itself, but generally either penalty functions, repair functions or decoder can be used [95]. For deterministic algorithms constraints are rather included in the local approximation of the problem.
Most presented options focus on solving single-objective optimization problems. To solve multi-objective problems, usually sequences of single-objective problems are calculated. Several techniques are available how the sequence of single-objective problems is defined. A common approach is the ϵ-constraint method, in which only one of the objectives is minimized while the others are considered as constraints [96]. Another approach is called weighting scalarization, for which all objectives are multiplied with weighting factors $\boldsymbol{w}$ and summed up to one combined objective function f. The weights are chosen differently for each single-objective problem that is solved. Again, several approaches can be used to choose the weights. Frequently techniques are applied determining results with equidistant space on the Pareto-front [97, 98]. However, this requires solving a relatively high number of single-objective optimization problems. One approach to reduce the calculation time is to apply a neural networks [89]. However, still a high number of optimization runs has to be performed in advance to train the network. Afterwards, the network can be used to predict possibly optimal designs with reduced calculation time. A different approach is to calculate only a minimum number of optimal points that still represent the Pareto-set with a certain accuracy. This goal can

be reached by an adaptive scalarization method called sandwiching [23, 99, 100]. The approach is only applicable for convex Pareto-fronts [81]. Since this kind of algorithm is used in this work it is discussed in more detail in the following.

Figure 2.6 shows the general steps performed to approximate the Pareto-front with the sandwiching algorithm using the example of a bi-objective problem. However, this procedure can also be applied to higher dimensions. As already stated, a sequence of single-objective optimization problems is solved. In a first step the extreme compromises between the objective functions are determined. For this purpose, the weighting factors of all objectives but one are set to zero. The objective function which has a weighting factor different from zero is afterwards minimized. This procedure is repeated until the extreme points of all objectives are found. Based on the extreme compromises the so called Nadir Point is constructed, which represents the worst value for each objective [23]. This point is required to determine the approximation quality of the solutions. For this purpose, between all yet calculated Pareto-optimal points an inner and outer approximation is determined as shown in Figure 2.6 at the bottom on the right. The inner approximation is a straight line between the two points and the outer approximation results from the tangents of them. The resulting facet has a shape like a sandwich which is the namesake of the method. The current approximation quality is set by the maximal distance between the inner and outer approximation. If the quality is not sufficient according to the specification of the user, another single-objective run is performed. The applied weighting factors are determined by the slope of the connecting line between the two evaluated Pareto-optimal points of the facet as indicated in Figure 2.6 at the bottom left. Minimizing the resulting single-objective problem with the corresponding weighting factors is basically a shift of the inner approximation/connecting line until a minimum is found. By calculating an additional point on the Pareto-front like this, one facet is split into two and correspondingly the approximation quality is increased. This procedure is repeated between all other available facets. Like this, additional Pareto-points are calculated exactly there, where the approximation quality is worst. This is usually at another location as it would be chosen during equidistant weighting. Accordingly, only a minimal number of Pareto-optimal points has to be calculated in order to reach a certain approximation quality to describe the convex multi-objective problem [23].

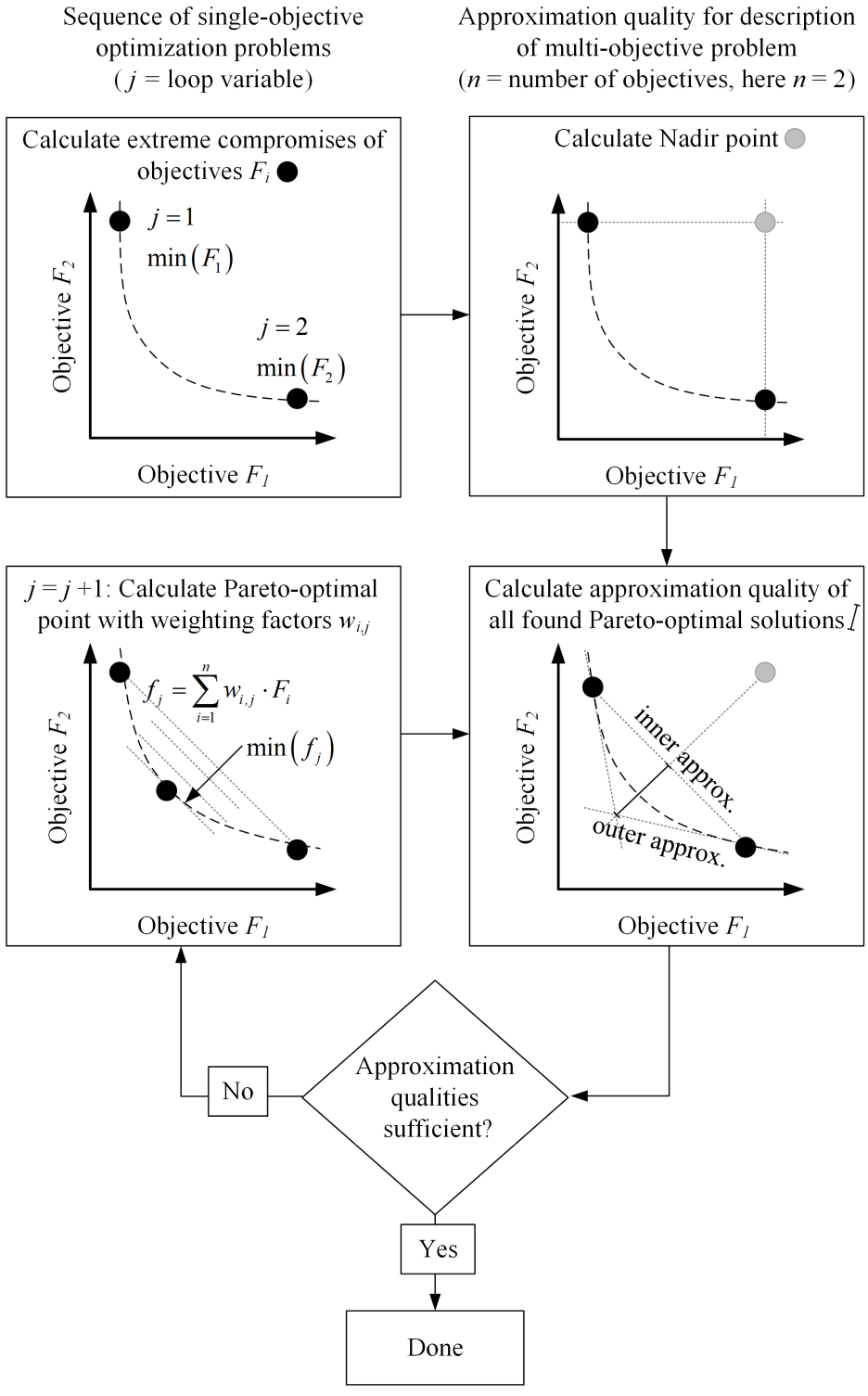

Figure 2.6: Principle of sandwiching algorithm to approximate convex multi-objective optimization problems explained for a bi-objective problem.

2.3.2 Engineering point of view

The optimization of distillation columns simulated with the theoretical stage model includes discrete (stage numbers) and continuous variables (energy input etc.). Additionally, it has a non-linear nature due to the thermodynamic models included. Mathematically this is denoted as mixed-integer non-linear programming problem, often simplified to MINLP. If the number of stages is not included in the optimization, it simplifies to a non-linear programming problem, NLP. Accordingly, with which algorithm the problem is solved mainly depends on its initial definition. Additionally, the problem definition in terms of chosen objective functions affects the outcome of the optimization. Accordingly, common approaches used for distillation columns are summarized in this section.
In engineering most frequently single-objective optimizations are performed to compare distillation options. For this purpose, often a combined cost function [45, 67, 101], which is also denoted as Total Annual Costs (TAC) [16, 26, 71, 85, 86, 88, 90, 102, 103] is defined and minimized. A well-known method for the derivation of the cost function is presented by Luyben [25], however, many other versions are also applied. Due to the non-uniform evaluation method of cost functions a detailed comparison of the presented results is difficult. Nevertheless, most of the just quoted authors find cost savings in the range of 20 % to 44 % for the dividing wall column compared to the conventional direct split sequence.
From an economic point of view, the derivation of a combined cost function is a useful tool to compare different options. From the perspective of research, the combination of real objectives with empirically determined factors to fit everything into one equation is an unnecessary restriction of the solution space which is performed without sufficient information. Actually, the optimization of most separation processes including the dividing wall column are of multi-objective nature. Since objectives can be contradicting, there is not just one optimum but a high number of Pareto-optimal compromises. Accordingly, the result of a single-objective problem like a cost function represents only one small part of the whole possible space.
Correspondingly, several publications perform bi-objective optimizations of distillation columns. For this purpose, some authors again include cost functions into the optimization, while for example a product purity [29, 83], ecological factors [30] or control properties [104] are maximized or minimized. On the other hand, there are also some authors that perform bi-objective optimizations of actual design variables of the column, like the the reboiler duty $\dot{Q}$ and product flows or purities [31] or the reboiler duty and number of theoretical stages ΣN_{Ci} [28, 32, 89, 105]. In both cases the result is a convex curve on which all Pareto-optimal solutions are located. In this work the Pareto-front describing compromises between the stage number and energy input is denoted as $N\dot{Q}$ curve. Note that for simplicity reasons the term N is used instead of ΣN_{Ci}.
The main advantage of such a bi-objective optimization is the possibility of an *a posteriori* evaluation. In other words, the results can be evaluated several times considering different cases and be used for comparison of different distillation options.

An example: if the focus is more on reducing energy demand, the end of the Pareto-front at high stage numbers is compared. If on the other hand strong height limitations are to be considered, N has to be small and thus the other end of the front should be evaluated. One author found for example, that the Pareto-fronts of different distillation options might intersect [104]. Therefore, it makes sense to allow the final decision maker to weight the considered objectives differently after the calculation has been completed. However, in order to perform bi-objective optimization, constraints usually have to be used. Correspondingly, the applicability of the results is still limited, even though this limitation is less severe compared to the single-objective optimization of a cost function. In case of the optimization of N and $\dot{Q}$, the constraints usually concern the purities or recoveries of the products or in other words the sharpness of the separation [106]. Accordingly, the results cannot be transferred to a column with different product requirements. Consequently, a new calculation has to be run. Additionally, the impact of the simplified optimization problem definition on the results is usually not questioned. Thus, this topic is investigated in Section 4.2.
A more universal *a posteriori* approach enabling for multiple-use optimization results is considering more than just two objectives. For example, while minimizing the energy demand and total stage number, also the the product purities could be maximized. The resulting optimization problem is accordingly multi-objective [107]. Even though such a kind of optimization can offer a significant knowledge gain about when to use which kind of distillation setup, to the best of the authors knowledge only one similar publication has been published in which three objectives are considered [108]. In the latter cited paper, a ternary feed stream with three different compositions should either be separated in a dividing wall column, side draw column, a direct or indirect split sequence. The objectives are to minimize total costs while a product purity and a product flow are maximized. In some cases again the Pareto-fronts intersect, so it cannot be said generally, that one option is always more suitable. However, again a cost function is used and the results are only presented normalized which makes a comparison to other publications difficult. Apart from this, to the best of the authors knowledge no further scientific contributions have been published yet in this context. Correspondingly, multi-objective optimizations of dividing wall columns are evaluated in detail for two examples in Section 4.1 of this work. The comparison of suitable distillation options based on Pareto-optimal column designs is presented in Section 4.4. In any case, the result of a multi-objective optimization is, independent on the problem definition, high-dimensional, especially if the optimization variables should also be presented. Accordingly, data visualization is an important issue which is summarized in the following Section 2.4.

2.4 High-dimensional data visualization

In order to present the design of a dividing wall column including all degrees of freedom, especially in the context of optimization and multiple steady states, high-dimensional data visualization techniques are needed. In literature lots of methods are presented

addressing this topic, an extensive review can be found in [109, 110]. The following section focuses only on fundamentals.
The main challenge visualizing a high-dimensional data set lies in its conversion to lower dimensions that can be plotted. Direct data mapping summarizes methods in which sub projections of the higher dimensions are plotted directly. This method includes the use of parallel coordinates [111], enhanced versions of those [112, 113] or scatter plot matrices [114]. All have the disadvantage that they get unclear or space consuming for higher dimensions. Accordingly, for very complex data sets further data processing is a good alternative. The two most important kinds of data transformation are clustering and dimension reduction. Both of them can be implemented as unsupervised machine learning algorithms [115, 116]. Clustering of data means that scattered data points or patterns are classified according to similarity into groups called cluster [117]. This method is well suited to get a general overview over the data classes. However, it does not solve the visualization problem itself. For this a dimension reduction is needed which again can be differentiated into sub categories. A commonly used linear reduction technique is the principal component analysis [118]. Non-linear approaches are isomap [119] and t-distributed stochastic neighbor embedding (t-SNE) [120]. A combination of clustering and dimension reduction is the self-organizing map (SOM) [121]. Since a variation of these, the self-organizing patch plots (SOPPs), are used in this work those two is explained in more detail in the following Section 2.4.1, followed by an introduction how to read them in section 2.4.2.

2.4.1 Self-organizing maps and self-organizing patch plots

A SOM is an artificial neural network that is trained unsupervised resulting in a discretized and typically two-dimensional representation of the training data. Thus, the training set is basically the data which should be reduced in dimension and/or visualized. During the training, the network is organized in a way to reproduce the topology of the input data. For this purpose first the SOM has to be initialized which means that weighting factors have to be created for each neuron in the network. Usually, this is done randomly. Then, in a training step a representative part of the training set called stimulus is handed over to the network, where the best matching unit (BMU) is searched. Based on the BMU the neurons are migrated and the weighting factors are updated. The training ends after a defined number of iteration steps. However, the overall creation of a SOM is complex and extensive. A detailed explanation would exceed the scope of this work and thus the author refers to special literature about this topic [121–124]. When the training is finished, the low dimensional SOM which represents the topology of the input data can be plotted.
SOMs are an established technique for dimension reduction which is useful especially for a visualization of high-dimensional data [122]. Nevertheless, not the data set itself is shown but a network which was trained with it. Even though the map represents the topology of the input data, not the exact numbers are shown and part of the solutions could be distorted. As the objective of this work is to plot exact optimization or

screening results, this is a crucial disadvantage. Accordingly, Stöbener *et al.* combined the self-organizing maps with Voronoi diagrams to so-called self-organizing patch plots that can exactly represent high-dimensional data [125].
For the transformation of a SOM to a SOPP, only the position of the BMUs corresponding to the training data points in the SOM is used. Each of these data points is taken as a seed point for the Voronoi diagram. In Voronoi diagrams the plane diagram area is divided into irregular shaped regions. This division is performed around scattered seed points (data points), in a way that each patch represents one seed point. All points inside the patch are closer to the corresponding seed point than to any other. The term close can have different mathematical meanings, in most cases the minimum Euclidean distance is meant [126]. Afterwards, the Voronoi patches are colored according to the absolute value of the seed point. How the resulting diagrams look like and how they are read is explained in the following Section 2.4.2.

2.4.2 How to read self-organizing patch plots

In SOPPs there is always one diagram per quantity. If in the context of distillation for example an $N\dot{Q}$ curve is calculated for fixed product specifications while varying the feed stage height, there are three quantities and accordingly three subplots. These diagrams relate to each other and always have to be read in combination. In all diagrams the same patch pattern is found and each patch represents one high-dimensional data set. Note that the shape of the patches, their black borders and the axes of the diagrams do not directly have a meaning. For the understanding only the location of the patches in the plot area in combination with the other diagrams and the color of the patch are important. With the help of the legend next to the diagram, the color of the patch can be translated into the value of the corresponding data point. The related values of the other quantities is read in the same patch in the other subplots.
Considering this background one can have a closer look on Figure 2.7, where the two-dimensional $N\dot{Q}$ curve from Figure 2.7a is transferred into a SOPP in Figure 2.7b. For simplicity reasons the optimization variables which lead to the optimal results are not shown. However, it is easy to include them in terms of an additional subplot. First of all, since considered the data set is two-dimensional there are two subplots, one for ΣN_{Ci} and one for $\dot{Q}$. All data points that are plotted in the diagram in Figure 2.7a can also be found in Figure 2.7b, indicated by small crosses. Around each cross, a Voronoi patch is formed. As nine data points are plotted, there are also nine patches in each SOPP. The nine patches inside one diagram are irregularly shaped and the resulting irregular pattern is identical in all corresponding subplots. The data point at a high total stage number ΣN_{Ci} and low reboiler duty $\dot{Q}$ can be found in the upper left corner of the SOPPs. In the subplot of ΣN_{Ci} the corresponding patch is colored in dark red while the patch in the subplot of $\dot{Q}$ is dark blue. The proceeding to lower stage number in Figure 2.7a equals the path from the upper left corner to the lower left, lower right and upper right corner in the SOPPs in Figure 2.7b. Note that this path can also be totally different for another data set. Taking a look at the SOPPs as a whole, it is

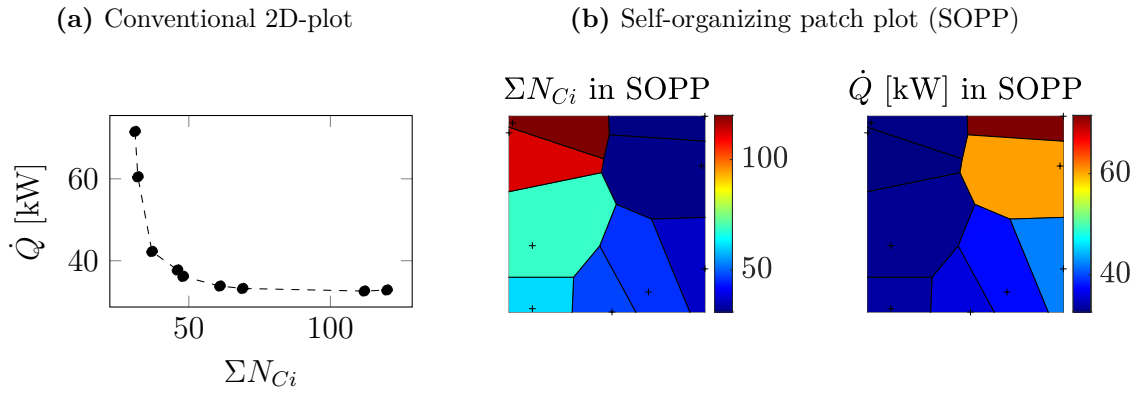

Figure 2.7: Representation of same data points in a conventional two dimensional plot and in a SOPP.

obvious that the stage number is high in another edge of the diagram than the reboiler duty. Accordingly, it can easily be read that the two objectives are contradicting.
All in all, the same knowledge as from the conventional axis based visualization can be read. For this simple two-dimensional case there is no real benefit of the visualization in SOPPs. Considering that for example the optimization of a dividing wall column results in a 13-dimensional space these correlated diagrams are well suited to determine tendencies.

3 Methodology

All presented results are obtained from theoretical calculations. For this purpose Aspen Plus® (V10 and 11) is used and for automation reasons coupled to Microsoft® (MS) Excel® (2013) by ActiveX. For simplicity reasons the registered trade mark symbol is neglected in the rest of this work. All calculations are performed on standard computers (CPU: Intel® Core™ i5-6500 CPU @ 3.2 GHz, RAM: 16 GB or CPU: AMD Ryzen 5 PRO 2400G 3.6 GHz, RAM: 16 GB).
Section 3.1 summarizes the settings used for the interface between the two programs and the chosen settings in Aspen Plus. The interface is either used for an optimization (see Section 3.2) or a screening to determine the split flexibility (see Section 3.3). In case of high-dimensional results, self-organizing patch plots (SOPPs) are computed in MATLAB® (R2018a and R2020a) for visualization (Section 3.4). To obtain a easier comparison between the results, standardization methods are applied for some variables which are summarized in Section 3.4. Last, the mixtures which are used for the calculations in this word are presented in Section 3.5.

3.1 Setup of automated flow-sheet simulation

As already mentioned Aspen Plus is used for the flow-sheet simulations. In this context, three aspects have to be considered. First the thermodynamic modeling, second the implementation of columns and third the setup of the data exchange through the interface.
For the first aspect about the thermodynamic modeling supporting information can be found in the appendix in Section A.2.1. However, it should be mentioned that Non-Random-Two-Liquid (NRTL) is used for the thermodynamic modeling. The applicability of the parameters from the data base to the chosen systems is validated with literature data.
Considering the second aspect, several options are available to implement the dividing wall column in Aspen Plus. The models in question are shown in the appendix in Figure A.2. All of them are equilibrium stage models including the *MultiFrac* model *Petlyuk* (note that the italic font is used to indicate that the Aspen Plus model is meant an not the column sequence itself) and several sequences of *RadFrac* models. All options are thermodynamically equivalent to the dividing wall column. In any case the stages inside the columns are counted from the top to the bottom. In order to determine the best suited model for the optimization and screening runs, two aspects are relevant, first the calculation time and second the prone to errors. These two objectives are evaluated for all suited column models. For this purpose a sequence of 200 randomized calculation runs is performed automated with the interface between Aspen and Excel. Thus to fully understand the method, the third aspect, the data exchange through the interface, is briefly summarized prior to the presentation of the chosen column model.

For the third aspect, the automated simulation setup, input and output data are managed in MS Excel. The corresponding Aspen Plus simulation hat so be in a .bkp format. In MS Excel a Visual Basic for Applications (VBA) code exploiting ActiveX is used to access specific paths leading to the desired process variables. These paths have to be implemented differently for each column model. Overall with the procedure an automated data exchange between Aspen Plus and Excel can be obtained.
With the above mentioned interface the best suited column implementation option is determined using the example of a simple dividing wall column. As already mentioned 200 randomly generated simulations are automatically run one after another for each of the column options (Figure A.2 in the appendix). For each of the implementation options a different VBA code needs to be programmed. In any case, varied input parameters are the stages in all six column sections, the reboiler duty and the liquid and vapor splits. Due to variable standardization it was guaranteed that only theoretically feasible variables are used. The results of all models are compared and have identical outputs which validates the fact that all models are thermodynamically equivalent. The number of non-convergent runs (also denoted as error in the following) and the necessary calculation time of all tested models can be seen in Figure 3.1a and Figure 3.1b, respectively. Two of the randomly generated runs resulted in errors for all models and are thus assumed to be infeasible. Accordingly, in the figures only the results of 198 runs are compared. It can be seen that the lowest number of errors is reached by the three

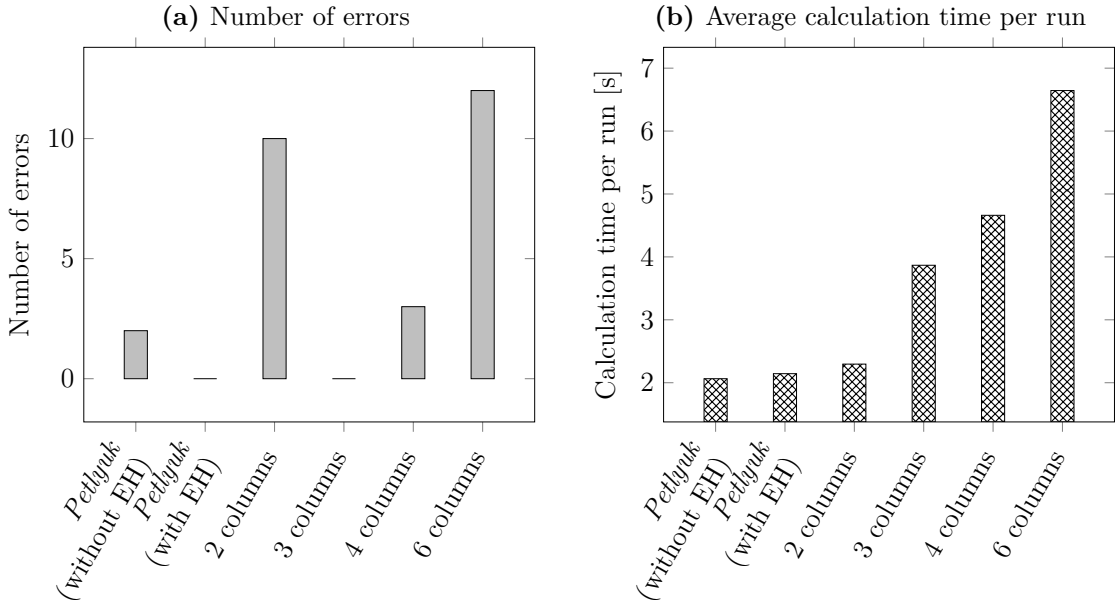

Figure 3.1: Comparison of different flow-sheet implementations of a dividing wall column in Aspen Plus: Results for 198 randomized simulations (EH = error handler).

column model. Nevertheless, the calculation time increases continuously with increasing column numbers and thus the three column model needs approximately double the calculation time as the *Petlyuk* model. Accordingly, it is decided to implement an additional error handler (EH) in the VBA code of *Petlyuk* model interface. The code of

this error handler can be found in the supporting material [62]. It is briefly described in the following paragraph.
The error handler works as follows. In case of a non-convergent run, in a first step the total number of iterations to evaluate the simulation is manually increased to 600. As Aspen Plus has an internal limit of 200 iteration steps, a workaround is needed to be programmed in VBA. For this purpose, one variable, for example an internal flow between column sections, is multiplied with a factor of 1.001 and the new, only slightly changed parameter set is sent to Aspen. Then, a simulation can be run witch applies again 200 iteration steps. Afterwards, the variable is divided by 1.001 and thus set back to the original value. Then, again the inputs are sent to Aspen Plus and a simulation is run. Consequently, the number of iteration steps in increased to 600 instead of just 200. If this is not sufficient to reach convergence, the Aspen Plus internal solver of the *Petlyuk* Block is changed (path in Aspen Plus: Blocks - (Block name) - Convergence - Methods - Overall, either Standard, Sum rates or Newton).
The *Petlyuk* model in combination with the described error handler in VBA is then also used to simulate the simulation sequence with 198 random variable sets. The corresponding results are also shown in Figure 3.1. The *Petlyuk* model with error handler solves all 198 simulations successfully without error while maintaining the comparably low calculation time of the model without EH. Accordingly, the *Petlyuk* model in combination with the error handler is used as model for all simulations in this work. Similar observations are made for the implementation of a multiple dividing wall column. Accordingly, these results are not shown here.
The final code used for the data exchange through the interface for the simple and multiple dividing wall column can be found in the supporting material [62]. A graphical visualization for the simple dividing wall column can be found in the appendix in Figure A.3. It is visible that several variables have to be transformed, which avoids that infeasible inputs are sent to Aspen Plus. This concerns the stage allocation and the liquid and vapor split at the dividing wall. As the standardization procedure might be relevant for some of the results, it is explained in more detail in the following paragraph for a simple dividing wall column.
The required input for the *Petlyuk* model is the total stage number of the main column (C11-C14 from Figure 2.2a) and of the prefractionator (C21-C22 from Figure 2.2a). These columns are then thermally coupled by inserting the stage numbers at which streams enter and leave one of the two columns. Also the flow of the coupling streams has to be inserted as absolute quantity. Consequently, during the optimization it could on the one hand happen that the coupling stages are entered in a wrong order or on the other hand that the absolute flow of a coupling stream is larger than the one available. Both problems cause non-convergent runs and are avoided by the parameter transformation done in the VBA code. Thus, instead of specifying the stage numbers as required for Aspen Plus, they are specified for each section individually. Then, in the VBA code they are translated to the Aspen Plus notation and sent as inputs. Additionally, the *Petlyuk* model requests temperature estimations on the top and bottom stage of each column. These are calculated from the boiling points of the components assuming a linear temperature profile inside the column. Last, the vapor and liquid split

are inserted in Excel as relative values defined as the flow on the right/product side of the dividing wall divided by the total flow that is split. In Aspen Plus the absolute coupling flow is needed as input. This is then calculated by multiplying the split ratios with an estimated total flow that is split. The total flow that is split is approximated based on the reboiler duty, the enthalpy of the bottom stream for almost pure products and mass balances assuming constant molar flows. The enthalpy used for each system is listed in the supporting material [62]. The use of relative vapor and liquid split fraction is needed in order to guarantee that the absolute flows inserted in the simulation do not exceed the available amount of vapor or liquid. However, these vapor and liquid splits are only estimated values based on the given assumptions. The actual vapor and liquid splits are calculated after the simulation has converged successfully based on the used absolute coupling flows and the resulting column profiles. All values of liquid and vapor split ratios shown in this work are the actual split ratios and not the estimated ones.
Summarizing, the stage number in all sections and the estimated relative split ratios are the variables that are actually inserted in the Excel sheet. The VBA code transforms the variables to the Aspen Plus notation and inserts them in the flow-sheet simulator. A similar transformation is done when data is read from Aspen and written into the Excel sheet.

3.2 Multi-objective optimization

Prior to the optimization itself, an initial converging simulation in Aspen Plus is required. Especially the definition of the vapor and liquid splits at the dividing wall(s) is challenging to reach convergence. For this purpose, $\dot{V}_{min}$ diagrams are applied [63]. In order to enable a fast calculation of $\dot{V}_{min}$ diagrams for different column types and systems, a MATLAB code is implemented, which can be found in the supporting material [62].
However, especially for the multiple dividing wall column pilot plant, in some cases the method does not result in sufficiently high purities. The reason for this deviation is explained in Section 5.2.1. In the case of low purities, the optimization is much more time consuming and may not even find a solution. Accordingly, if too low purities result, the vapor and liquid splits are further adapted manually to end up closer to the desired specifications. Since a manual adjustment of the splits is inaccurate and time consuming, an extended approach to estimate initial splits with $\dot{V}_{min}$ diagrams is presented in Section 5.2.3.
The optimization problem itself is defined in the MS Excel file coupled to Aspen Plus, which is described in section 3.1. A multi-objective optimization problem is then solved as a sequence of single-objective problems applying the sandwiching algorithm. The solver used to solve single-objective problems is depending on the presence of integer variables. With integer variables, the MISQP solver is used [127], otherwise the NLPQLP solver [128]. The solvers consider constraints as penalty terms and are gradient-based, thus less convergence problems occur in the Aspen Plus simulations. The set up and programming of the optimization routine itself was not part of this

work as this was performed by the Fraunhofer ITWM. For more details about the implementation, the reader is referred to literature [23, 31].
As already discussed in Section 2.3.1 the sandwiching algorithm is only suited for convex Pareto-fronts and the gradient-based solvers show a tendency to get stuck in local optima before finding the global one. Correspondingly, often several multi-objective runs are performed using different initial simulation runs in Aspen Plus. The results of all runs are then merged and dominated solutions are sorted out. Thus, in some cases the distance between the Pareto-optimal data points might be irregularly resulting in deviations in the approximation quality.

3.3 Screening

A screening is performed to determine all liquid and vapor splits in dividing wall columns leading to certain product specifications for different column designs. The following procedure is the foundation of all calculations presented in Section 5. For the calculation also the interface described in section 3.1 is used. A VBA code is applied to automatically perform a series of simulation runs. The code is slightly differing depending on the column type, thus in the following first the code for the simple dividing wall column is presented followed by one for the smDWC.

Simple dividing wall column

For the simple dividing wall column, the code basically performs the following steps. Note that the full version of the code can be found in the supporting material [62].

```
' Set min and max values of R_V,r,est and R_L,r,est and Q
Q = Q_min
Do While Q <= Qmax
       R_V = R_V,min
       Do While R_V <= R_V,max
              R_L = R_L,min
              Do While R_L <= R_L,max
                     Send R_V and R_L and Q to Aspen Plus
                     Run Aspen Plus Simulation
                     Read and save corresponding purity outputs
                     R_L = R_L + stepsize(R_L)
              Loop
              R_V = R_V + stepsize(R_V)
       Loop
       Q = Q + stepsize(Q)
Loop
```

A grid of specified combinations of the liquid and vapor split and the reboiler duty is screened. For this purpose the minimum and maximum values of the screened variables

and the number of steps are specified by the user.The objective when choosing these variables is to map split ranges resulting in the specified purities with a sufficient accuracy while still requiring an acceptable calculation time. All resulting combinations are then run automatically one after another. The resulting product purities are saved in the Excel sheet. After finishing all runs, the results are filtered according to the desired product purities.
Usually two of this kind of runs is performed. The first run screens most of the feasible range (given by the standardization of the splits) and the second run should enhance the resolution of the results in a smaller range, if desired. Accordingly, in the first run the minimum value of the liquid split is set to 0.2 and for the vapor split to 0.15. The liquid split is set to a higher value since low values can cause convergence problems in Aspen Plus due to the liquid side draw of the column. The maximum value is usually set to 0.9 for both splits. The range of the reboiler duty is chosen according to optimization results. The number of steps is always set to be 12, accordingly 1728 data points are calculated. From the parameter ranges and the number of steps the step size of the three screened variables is calculated. The split ranges used for the second run are based on the results of the first run. Accordingly, they are only screened in the range where the desired product purities can be reached. Afterwards, another macro is run which determines the resulting ranges of the splits for a two-dimensional plot.

Simplified multiple dividing wall column

For the simplified multiple dividing wall column four splits have to be varied which results in a more complex grid of the screening and thus higher calculation time (days up to weeks). Accordingly, the energy input could no more be included as screening variable. Despite this fact the automated screening is performed similar to the one of the simple dividing wall column. An abstracted version of the code is shown in the following, the full code can be found in the supporting material [62].

```
' Set min and max values of R_V,C1C3,r,est and R_V,C1C2,r,est and R_L,
   ↪ C1C2,r,est and R_L,C2C3,r,est
R_V1 = R_V1,min
Do While R_V1 <= R_V1,max
       R_V2 = R_V2,min
       Do While R_V2 <= R_V2,max
              R_L1 = R_L1,min
              Do While R_L1 <= R_L1,max
                     R_L2 = R_L2,min
                     Do While R_L2 <= R_L2,max
                            Send R_V and R_L and Q to Aspen Plus
                            Run Aspen Plus Simulation
                            Read and save corresponding purity outputs
                            R_L2 = R_L2 + stepsize(R_L2)
                     Loop
                     R_L1 = R_L1 + stepsize(R_L1)
```

```
            Loop
            R_V2 = R_V2 + stepsize(R_V2)
        Loop
        R_V1 = R_V1 + stepsize(R_V1)
Loop
```

Due to the higher number of screening variables, the number of steps is reduced to eight instead of 12 for the simple dividing wall column. Correspondingly, around 4096 simulations are run for one screening set. The ranges of the splits are chosen similar to the procedure of the simple dividing wall column stated above. Again usually two runs are performed to enable a sufficient resolution of the results. After finishing the screenings the results are again filtered according to the specified product purities. This data is either visualized directly in SOPPs (see Section 3.4) or further processed by another VBA code to enable a conventional two-dimensional visualization.

3.4 Data visualization and standardization

This section summarizes several methods applied for visualization, standardization and evaluation of the results.

Visualization of high-dimensional results

Self-organizing patch plots are used for the visualization of high-dimensional data. The diagrams are calculated in MATLAB®. First, the code by Azzopardi [129] is applied to calculate self-organizing maps. Afterwards, the maps are combined with Voronoi patches resulting in the final SOPPs, this implementation was developed by Stöbener *et al.* [125]. The corresponding code can be found in the supporting material [62].
The MATLAB code is then extended with an user interface in AppDesigner which is shown in Figure 3.2. The user interface should simplify the exploration of the visualized solution space and enable the *a posteriori* selection of an operating point. In the interface the decision maker can select a result filtration. The first step is the specification of the upper and lower borders of one or several of the objectives. Then, in the SOPPs all data points which do not fulfill the restrictions are colored black. Also, an option can be activated enabling to click on one of the patches and get the underlying data set as output.

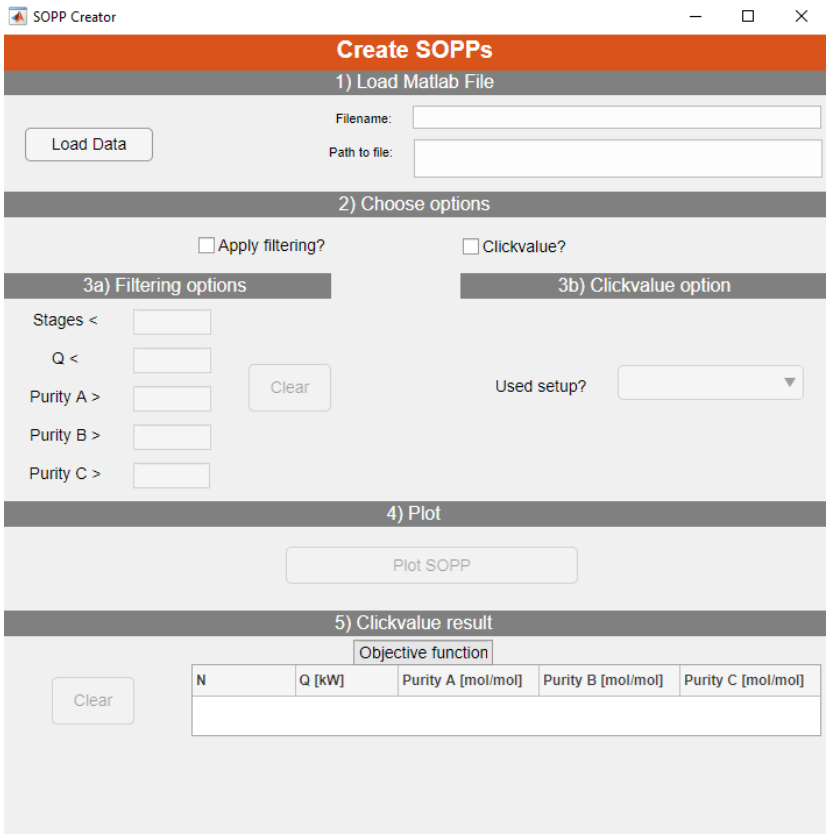

Figure 3.2: Interface for the creation and filtering of the SOPPs. As additional tool, one can click on one patch and get the underlying data as output.

Standardization of theoretical stages

For the visualization of optimization results in SOPPs, several stage specifications in the column sections of the dividing wall column have to be standardized. These are shown in Figure 3.3 for a simple dividing wall column. Also, the product flows are

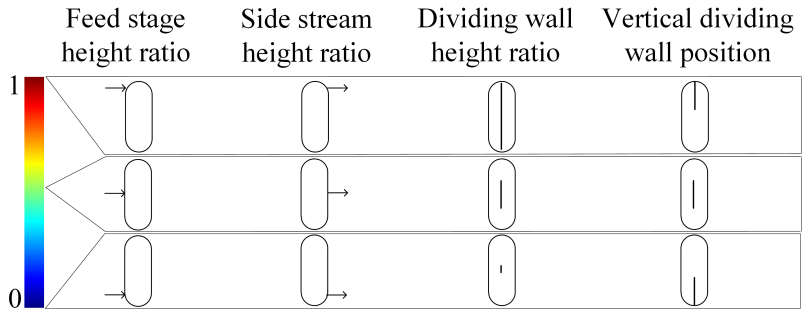

Figure 3.3: Standardized parameters used for dividing wall columns.

divided by the flows of the corresponding components in the feed stream. Accordingly, for example the distillate flow is divided by the flow of component A in the feed stream. Thus, a value of one means, that both flows are equal, above one the distillate flow is higher and vice versa. Note, that the standardized parameters are not exactly the optimization variables. During the optimization, the stages in all sections are varied

and not their standardized values, similar applies for the product flows. However, the numbers itself are not as important as their relation to each other. Accordingly, the standardized relations are visualized and not the absolute numbers.
For the vapor and liquid split ranges another stage standardization is relevant. The relative stage number n describes the ratio of the theoretical stages to the minimum one as shown in Equation 3.1. The parameter can be understood as distance from the minimum stage number, which is reached at $n = 1$.

$$n_i = \frac{N_i}{N_{min,i}} \tag{3.1}$$

i can either represent a column sections (for example $i = C12$) or a column region performing one split (for example $i = AB$, see Section 2.1.3.1 for more details). The factor can also be applied for a whole column or column sequence ($i = column$). Note that in this case the minimum stage number of the column setup j is denoted and calculated according to Equation 3.2.

$$\begin{aligned} n_{column} &= \frac{N_j}{N^j_{min}} \\ N^j_{min} &= \Sigma N_{min,i} \\ N^j &= \Sigma N_i \end{aligned} \tag{3.2}$$

A less commonly used standardization is the ratio m_i which describes the stages in one column section in relation to the total one (Equation 3.3). It can be understood as parameter describing the stage allocation inside the column sections.

$$m_i = \frac{N_{Ci}}{\Sigma N_{Ci}} \tag{3.3}$$

Energy saving quantification

In order to quantify the energy saving of one setup compared to another at the same stage number the energy saving E^j_i is introduced which is defined according to Equation 3.4.

$$E^j_i = \frac{\dot{Q}^i_{opt} - \dot{Q}^j_{opt}}{\dot{Q}^i_{opt}} \tag{3.4}$$

3.5 Systems used for case studies

Four ternary and six quaternary systems are chosen for the case studies in this work. In any case, the feed stream is assumed as saturated liquid (thermal state $q = 1$) and the composition is in most cases equimolar. This composition is chosen in order to be as neutral as possible towards the evaluated distillation variants. However, as stated Section 2.1.1 the dividing wall column is assumed to require the lowest energy demand

in any case. In Section 2.1.1 it is also mentioned that the energy saving can differ, if the ratio of one component in the feed stream is higher, thus feed variations are performed in sections 4.4.2.3 and 5.4. The corresponding compositions of the feed stream are then given in the related paragraphs. All test systems are summarized in Table 3.1. The

Table 3.1: Systems used for case studies.

Name	Component A	Component B	Component C	Component D
3.1	Benzene	Toluene	*p*-Xylene	–
3.2	Hexane	Heptane	Octane	–
3.3	Methanol	Ethanol	*n*-Butanol	–
3.4	*n*-Butane	2-Methylbutane	*n*-Pentane	–
4.1	Ethanol	*n*-Propanol	Isobutanol	*n*-Butanol
4.2	Methylacetate	*n*-Propanol	Isobutanol	*n*-Butanol
4.3	Butanal	*n*-Propanol	Isobutanol	*n*-Butanol
4.4	Methylacetate	Butanal	*n*-Propanol	*n*-Butanol
4.5	Methylacetate	Butanal	*n*-Propanol	Isobutanol
4.6	Benzene	Toluene	*p*-Xylene	Cumene

feed stream properties including the flow, composition and the K-values of all systems is summarized in Table 3.2. As already mentioned, the thermodynamic modeling of all

Table 3.2: Properties of feed streams for equimolar cases and $q = 1$.

System	$\dot{F}$ $\left[\text{kmol} \cdot \text{h}^{-1}\right]$	z_i [–]	K_A [–]	K_B [–]	K_C [–]	K_D [–]	ESI_{ABC} [–]	ESI_{BCD} [–]
3.1	3	$0.\overline{33}$	1.91	0.73	0.33	–	1.08	–
3.2	3	$0.\overline{33}$	1.79	0.87	0.34	–	0.82	–
3.3	3	$0.\overline{33}$	1.79	0.99	0.21	–	0.39	–
3.4	3	$0.\overline{33}$	1.84	0.65	0.5	–	2.15	–
4.1	0.1	0.25	1.96	0.94	0.65	0.45	1.44	1.01
4.2	0.1	0.25	2.87	0.56	0.35	0.22	3.28	1.00
4.3	0.1	0.25	1.93	0.90	0.67	0.50	1.59	1.00
4.4	0.1	0.25	2.34	1.00	0.45	0.20	1.05	0.99
4.5	0.1	0.25	2.27	0.99	0.42	0.32	0.96	1.81
4.6	0.1	0.25	2.30	0.98	0.42	0.29	1.02	1.57

systems is based on NRTL, details about the corresponding parameters can be found in the appendix in Section A.2.1.
The main reason for the choice of the ternary systems are their $\dot{V}_{min}$ diagrams which can be found in Figure 3.4. For system 3.1 and 3.4 the CD peak is significantly higher than

AB. The difference between these two is the minimum stage requirement. For system 3.1 almost the same stage number is required to split AB and BC, this is indicated by an ESI close to one. For system 3.4 the BC split requires more stages, which is reflected by the high ESI of the system. The $\dot{V}_{min}$ peaks of system 3.2 are almost the same and for system 3.3 the AB peak is the highest one.

Most quaternary systems are chosen based on the recommendation of suited systems

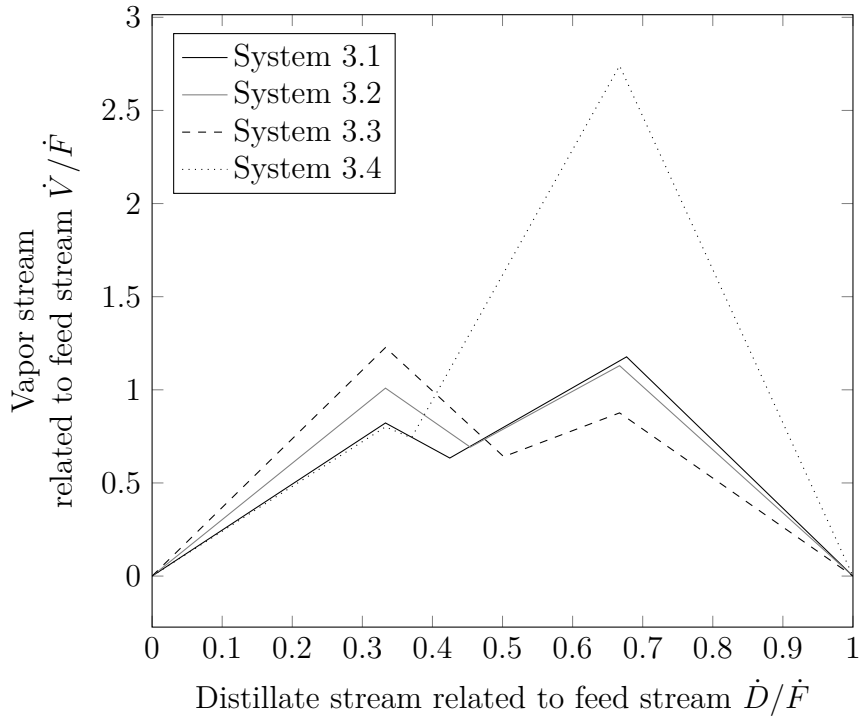

Figure 3.4: $\dot{V}_{min}$ diagrams of the ternary case study systems.

for the multiple dividing wall column pilot plant presented by Preißinger *et al.* [22]. Accordingly, also the feed flow is chosen as suggested in the latter cited paper to be $\dot{F} = 100\,\mathrm{mol} \cdot \mathrm{h}^{-1}$. Additionally, system 4.6 is chosen as extended version of system 3.1 with a fourth component. The $\dot{V}_{min}$ diagrams of the quaternary systems are presented in Figure 3.5. Based on the fact that systems 4.1 to 4.3 only differ in the light boiling component, their $\dot{V}_{min}$ diagrams are relatively similar. System 4.4 shows the lowest energy demand of all quaternary systems. System 4.5 and 4.6 have a very similar behavior with a BC peak lower than AB, which is also reflected by the ESIs of these systems.

Note that in the following result sections most calculations for ternary systems assume product purities of 95 mol %, while for most quaternary system calculations 98 mol % are used. This discrepancy can be explained with external conditions. 95 mol % were chosen in an early project phase of the author of this work. For quaternary systems, purity requirements were set later by Preißinger [22], who was responsible for the design of the pilot plant (Section 2.1.2), to 98 mol %.

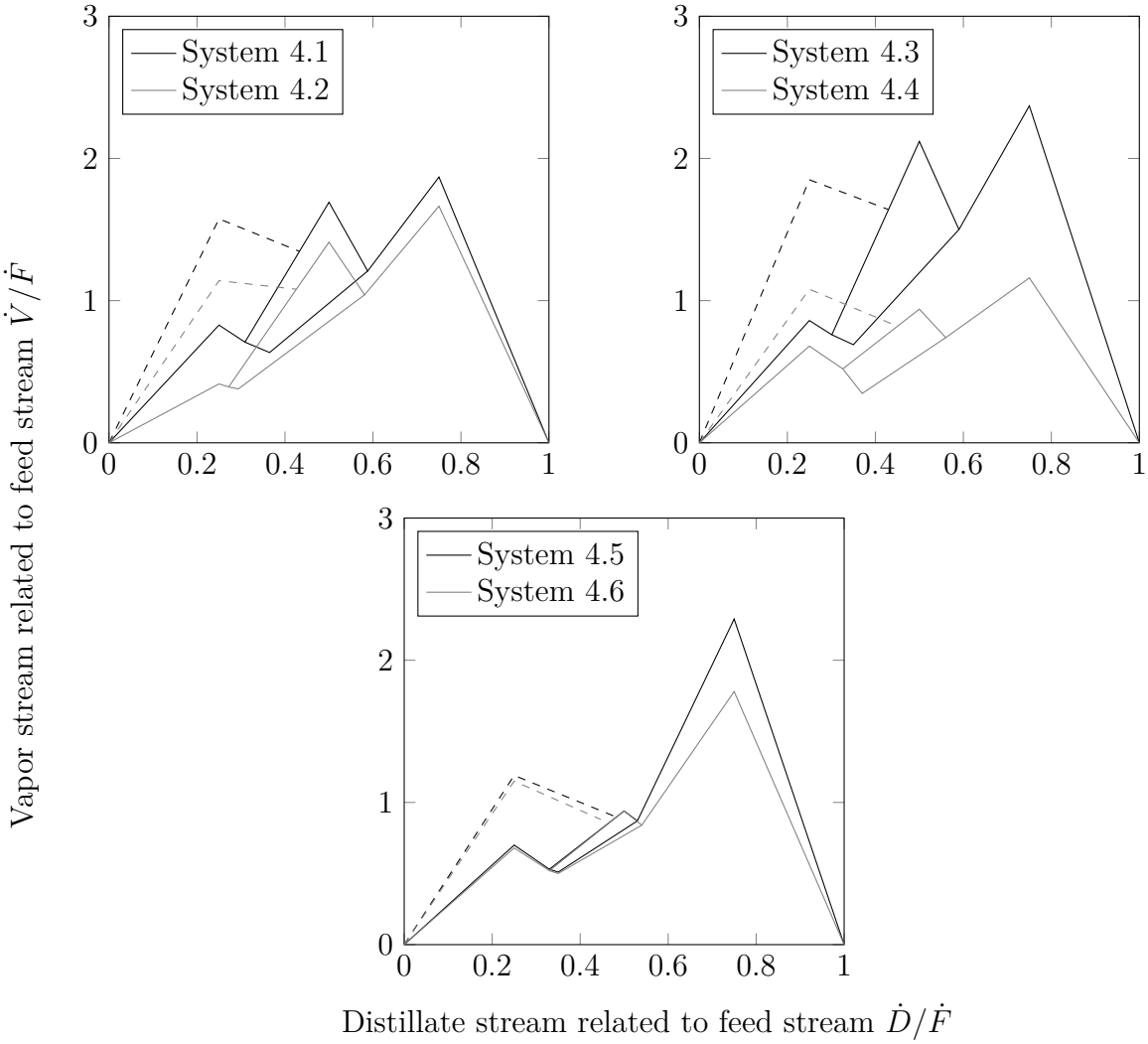

Figure 3.5: $\dot{V}_{min}$ diagrams of the quaternary case study systems. Dashed lines in indicate the adaptation of the diagram for the simplified version of the multiple dividing wall column.

4 Results part I: Multi-objective optimization

In this chapter multi-objective optimizations of different column configurations are performed as described in Section 3.2. The goal is to obtain a full understanding of the optimal space and the related variable sets. In any case two of the objective functions are the reboiler duty $\dot{Q}$ and the sum of the theoretical stages in all sections ΣN_{Ci}, which is for simplicity reasons sometimes only denoted as N. First, a large part of the optimal solution space is calculated by including the product purities as objectives in Section 4.1. Note that the term large is used and not whole for two reasons. First, the part of the solution space with very low product purities is neglected because it is assumed not to be relevant. Second, in order to still maintain convergence in Aspen Plus, some of the variables like the vapor and liquid splits could not be varied in the whole feasible range but only in a large part of it. Correspondingly, probably only a large part of the solution space is calculated and not the whole one. Afterwards the bi-objective subspace resulting in compromises between N and $\dot{Q}$, the so called $N\dot{Q}$ curves, are investigated further. The main objective of the corresponding Section 4.2 is to evaluate the impact of the initial optimization problem definition on the results. Then, an approximation method for $N\dot{Q}$ curves as shortcut approach is developed and presented in Section 4.3. Last, this approximation method is used in combination with full optimizations to evaluate the energy saving potential of different kinds of dividing wall columns compared to column sequences in Section 4.4.
Please note that each optimization is assigned a number, under which the corresponding initial simulations, the definition of the optimization problem and its solution can be found in the supporting material [62]. A brief summary can be found in the appendix in Section A.4. The run number corresponding to a data set is always given in brackets in the legend or caption of each diagram. It is always build according to the principle "Opt531", where the first number defined the number of objectives, the second number the number of components and the following numbers are identification numbers.

4.1 Large part of solution space

The optimization problem of distillation columns is complex and its solution is significantly affected by its initial definition. Usually several assumptions are made prior to the optimization to reduce the solution space in advance. However, this basically excludes a part of the results which is not known. Thus the objective of this section is to present an approach to calculate most of the solution space which enables an *a posteriori* investigation of the results after the optimization. Accordingly, the optimization results can be analyzed several times from different points of view without the need of an additional calculation run. The foundation of this approach is to consider

more than just two objectives, thus include the product purities, energy demand and total number of theoretical stages.
In the following Section 4.1.1 the optimization procedure is performed for a ternary system split in a simple dividing wall column. For this system five objective functions result, thus this problem is called penta-objective. Afterwards, the split of a quaternary system in the pilot plant of a simplified multiple dividing wall column (see Section 2.1.2) is optimized in Section 4.1.2. Since this column already has a defined number of theoretical stages in the sections, the number of theoretical stages is no more an objective function. Consequently, with one more component in the feed stream this is also a penta-objective problem.
Obviously the visualization of this five-dimensional objective space is an issue, which is solved with self-organizing patch plots (see Section 2.4.1). This technique has the additional advantage, that not only the objectives but also the optimization variables can be presented in one diagram with several subplots. Accordingly, the visualization of all degrees of freedom of the column is enabled, which is often omitted.

4.1.1 Dividing wall column

For system 3.1 the penta-objective optimization is performed [107]. As objectives the total stage number, the reboiler duty and the purities of component A in the distillate, B in the side draw and C in the bottom product are specified. The optimization variables are the vapor and liquid splits, the product flows of distillate and side product, the number of stages in all column sections and the reboiler duty. Note that the reboiler duty and the stage numbers have to be defined as objectives and variables. This problem arises from the variable definition in Aspen Plus. The two parameters are required as input for the simulation and thus have to be varied and optimized simultaneously. Figure 4.1 presents the resulting optimal space in SOPPs. Note that the legend definition is presented in Figure 3.3 in Section 3.4. The first row of plots represents the objectives and the following two rows the corresponding optimal variables. First of all, it can be seen that the objectives show high values in different regions of the subplots, which again underlines their contradicting nature. Especially N and $\dot{Q}$ are clearly contradicting. The impact of the optimization variables on these two objectives is investigated in more detail in Section 4.2 and thus the focus here is on the resulting product purities. Even though the product purities are high in different regions of the subplots, there are overlapping regions in which all of them can be obtained in high purity. For simplification of the data analysis the patches are filtered according to the product purities. Either component A, B or C are specified to be above 95 mol %. The filtered patch plots can be found in the Figures 4.2, 4.3 and 4.4, respectively.

The liquid and vapor splits resulting in the optima are roughly in the range predicted by the $\dot{V}_{min}$ method. If a lower vapor split is used, the corresponding liquid split is also lower and vice versa. It should be noted that not only one combination of the liquid and vapor split results in one optimum patch. Consequently a set of vapor and liquid splits results in a flexibility of the optimization variables which result in the same

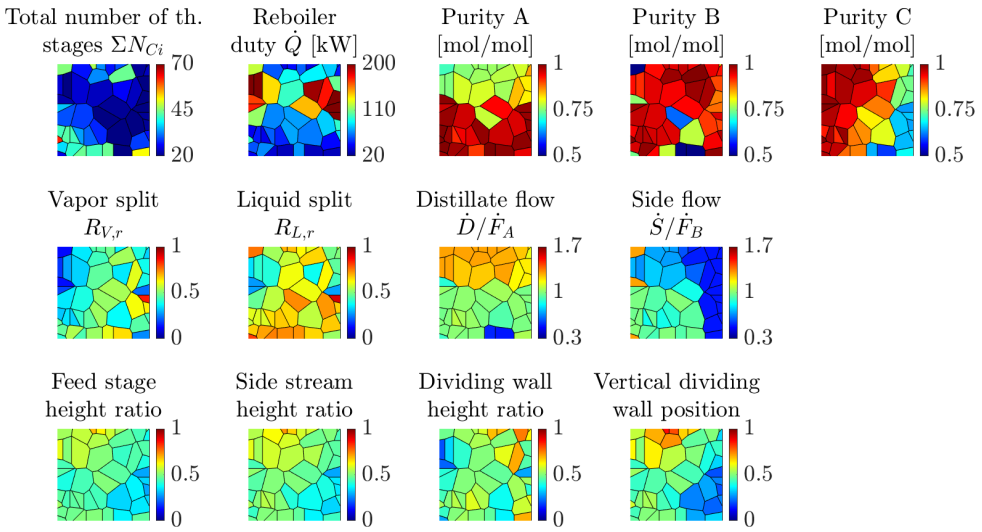

Figure 4.1: Results of penta-objective optimization of system 3.1 in dividing wall column in SOPPs (Opt531).

optimum output. This topic has been introduced in the theory sections 2.1.3.1 and 2.2. Additionally, it is discussed in more detail in the second result part in Section 5.
A clear impact of product flows on the product purities is observable. This is illustrated by an example. In the upper left region of the subplots component A has a low purity, accordingly in the corresponding single-objective runs the weighting factor for the purity of component A was significantly lower than for B and C. As a consequence, the distillate stream related to the feed stream of component A is increased above one (orange color in subplot eight) and the side product stream is reduced. Accordingly, the distillate flow is contaminated with component B and the purity of A is reduced. On the other hand, this guarantees that no component A is in the side product and thus B is obtained in a higher purity. This principle applies for all product flows. However, while the distillate and bottom flows are most likely only contaminated with one component, the side product stream can contain impurities of two. Thus, it can be observed that for many Pareto-optimal points the side product flow related to the feed stream of component B is reduced below one. This applies to all data points where component A, B and C are obtained in approximately the same purity and where these purities are below one. As a consequence the distillate of bottom flow of the column are increased. If the distillate or bottom stream is higher depends on the system (observed in Section 4.4.2).
Also the optimum stage allocation for different cases can be read. At higher total stage numbers, the allocation stays at the initially used uniform distribution (last row of subplots, patches in lower left corner). At lower total stage numbers the allocation of the stages in the column sections gets more important and thus deviations from the initial setup are observable. For component A at higher purities (Figure 4.2) blue patches dominate in the plots of feed and side stream height ratio and vertical dividing

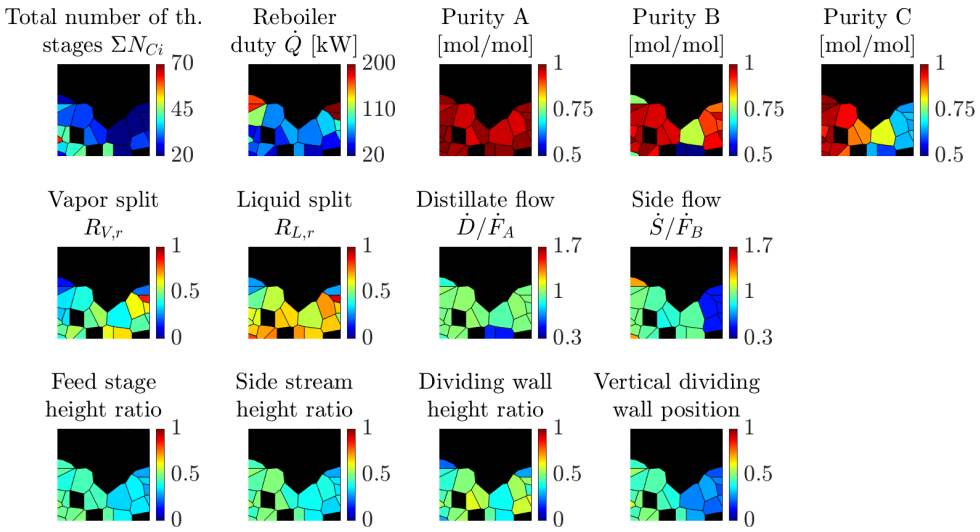

Figure 4.2: Results of penta-objective optimization of system 3.1 in dividing wall column (Opt531): Purity A above 95 mol %.

wall position. Accordingly, more stages are provided for the AB split performed in the upper column region. An opposite effect is observable for component C (Figure 4.4). Generally, for components A and C in high purity the dividing wall height ratio shows a less distinguished trend, but interestingly for both the dividing wall appear to be rather short. This can be explained with the fact, that the AB and BC splits are performed in two sections, from which one has less vapor than the other due to the vapor split at the dividing wall. For the BC split, section C14 is operated at the full vapor amount and C13 at a reduced one, for AB C13 is the reduced and C11 the full one. Thus, if the dividing wall is shortened, the total stage number for the AB and BC split can be maintained, the region with less vapor are minimized and simultaneously the product purities maximized. Meanwhile, it still has to be guaranteed that the sections C21 and C22 have sufficient stages and vapor to prevent component A to reach the bottom of the column. However, the AC split always requires less energy and stages than the AB and BC splits. For component B having a high purity in the side product stream no clear trend for the feed and product stream stage height ratios and vertical dividing wall position is observable. However, it gets clear that a longer dividing wall (higher value of vertical dividing wall height ratio) is beneficial. Generally a notable fact is that the feed and product stage height ratio are always close 0.5 and thus are less sensitive to product stream specifications than the dividing wall height ratio and its vertical position. Summarizing, it can be concluded that all optimization variables have a notable impact on the resulting product purities.

To illustrate the superiority of SOPPs compared to a conventional visualization techniques, the results from Figure 4.1 are also presented in a conventional radar chart in Figure 4.5. The chart is quite convoluted and difficult to interpret. Even though the line orientation indicates that the number of stages and reboiler duty are

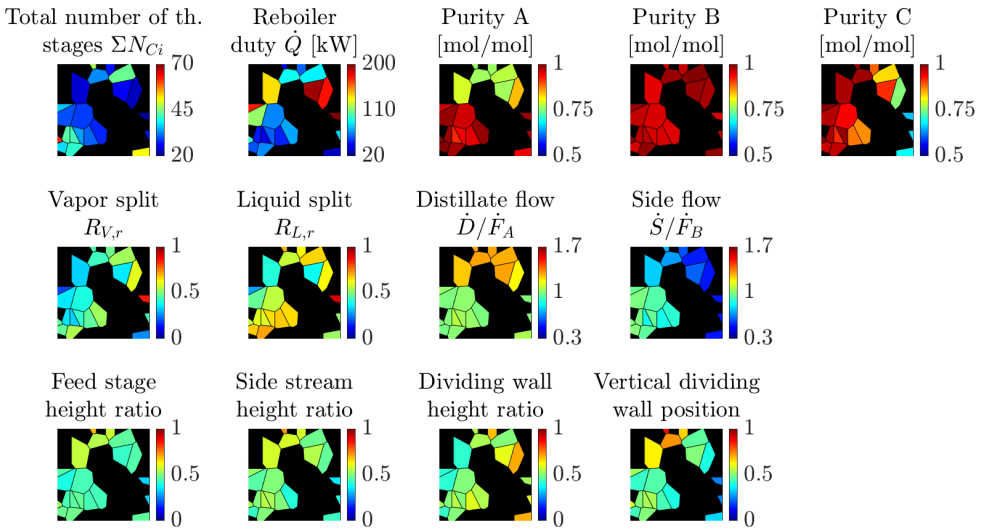

Figure 4.3: Results of penta-objective optimization of system 3.1 in dividing wall column (Opt531): Purity B above 95 mol %.

contradicting functions, the interaction of the optimization variables is almost impossible to understand. Thus, the visualization in SOPPs are better suited for the interpretation of the results.

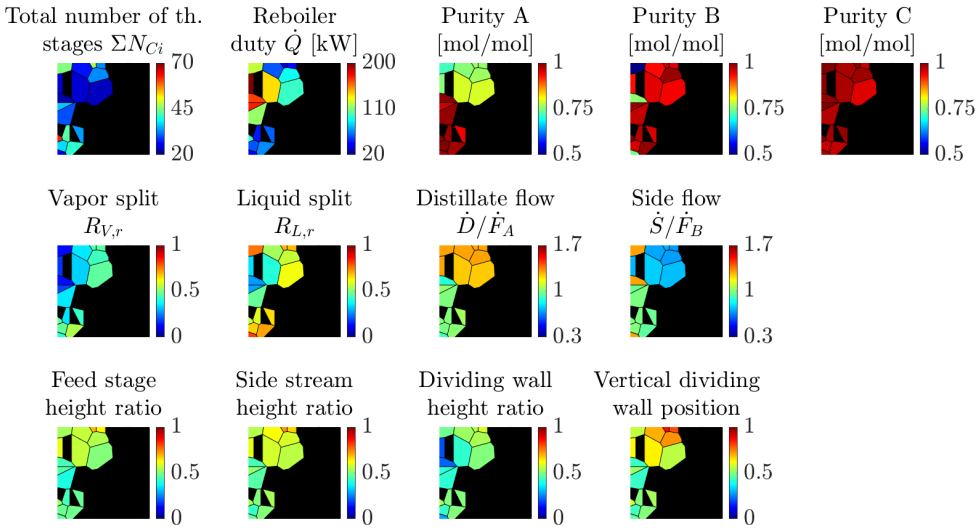

Figure 4.4: Results of penta-objective optimization of system 3.1 in dividing wall column (Opt531): Purity C above 95 mol %.

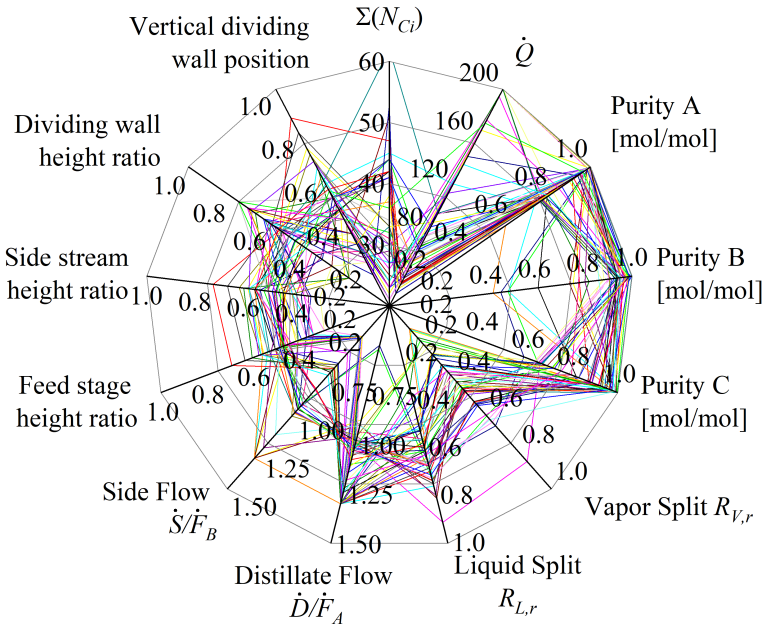

Figure 4.5: Results of penta-objective optimization of system 3.1 in dividing wall column in radar chart (Opt531).

4.1.2 Pilot plant of simplified multiple dividing wall column

For the simplified multiple dividing wall column pilot plant the stage allocation is already given (see Section 2.1.2). Accordingly, the multi-objective optimization problem no more includes the integer variables for the theoretical stages in all column sections. The resulting problem is also penta-objective and considers two vapor splits, two liquid splits and the product flows as optimization variables. The results of the penta-objective optimization are shown in Figure 4.6.

It is observable that the vapor and liquid splits to column C2 can be chosen in a

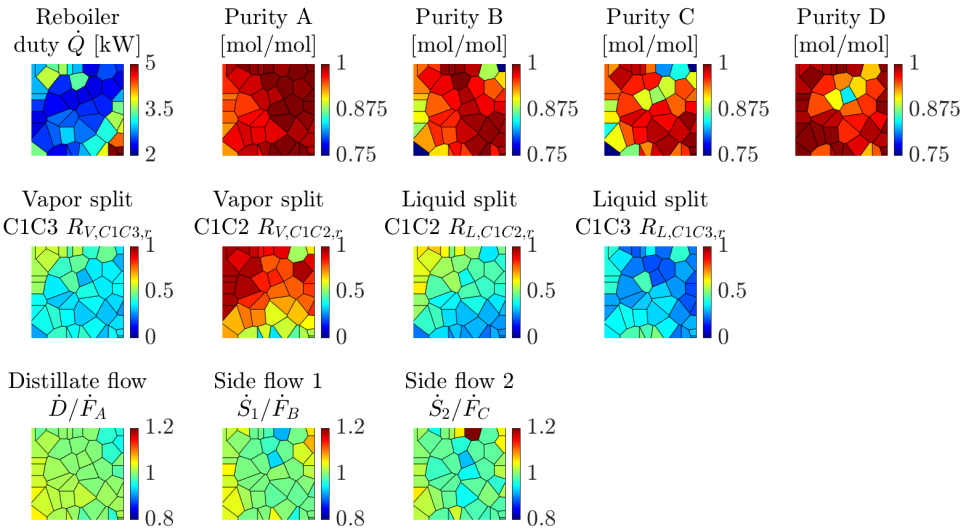

Figure 4.6: Results of multi-objective optimization of system 4.1 in simplified multiple dividing wall column for 220 stages in total (Opt541).

relatively broad range while the splits to column C3 are more limited. However, again several combinations of these splits can result in the same energy demand which is discussed in more detail in Section 5. Additionally, similar as for the ternary system in a simple dividing wall column in Section 4.1 the product purities are partly adapted by the chosen product flows. For purer side products the side flows are reduced. It is observable that the side product flow 2 is reduced stronger than side draw 1 (more patches in darker blue). Probably this behavior is a compensation of missing stages in certain column sections. By implication a stronger flow reduction also means, that the purity of component C limits the process. This statement can be verified by reading the minimum energy required to obtain the four products in certain purities. Since the column should reach product purities of at least 98 mol %, the following discussion focuses on the data fulfilling this specification. The evaluation is performed with the data filtration tool presented in Section 3.2. However, the filtered SOPPs are not shown here but the most important conclusions from the diagrams are summarized.

The components A, B and D can be obtained at purities above 98 mol % at $\dot{Q} = 2.3$ kW, which equals the lower border of the variable during optimization. Note that an even lower value of the reboiler duty could have caused instability of the simulation and

thus no repetition was performed with a reduced lower border. However, the minimum energy demand for component C to reach that purity is higher at around 2.7 kW, which equals the overall energy demand for all components at that purity. From this it can already be concluded that component C actually limits the energy demand of the column.
A clearer distinction for the limitation order of the other components can be made considering the purities to be at least 99.8 mol %. The energy demand for each component is as follows: $\dot{Q}_{min}(x_A^{\dot{D}} \geq 0.998) < 2.3\,\text{kW}$, $\dot{Q}_{min}(x_B^{\dot{S}_1} \geq 0.998) < 3.4\,\text{kW}$, $\dot{Q}_{min}(x_C^{\dot{S}_2} \geq 0.998) = 5\,\text{kW}$, $\dot{Q}_{min}(x_D^{\dot{B}} \geq 0.998) = 3.0\,\text{kW}$. Note that the energy demand for component A and B might be slightly lower since the purities were in both cases above 99.9 mol %.
All in all, it can be concluded that component C is limiting the process, followed by component B and D. Even though an adjustment of the product flows reduces the limitation, it cannot be totally avoided. Probably this behavior is supported by the chosen allocation of the theoretical stages. The results from the following Section 4.2.2 show, the BD split requires significantly more theoretical stages than the AB split. If these stages are not provided, the limitation of the CD split gets more pronounced as it is observed here.
At this point, a transition can be made to the following chapters. There, only bi-objective optimizations minimizing N and $\dot{Q}$ while using constraints on the product purities are performed. In most cases, the same constraints are used on all product purities simultaneously. This assumption equals optimal points from the penta-objective optimizations, for which similar weighting factors (see Figure 2.6) are used for all product purities. Thus, if the same systems from this chapter are considered, the corresponding result of the constrained bi-objective optimizations can also be found in the SOPPs from Figure 4.1 or 4.6. As an example, in Figure 4.6 of system 4.1 one patch represents all products to be at least 98 mol %. A similar optimal point can be found in the following Section 4.2.2.2 in Figure 4.10. In both cases the corresponding optimal energy demand is at around 2.7 kW.

4.1.3 Transferability of the results to other mixtures

In the previous sections 4.1.1 and 4.1.2 a new multi-objective optimization approach for distillation columns has been introduced. However, the procedure was only presented using the example of two test systems. Thus, the question arises whether the results are universally valid or not. Generally, the objective of this chapter is to highlight the advantages of the approach to include more than just objectives. Like this, only one optimization run has to be performed for one mixture and the results can be evaluated several times depending on the needs of the user. For example, if the product requirements of an industrial plant change, the corresponding new minimum energy requirement can easily be read from the diagram without performing new calculation runs.
Nevertheless, general trends are assumed to be valid in any case which includes the

partly adjustment of product purities by changing the corresponding product flows. On the other hand, properties like the exact value for the energy demand corresponding to the total stage number is of course depending on the mixture itself. This part of the whole solution space presented is investigated in more detail in the following Section 4.2 for a larger set of systems.

4.2 Impact of optimization problem definition and simplification

Despite the definition of the objective functions also the optimization variables and constraints have to be chosen to optimize a dividing wall column. Often they are just set prior to the optimization and it is not questioned how the result could have been affected by their initial choice. However, based on the results from Section 4.1 it can be expected that their selection can affect the outcome of the optimization. Accordingly, the focus of this section is to perform optimizations with varying definitions of the optimization problem including the variables and constraints. The investigations are first performed for a simple dividing wall column in Section 4.2.1 in order to get a understanding of the parameter relations. Afterwards, the knowledge is used to simplify the complex optimization problem of a simplified multiple dividing wall column (Section 4.2.2).

4.2.1 Dividing wall column

System 3.1 is chosen for the investigation in a simple dividing wall column. In any case, the number of theoretical stages and the reboiler duty are minimized as objectives. For the optimizations, different variable simplifications and/or constraints are investigated. First, three optimizations are performed in which constraints are set on the purity of one of the components (A, B or C $\geq 95\,\mathrm{mol\,\%}$), respectively, while the product flows are set to $\frac{\dot{D}}{\dot{F}_A} = \frac{\dot{S}}{\dot{F}_B} = 1$ (Opt 231, 232 and 233). These results are compared to one run in which the same purity constraint is used for all three products simultaneously while the product flows are either still set to $\frac{\dot{D}}{\dot{F}_A} = \frac{\dot{S}}{\dot{F}_B} = 1$ (Opt234) or considered as optimization variables and thus varied (Opt 235). For an exact definition of the optimization problems, please refer to the appendix (Table A.8 in Section A.4) and supporting material [62].
Figure 4.7 shows the resulting $N\dot{Q}$ optima, the corresponding optimal variables can be found in the supporting material [62]. The location of the $N\dot{Q}$ optima shows obviously, that the intermediate boiling component B is limiting the process in both dimensions (Opt232). Component A is much easier to obtain in the specified purity in terms of energy demand and total stage number (Opt231), while component C shows an interesting behavior (Opt233). Its minimum stage number is almost identical to the one of component A, while its minimum energy demand matches the one of component B. Another fact that should be noted is observed from the optimization of component A at high stage numbers and lower purities. The energy demand to reach the specified

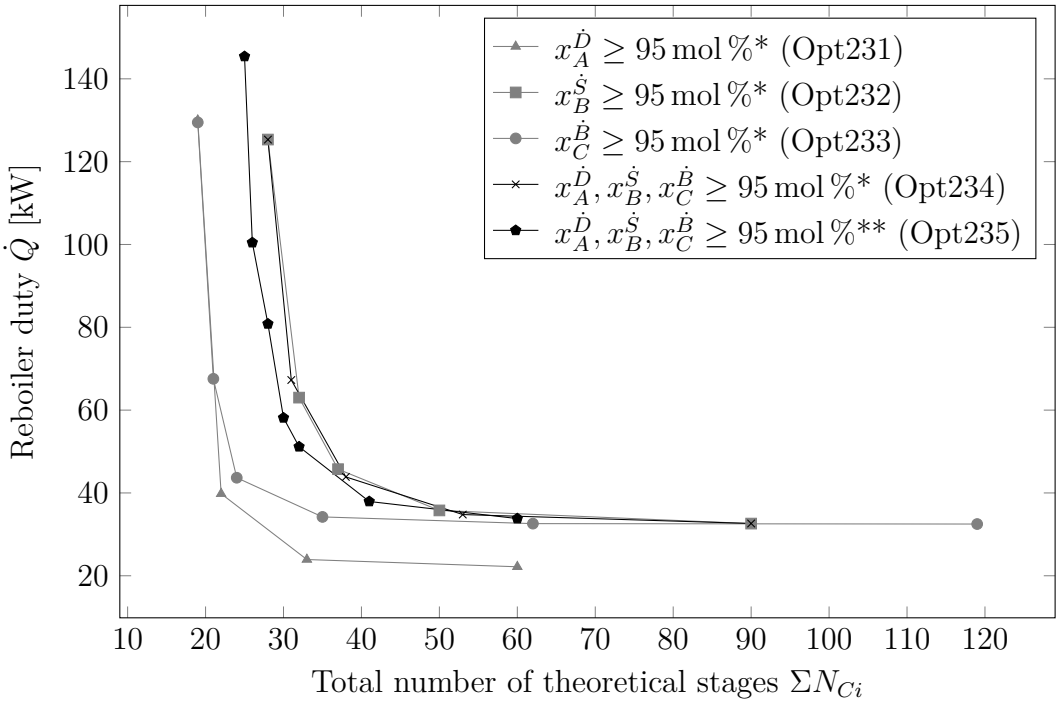

Figure 4.7: $N\dot{Q}$ optima for system 3.1 in a dividing wall column: Impact of product purity constraints and product flow setting. * Product flows set to $\frac{\dot{D}}{\dot{F}_A} = \frac{\dot{S}}{\dot{F}_B} = 1$, ** Product flows included as optimization variables.

purity is quite low and thus not much vapor is provided. Correspondingly, also low liquid flows are available inside the column. However, the side draw of the column is taken in liquid state. Thus, it has to be guaranteed, that a sufficient liquid flow is sent to the side draw stage of the column. In the case of a very low energy demand for the product split it can happen, that the reflux flow at the top of the column is already too low to enable a liquid side draw. This restricts the vapor flow inside the column to a minimum feasible value. Accordingly, for product splits with a very low energy demand the dividing wall column is not suited since it has to be operated above its minimum energy demand to enable a liquid side product. This is for example observable for component A of system 3.1 at purities below approximately 95 mol %. An alternative to avoid this problem would be the use of a vapor side draw.

The application of constraints on all three product purities while maintaining the same product flows results in an $N\dot{Q}$ curve lying totally on the one of component B (Opt 234). Accordingly, for set product flows the use of only one purity constraint on component B is sufficient for the calculation of optimal setups. However, the other two components are in most cases obtained in higher purities (not shown here, consider supporting material [62]). This can be explained with the fact that simply more energy or stages are provided than necessary and thus the purity increases as shown exemplary for component B in Figure 4.8a. In order to reach exactly the same purities in all product flows, the flows have to be included as optimization variables. Using restrictions on all three product purities while varying also the product flows (Opt235) results in a lower

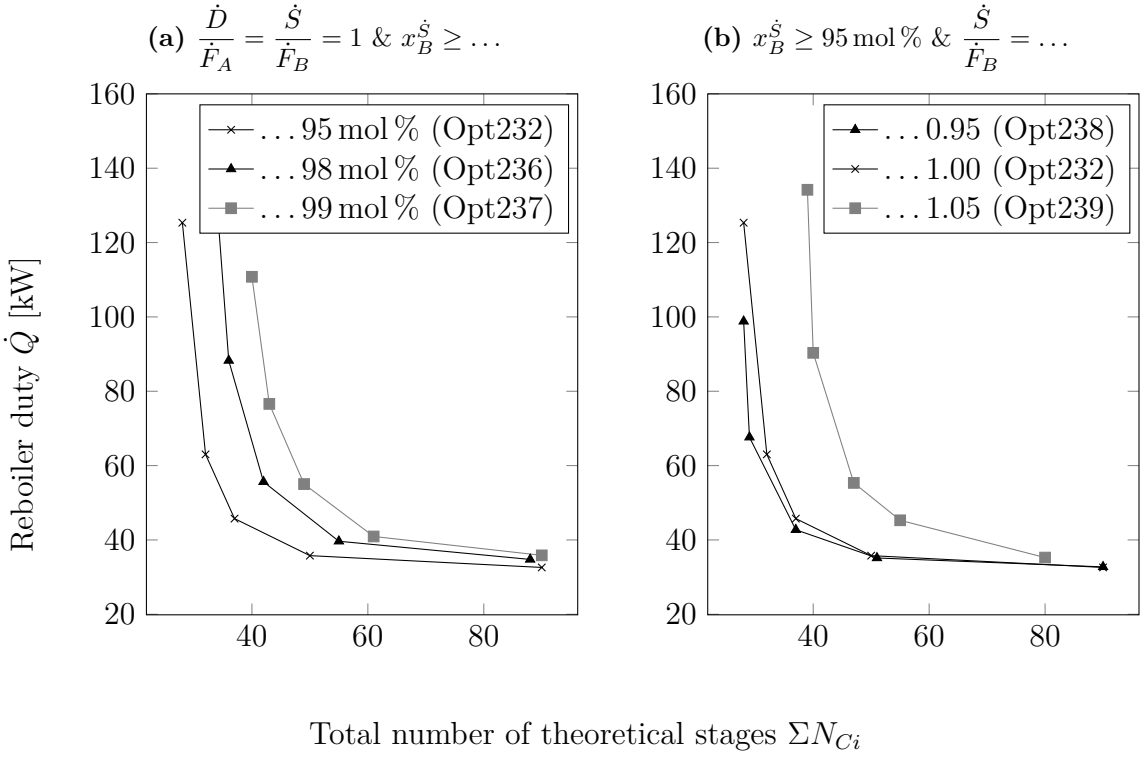

Figure 4.8: $N\dot{Q}$ optima for component B of system 3.1 in a dividing wall column: Shifts for different product flows and purity constraints.

minimum stage number than needed for component B only at non-optimally set product flows. This is caused by a decreased flow of the side product flow while the flow of the distillate and bottom are increased. The behavior is also shown in Figure 4.8b for the optimization with a constraint on component B only. Also, the curves of components A and C are shifted to the right and thus to a higher minimum stage number. This can be explained relatively easy. For a constrained purity of component A of course the sections C11 and C12 have a high number of theoretical stages while the numbers for section C13 and C14 are relatively low (see supporting material in [62]). Thus, the resulting purity of component C is quite low at around 70 mol % to 80 mol %. However, since component C is now also required in a higher purity, the stages in sections C13 and C14 have to be increased corresponding to the number needed component C. Vice versa applies for the $N\dot{Q}$ curve of component C being constrained.
Another interesting fact can be observed considering the optimal stages in the prefractionator for the different runs (not shown here, consider supporting material [62]). For component A being constrained, the optimum feed stage in the prefractionator is allocated in the upper region while for component C it is preferred to be in a lower region. Also the total stage number in the prefractionator is lower for component A than for component C. The average of the optimum stage allocations of component A and C almost equals the results of the optimization using a constraint on the purity of component B. The optimum feed stage is in the middle of the prefractionator.
Summarizing, the adjustment of the stage allocation in the column sections and the

product flows shifts the $N\dot{Q}$ curves of the three components to one at which all components can be obtained in the same purity. However, the adjustment of the product flows is only useful, if no high purities are needed. For high-purity products the product flows have to equal the flow of the corresponding component in the feed stream. Another fact that has to be noted is that the energy input for component A is also increased to an unnecessary high value. This, as also predicted by the $\dot{V}_{min}$ diagram, causes a flexibility of the vapor and liquid split during the operation of a dividing wall column which will be discussed in more detail in chapter 5.
If different purities than 95 mol % are required, the same effects occur. However, the $N\dot{Q}$ curves are shifted as shown in Figure 4.8a for component B at set product flow. Similar diagrams are obtained for components A and C. As expected, the Pareto-optimal curves shift to higher minimum stage numbers for higher purities. Nevertheless, the change in minimum energy demand at high stages number is relatively low. Thus, the curve is shifted more to the right than to the top when the purity constraints are increased.

Transferability of results

Again these calculations are only performed for one mixture. However, the transferability on other mixtures can be derived based on theoretical knowledge. Of course, absolute values of stage number and energy demand are different for different mixtures. However, the directions in which the $N\dot{Q}$ optima shift are expected to be still applicable. The results from Figure 4.7 are partly transferable. In any case it applies that the $N\dot{Q}$ optima of the side product is limiting the process (Opt232). Also, lower energy demands can be reached, if the product flows are considered as optimization variables (Opt235). The relative location of the $N\dot{Q}$ optima of component A (Opt231) and component C (Opt233) can differ according to the $\dot{V}_{min}$ diagram and ESI of the system. For the considered system the BC peak is the highest one, thus for component C more energy input is required than for A. If a system with a different $\dot{V}_{min}$ diagram is considered, the right end on the $N\dot{Q}$ optima would correspondingly be shifted. The trends from Figure 4.8 are assumed to be universally valid.

4.2.2 Simplified multiple dividing wall column

The full optimization problem to calculate the $N\dot{Q}$ optima of the simplified multiple dividing wall column consists of 18 variables, which results in a significant calculation time of several days. However, one run in which all variables are considered in order to minimize N and $\dot{Q}$ is performed and used as reference for all other runs (Opt245). Then, several simplified runs are performed to reduce the calculation time and obtain new insights into correlations. For this purpose, some of the variables are set and thus the total number of variables is reduced. In order to evaluate the effect of the chosen set variables and their values, the $N\dot{Q}$ optima of system 4.1 are calculated for several versions of the optimization variable set. For all runs, inequailty constraints are applied

on all four products to reach at least 98 mol % pure products. Section 4.2.2.1 focuses on the effect of given flow specifications and Section 4.2.2.2 on the impact of set stage allocations in the column sections.

4.2.2.1 Assumption of set internal or external flows

In Section 4.2.1 is was already observed that the $N\dot{Q}$ curves shift in dependence on the product flows. Accordingly, in this section it is investigated how significantly the optima shift for different product flows in a simplified multiple dividing wall column. Fixed product flows would reduce the number of optimization variables by three to 15. Additionally, the impact of the vapor splits set to 0.5 is tested. The value is chosen since the vapor splits are usually not controlled during the operation of a column and are rather resulting from the pressure drop on both sides of the dividing wall. Accordingly, for a centered dividing wall, a split ratio around 0.5 can be expected. Thus, the number optimization variables is reduced by two to 16. For the optimization runs again ΣN_{Ci} and $\dot{Q}$ are minimized while varying the stages in all sections and the liquid splits. For set product flows additionally the vapor splits are varied and for the optimization at set vapor splits the product stream are varied. For clarification of the optimization setup please consider the appendix (Table A.10 in Section A.4) and the supporting material [62].
Figure 4.9 summarizes the optima resulting for setting the product flows or the vapor splits. First, the values of the product flows are set to the corresponding flow of the

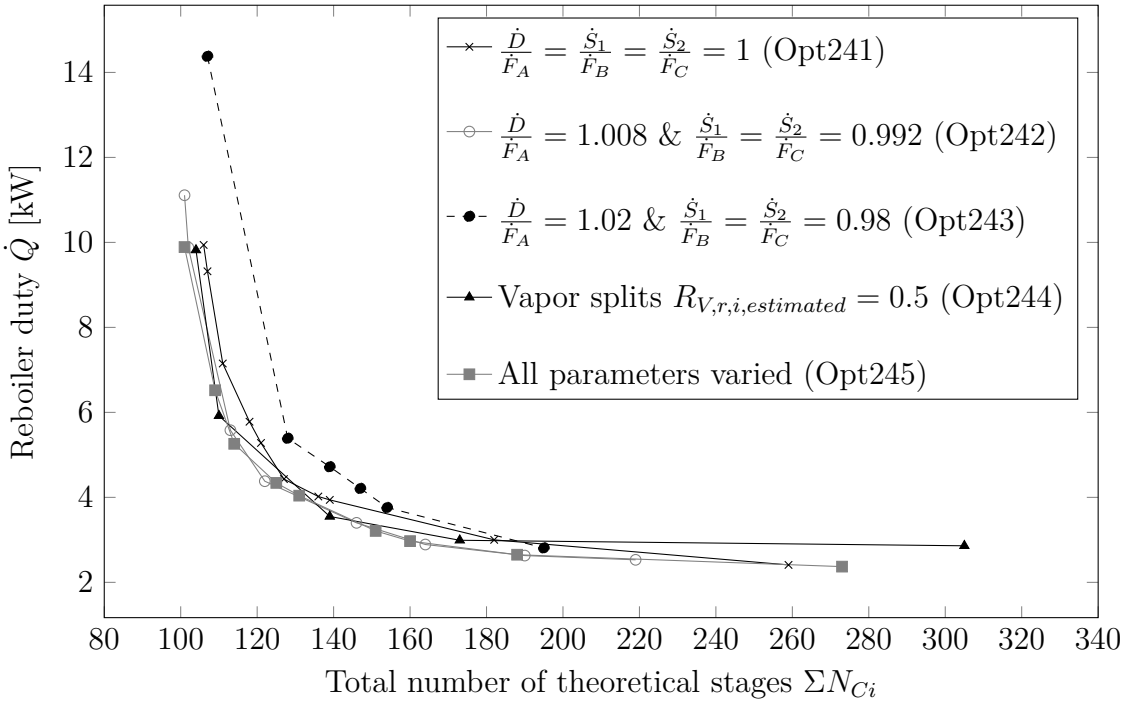

Figure 4.9: $N\dot{Q}$ optima for system 4.1 (98 mol % pure products) considering set flow simplifications.

components in the feed stream, thus they fulfill $\frac{\dot{D}}{\dot{F}_A} = \frac{\dot{S}_1}{\dot{F}_B} = \frac{\dot{S}_2}{\dot{F}_C} = 1$ (Opt241). The

resulting $N\dot{Q}$ optima are a deterioration compared to the case in which all variables are included. However, in Section 4.2 it was already stated that, in a simple dividing wall column, the reduction of the side flow can be advantageous for purities lower than one. Accordingly, the side product flows are reduced considering that the product quality of 98 mol % should still be reachable in the distillate and bottom stream. The resulting maximum possible distillate and bottom flows are $\frac{\dot{D}}{\dot{F}_A} = \frac{\dot{B}}{\dot{F}_D} = 1.02$ while the side product flows can be reduced down to $\frac{\dot{S}_1}{\dot{F}_B} = \frac{\dot{S}_2}{\dot{F}_C} = 0.98$ (Opt243). One flow combination in between is also tested at $\frac{\dot{D}}{\dot{F}_A} = \frac{\dot{B}}{\dot{F}_D} = 1.008$ and $\frac{\dot{S}_1}{\dot{F}_B} = \frac{\dot{S}_2}{\dot{F}_C} = 0.992$ (Opt242).
It can be seen that the first reduction of the side product flows divided by the corresponding feed flows to 0.992 is beneficial and shifts the $N\dot{Q}$ curve to the left. However, a further reduction results in a significant shift to the right to a position worse than the initial one for same product flows. It can be concluded that the product purities are very sensitive to the product flows. Due to the high sensitivity to the product flows, these should be included as optimization variables.
Another interesting result is found for set vapor splits at 0.5 (Opt244). The energy demand at high stage number is slightly increased while at lower total stage numbers the behavior is almost similar as for the best found options. However, the allocation of the theoretical stages in the column sections is quite different for the two cases. This gives the impression that the non-optimal vapor split was compensated for by a different stage allocation. The connection of vapor and liquid splits and stage allocation will be discussed in more detail in Section 5.2.

Transferability of results

The results for system 4.1 can be assumed to be valid for different mixtures, too. Of course the absolute values for the optimal product flows might differ, but the tendency that side draw flows should be reduced to a certain extent still applies (Opt242 vs Opt241). The exact value of the optimal product flow is determined by the theoretical stage setup, the mixture properties and product specifications. There might be systems, for which no increase of energy demand occurs for set vapor splits at 0.5 (which was observed for Opt244). More details about this can be found in Section 5.5.

4.2.2.2 Assumption of set stage allocation

Figure 4.10 compares different options for setting the ratio of the theoretical stages in all Sections in relation to the total stage number (m_i). Thus not the stages in all ten Sections have to be optimized but only the sum of them and the stages in each section are calculated with their corresponding ratio m_i. With the product flows being varied the total number of variables is reduced by nine to nine. The investigation is performed for system 4.1. Again, for clarification of the optimization setup please consider the appendix (Table A.10 in Section A.4) and the supporting material [62].
First, the stages are set as suggested for the pilot plant of the column (see Section 2.1.2) (Opt246). Accordingly, the stages in all Sections are the same despite section C32, where they are double the amount of the others. Second, the doubled stage number in section

C32 is neglected resulting in the same number of stages in all sections (Opt247). Third, the Fenske equation is used to estimate the minimum stage number in all column regions. Note that the derivation of the method is presented later in this work in Section 4.3.2 and 4.3.3. Here two cases are tested, one in which the Kirkbride equation is applied to determine the optimum feed stage (in terms of dividing wall position) combined with stream estimations from the $\dot{V}_{min}$ diagram (Opt248) and one in which the stages of the coupling stages is assumed to be at the middle of each region performing one product split (Opt249). The ratios m_i used for each case are shown in the appendix in Table A.12. Additionally, for the optimization problem definition consider Table A.10 in Section A.4 and the supporting material [62]. All resulting $N\dot{Q}$ optima are compared to the results from a run optimizing all degrees of freedom of the column.

All options reach the same minimum energy demand of approximately 2.4 kW at high

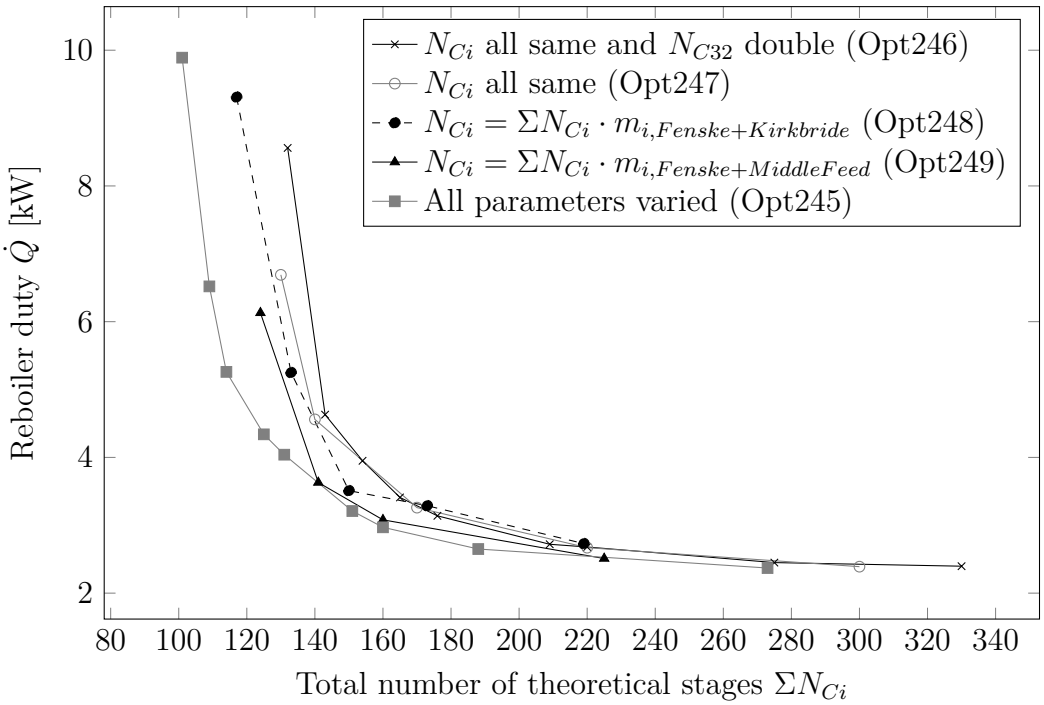

Figure 4.10: $N\dot{Q}$ optima for system 4.1 (98 mol % pure products) considering set stage simplifications. For Opt248 and 249 note that ΣN_{Ci} is defined as optimization variable and m_i are set.

stage numbers. However, the differences become more significant proceeding to lower stage numbers. Results closest to the overall optimum (Opt245) are reached estimating the total stage numbers with the Fenske equation and assuming the coupling stages at the middle of each region (Opt249), followed by the combination with Kirkbride (Opt248). Probably the flow specifications predicted by the $\dot{V}_{min}$ diagram in combination with the Kirkbride equation do not fit the actual composition profiles inside the column. This observation can be explained with the findings from Section 5.2.1. Generally, the accuracy of the $\dot{V}_{min}$ diagram to estimate the compositions of the coupling streams significantly decreases for lower total stage numbers. Accordingly, assuming the coupling streams to be located at the middle of the corresponding column regions is better suited

over the whole stage number range than inserting the results of the partly inaccurate $\dot{V}_{min}$ diagram in the Kirkbride equation. An increased minimum total stage number predicted by the Fenske equation compared to the optimum one is caused by an underestimation of the theoretical stages needed for the BC split in sections C13 and C14. In accordance with that the factor $(m_{C13} + m_{C14})$, defining the stages in the corresponding column region, is lower than the optimum ones. The necessary minimum stage number for the BC split resulting from the full optimization is 29. With the factors of the Fenske setups this stage number is reached at $29 \cdot (m_{C13} + m_{C14})^{-1} = 120$ stages in total. This observation fits the calculated limits of 124 and 117 stages for the Fenske setups.
Setting the stages in all sections equal (Opt247) results in a further increase of the minimum stage number, this is also valid for the use of doubled stages in section C32 (Opt246). Again the increase of total minimum stage number is caused by the limiting product split BC. Its minimum stage number is reached first and the stages in the other sections cannot be reduced further since their ratios m_i are fixed prior to the optimization.
Interestingly, the product flows are adjusted in a different way for each stage allocation (not shown here, see results in supporting material [62]). The side product flow of the limiting component C is reduced much stronger than the one of component B. Accordingly, the product flows can partly compensate a non-optimal stage allocation.
Summarizing, the reachable minimum total stage number is relatively sensitive to the allocation of the stages in the column sections. A misallocation, as for example by choosing same stages in all sections, can increase the total minimum stage number noticeable (in this case by approximately 30 %). However, an approximation with the Fenske equation is a suited tool to chose the stage allocation in an almost optimal way and like that reduce the optimization variables from 18 to 9. If the column should be designed in a flexible way for different systems, knowledge about the applicability the simplified column version (Figure 2.2c) based on the $\dot{V}_{min}$ method can be applied. In order to operate this column without energy penalty compared to the version with three dividing wall columns, the AB peak should not increase above the highest one. Correspondingly, for most systems suited for this kind of column the AB and AC split require less stages than the BC or CD split. Accordingly, the AB and AC split regions are well suited to reduce the total stage number of a simplified multiple dividing wall column from Figure 2.2c, all other sections should have a higher similar number. Like this, the increase of the minimum stage number is reduced while maintaining the flexibility of the column for different feed components. Additionally, the product flows should be included as optimization variables, since the energy demand is very sensitive to them. Also, they can be used to compensate slight misallocations of the theoretical stages.

Transferability of results

The trends found in this section totally apply for systems with ESIs similar to system 4.1. For all other systems, the data sets from Figure 4.10 should be differentiated into

"optimally" (Opt245) and "non-optimally" (all others) allocated theoretical stages in the column sections. Then, it can be concluded that a non-optimal stage number in the sections can significantly increase the energy requirements, especially close to the minimum stage number. In this case, it can happen that one column region is already operated at the minimum stage number, while the stages in the other column regions could still be reduced further. However, as the allocation of the stages is set prior to the optimization, the consequence is an increased overall minimum stage number of the column.

4.3 Approximation of Pareto-optimal solutions in distillation columns

In this section a new heuristic method to approximate $N\dot{Q}$ curves of dividing wall columns is presented. First, in Section 4.3.1 the general approach is explained. Second, the applicability of the Fenske equation to estimate the minimum stage number for a dividing wall column is tested in Section 4.3.2.

4.3.1 General approach

An approximation of the $N\dot{Q}$ curves is a useful tool to avoid a complete optimization run. The method by Gilliland and its extended version by Molokanov is compared to a set of results from the optimizations in the previous sections. The presented data points are randomly chosen from the previously presented optimization results and include various binary, ternary and quaternary mixtures which are split in simple columns, column sequences or dividing wall columns (Opt2x3, Opt2310, Opt235, Opt2314, Opt246). The results are shown in Figure 4.11a in comparison to the approximation with the Gilliland/Molokanov method (Equation 2.13 in Section 2.1.3.3) [130]. The optimization results are not well described by the equation. Additionally, the overall scattering range of the data points is relatively large and thus another standardization method might resolve this issue. Accordingly, a new method is developed to describe the Pareto-optimal solutions. For the new approach several options to standardize the optimization results are tested. The best agreement in the resulting plots is found for the standardization according to Equation 4.1, resulting in the relative total stage number N_{rel} and the relative reboiler duty Q_{rel}.

$$\begin{aligned} N_{rel} &= \frac{\Sigma N_{Ci}}{0.97 \cdot \Sigma N_{min,Ci}} \\ Q_{rel} &= \frac{\dot{Q}}{\dot{Q}_{min}} \end{aligned} \tag{4.1}$$

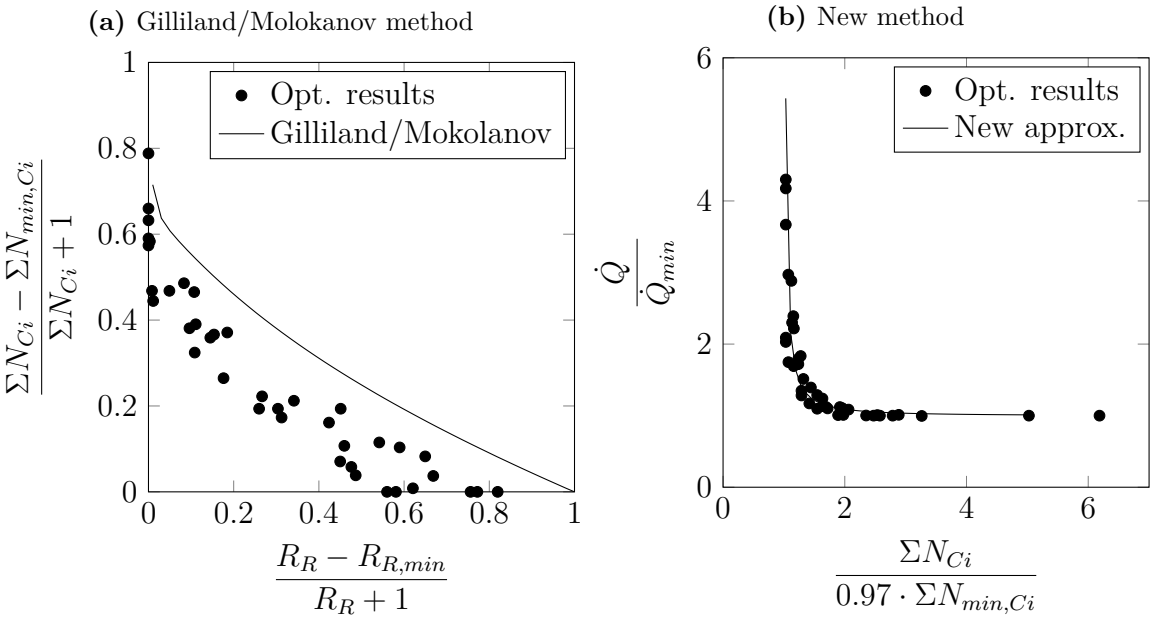

Figure 4.11: Comparison of standardized optimization data from this work with approximation methods. [130]

In Figure 4.11b the optimization results are plotted with the new standardization. All data points lie approximately on the same curve. The curve can be described with an equation of the type from Equation 4.2.

$$Q_{rel} = \frac{a}{N_{rel}^2 - b^2} + c \tag{4.2}$$

The parameters a, b and c have to be defined. b is the asymptote in x-direction and c in y-direction. For the approximation in Figure 4.11b both should actually be defined slightly below one, since the minimum reboiler duty and the minimum number of theoretical stages are actually reachable. However, for simplicity reasons these are set to be one. Like this, the minimum stage number cannot be approximated satisfactory due to its integer character. To avoid this problem, the relative stage number is defined by dividing the stage number by the minimum stage number times 0.97 instead of just the minimum stage number (as shown in Equation 4.1). The last parameter a is fitted to the data sets in Figure 4.11b to be 0.27. The final equation for the approximation is shown in Equation 4.3.

$$Q_{rel} = \frac{0.27}{N_{rel}^2 - 1} + 1 \tag{4.3}$$

Accordingly, for specified values of N_{rel}, the corresponding Pareto-optimal reboiler duty $\dot{Q}_{opt}$ can be calculated according to Equation 4.4.

$$\dot{Q}_{opt} = \frac{0.27 \cdot \dot{Q}_{min}}{\left(\frac{\Sigma N_{Ci}}{0.97 \cdot \Sigma N_{min,Ci}}\right)^2 - 1} + \dot{Q}_{min} \tag{4.4}$$

In order to apply Equation 4.4, shortcut methods are needed to estimate the minimum stage number and minimum energy demand. The applicability of the Fenske equation for this task is investigated in more detail in the following Section 4.3.2. The minimum energy demand can be determined with the $\dot{V}_{min}$ diagram. For detailed calculation information consider the supplementary material of this work [62].

4.3.2 Applicability of Fenske equation on dividing wall columns

In order to perform the approximation of $N\dot{Q}$ optima in a simple way, a shortcut method is required to estimate the minimum stage number of a dividing wall column. To validate whether the Fenske equation is applicable to dividing wall columns or not, two main questions are answered in this section. First, if on the one hand additional components and second, if the thermal coupling of the column sections influences the minimum number of stages. After answering the two questions, the Fenske equation is applied to the sections of a dividing wall column. Afterwards, all results are summarized and compared to the results of a rigorous optimization. For the evaluation binary, ternary or quaternary mixtures, each with equimolar compositions, are formed from system 4.6.

Optimization: Minimum stage number for multi-component mixtures

To answer the first question a simple rectification column with one feed stream and two outlet streams is $N\dot{Q}$ optimized (explained in Section 3.2). The feed stream is either binary, ternary or quaternary and either component A and B, A and C or B and C are split (an identical behavior for the other splits can be assumed). The nomenclature for the splits is according to the feed stream and the separated components as explained in Figure 4.12a using the AB splits. In any case, the recovery of the distillate product key component is defined to be 95 mol %. The detailed optimization setup can be found in the appendix (Table A.7) and supporting material [62], the resulting $N\dot{Q}$ optima can be seen in Figure 4.12b.

In all cases, it can be observed that the minimum reboiler duty for the splits increases with the number of components in the feed stream. This behavior is also predicted by the $\dot{V}_{min}$ diagram. Also, it can be observed that the minimum stage number does not change with additional components in the feed stream. The calculated minimum stage numbers can be found in Table 4.1. Thus to answer the first question it can be concluded that the Fenske equation, which is originally only applicable for binary feed streams, could also be applied for feeds consisting of more components since those do not affect the minimum stage number of the column.

Optimization: Minimum stage number in each section of a dividing wall column

To answer the second question, whether the thermal coupling of the column sections could render Fenske's results invalid, an $N\dot{Q}$ optimization for 95 mol % pure products of the ternary feed of system 3.1 is carried out in a dividing wall column. The resulting $N\dot{Q}$ curve is shown in Figure 4.13a in Section 4.4.2. As a result of the optimization

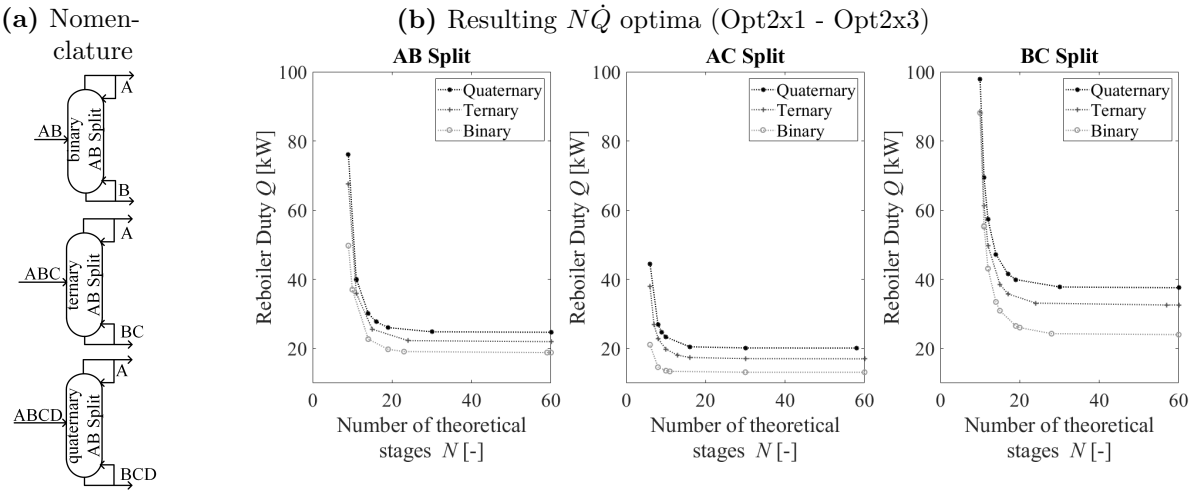

Figure 4.12: Bi-objective optimization results for different feed mixtures (light boiler related to heavy boiler in bottom stream $\leq 5\,\mathrm{mol\,\%}$ for the main distillate product). Note that in the DWC the AB split is performed in sections C11 + C12, AC in C21 + C22 and BC in C13 + C14 (as shown in Equation 2.3 in Section 3.4). [131]

a minimum stage number of 25 is calculated, similar as the sum of the splits in one column from Figure 4.12b. The internal distribution of the stages in the column sections resulting from the optimization is also listed in Table 4.1.

Conclusion: Comparison of optimization results and the Fenske equation

For the final conclusion, whether the Fenske equation predicts the same distribution of the stages, it is used for the calculation of the minimum stages in each section of the dividing wall column. The relative volatilities of the system 3.1 are shown in Table 3.1 in Section 3.5 and are assumed to be constant. The Fenske equation is then applied according to the method described in Section 4.3.3. In Table 4.1 the results of the Fenske equation and the previous paragraphs are summarized.

The calculated data from the Fenske equation matches the ones calculated by the optimization very well. Partly the optimization results are slightly higher than the ones determined by the Fenske equation. However, since the Fenske equations neglects real effects of the system in the column this does not mean that the optimization results are not reliable. On the contradictory, a single-objective optimization setting the number of stages according to Fenske did not lead to a permissible operating point at which the required product purities were achieved and thus the constraints were violated. All in all, the general trend of the stage distribution inside the column is well reproduced.
Similar calculations are performed for system 3.3. The Fenske equation predicts $N_{min,AC,Fenske} = 5$, $N_{min,AB,Fenske} = 12$ and $N_{min,BC,Fenske} = 5$. From the optimization of the system in a dividing wall column the resulting minimum stages are $N_{min,AC,Opt} = 5$, $N_{min,AB,Opt} = 13$ and $N_{min,BC,Opt} = 6$ (Opt2316). Again, the results from the Fenske equation are slightly lower for the reasons as stated above, but the trend is predicted correctly.

Table 4.1: Minimum stage numbers in each section of the dividing wall column splitting benzene/toluene/*p*-xylene ($\dot{F} = 3\,\mathrm{kmol} \cdot \mathrm{h}^{-1}$, $q = 1$) in 95 mol % pure products: Comparison of Fenske results with optimization results of splits in a simple column and in dividing wall column. For nomenclature, see Figure 2.2a in Section 2.1 and Equation 2.3 in Section 3.4.

Column Region	Column Section	Optimization: ternary splits in simple column	Optimization: DWC	Fenske equation according to Section 4.3.3
$N_{min,AB}$	$N_{min,C11}$	5	4	3
	$N_{min,C12}$	4	5	5
$N_{min,BC}$	$N_{min,C13}$	6	5	5
	$N_{min,C14}$	4	5	3
$N_{min,AC}$	$N_{min,C21}$	3	3	3
	$N_{min,C22}$	3	3	3
ΣN_{Ci}		25	25	22

In summary, the Fenske equation can and will be used in this work for the estimation of the minimum stage number in each section of a dividing wall column. However, it should be kept in mind that the result of this method is only a first estimated guess and in no case invalidates the results of an optimization. Especially if the binary subsystems show strong fluctuations in the relative volatilities, the equation will obviously not give reliable results. Nevertheless, the order of magnitude of the minimum number of stages can be well predicted.

4.3.3 Method to apply Fenske equation on complex distillation configurations

In this work the Fenske equation is applied to estimate the minimum stage number of dividing wall columns (for validation see Section 4.3.2 [131]), and column sequences. Both procedures are explained in more detail in the following paragraphs.

Dividing wall columns

To apply the Fenske equation on dividing wall columns the following assumptions have to be done. First, the minimum number of theoretical stages is only set by the two key components that are split and is not affected by the presence of additional components. Second, the composition of the vapor and liquid coupling flows between two columns is same, if they enter and leave at the same stages. Third, the recoveries of the key components split in the prefractionator are higher than the ones in the main column. For the product splits in the main column of a dividing wall column purity specifications x_i^{main} are usually given that can directly be inserted into the Fenske equation. Note

that the side draw flows are gained in two column regions and both product flows are mixed to obtain the final product flow. Thus, the impurities from both sections sum up. As a consequence, when the Fenske equation is applied the impurities in the side draw products have to be assumed with half of the final ones in the product for each region. An example is used to illustrate the procedure: The side draw product of a simple dividing wall column should be obtained in 98 mol % purity. The final side product is a mixture of the bottom product from the AB split and the top product of the BC split. Accordingly, for the bottom product B of the AB split a purity of 99 mol % is assumed, similar for the top product of the BC split.
Nevertheless, for prefractionating columns the molar fraction of the products x_i^j have to be guessed (for example the AC split). As a rule of thumb Equation 4.5 is applied for product purities above or equal 95 mol %. For product purities lower 95 mol % Equation 4.6 is applied. Note that x_i^{main} is the final purity of component i in the corresponding product stream of the dividing wall column.

$$\begin{aligned} x_{HK}^{\dot{D}} &= 10^{-73.1 \cdot x_{LK}^{main} + 67.5} \\ x_{LK}^{\dot{B}} &= 10^{-73.1 \cdot x_{HK}^{main} + 67.5} \\ x_{HK}^{\dot{B}} &= 1 - x_{LK}^{\dot{B}} \\ x_{LK}^{\dot{D}} &= 1 - x_{HK}^{\dot{D}} \end{aligned} \tag{4.5}$$

As an example, lets consider a simple dividing wall column with all product purities at $x_i^{main} = 95$ mol %. In order to estimate the minimum stage number of the AC split, the purities of the key component A and C have to be estimated with Equation 4.5. This results in $x_{HK}^{\dot{D}} = x_{LK}^{\dot{B}} = 0.011$ and $x_{HK}^{\dot{B}} = x_{LK}^{\dot{D}} = 0.989$. These values are inserted into the Fenske equation (Equation 2.10 in Section 2.1.3.2). With $\alpha_{LK/HK} = 5.76$ this leads to six stages when rounded up.

$$\begin{aligned} x_{HK}^{\dot{D}} &= 1 - x_{LK}^{\dot{D}} \\ x_{LK}^{\dot{B}} &= 1 - x_{HK}^{\dot{B}} \\ x_{HK}^{\dot{B}} &= x_{HK}^{main} + \frac{1 - x_{HK}^{main}}{2} \\ x_{LK}^{\dot{D}} &= x_{LK}^{main} + \frac{1 - x_{LK}^{main}}{2} \end{aligned} \tag{4.6}$$

In order to estimate the minimum stage number of a simple dividing wall column the Fenske equation has to be applied three times and for the smDWC five times. To calculate the total minimum stage number, the minimum stage numbers for all product splits are summed up.
For the applicability of the Kirkbride equation (Equation 2.14 in Section 2.1.3.2), the compositions of the flows that are fed to another section are estimated with $\dot{V}_{min}$ diagrams.

Column sequences

In order to estimate the minimum stage number of column sequences it is also assumed that the minimum stage number is only determined by the two split key components. Again the final product purities are given but mixed flows between the columns have to be estimated. The rule of thumb used for the application of the Fenske equation on each column before the last one in a column sequence is shown Equation 4.7.

$$\begin{aligned} x_{HK}^{\dot{D}} &= 10^{-22.6 \cdot x_{LK}^{main} + 18.4} \\ x_{LK}^{\dot{B}} &= 10^{-22.6 \cdot x_{HK}^{main} + 18.4} \\ x_{HK}^{\dot{B}} &= 1 - x_{LK}^{\dot{B}} \\ x_{LK}^{\dot{D}} &= 1 - x_{HK}^{\dot{D}} \end{aligned} \tag{4.7}$$

4.4 Energy saving potential of dividing wall columns

The overall energy saving potential of dividing wall columns is an interplay of the mixture, the number of theoretical stages and product purity requirements. The objective of this section is to clarify which parameters affect the saving potential and to which extend. For this purpose, bi-objective optimizations are performed to calculate $N\dot{Q}$ optima. For the evaluation of the energy saving potential, the results of dividing wall columns are compared to the ones of conventional split sequences. Which sequence is the one with the lowest energy demand is estimated with $\dot{V}_{min}$ diagrams, for most cases the direct or for the quaternary systems direct-direct split sequence requires the lowest energy input of all sequences. The quantification of the energy saving potential is challenging, which is explained in the following for a simple dividing wall column. Nevertheless, it also applies for multiple dividing wall column.

For all four ternary systems introduced in section 3.5 $N\dot{Q}$ optimizations are performed specifying product purities above 95 mol %. The results are shown in Figure 4.13. Considering the optimal variables of the dividing wall column (see supporting material in [62]), similar observations as described in Section 4.2 apply. Again, the side product stream is reduced while the distillate or bottom streams are increased. Whether the distillate or bottom stream is higher depends on the investigated system. For system 3.1 and 3.2, having a higher BC than AB peak in the $\dot{V}_{min}$ diagram, the distillate stream is larger. For system 3.3, having a higher AB than BC peak, the bottom stream is the highest one.

However, the more important aspect is that the direct split sequence always has a lower minimum stage number while the dividing wall column has a lower minimum energy demand at high stage numbers, which matches observations from literature as discussed in Section 2.3. A lower total stage number of column sequences can be explained with the fact, that no stages are needed for the AC split while the dividing wall column requires stages for this split in the prefractionator. The lower minimum energy demand of the dividing wall column comes from the fact that, due to the spatially separated execution of the AC split, there is no remixing of the intermediate boiling component B.

Accordingly, energy losses occurring for the direct split sequence are prevented by using additional stages. Since one extreme point of the Pareto-optimal curve is lower for the dividing wall column and one for the direct split sequence, there has to be an intersection of the curves. For all four systems this intersection is located at relatively low total stage numbers. Accordingly, for most columns at higher stage numbers the dividing wall column is the more energy efficient option. Nevertheless, if a column design is close to the intersection of the Pareto-optimal curves, not the whole energy saving potential of dividing wall columns of around 30 %, which is often reported in literature, can be exploited.
For the quantification of the overall energy saving potential of a dividing wall column compared to conventional split sequences considering the location of the intersection of the $N\dot{Q}$ optima no tool is available. Accordingly, the Decision Number DN is introduced to fill this gap. It is presented in the following Section 4.4.1. Based on the Decision Number and standardized variables, the energy saving of dividing wall columns is quantified in Section 4.4.2. Note that the presented results are partly based on actual optimizations and partly on approximations, the corresponding method is presented in Section 4.3. The input data for all approximations can be found in the appendix in Table A.14. Afterwards, the full energy saving potential of a simplified multiple dividing wall column based on optimizations is presented in Section 4.4.3. Last, the energy savings of the smDWC pilot plant is studied for six different quaternary mixtures based on optimizations in Section 4.4.4. Note that in all cases the liquid fraction of the feed is set to $q = 1$.

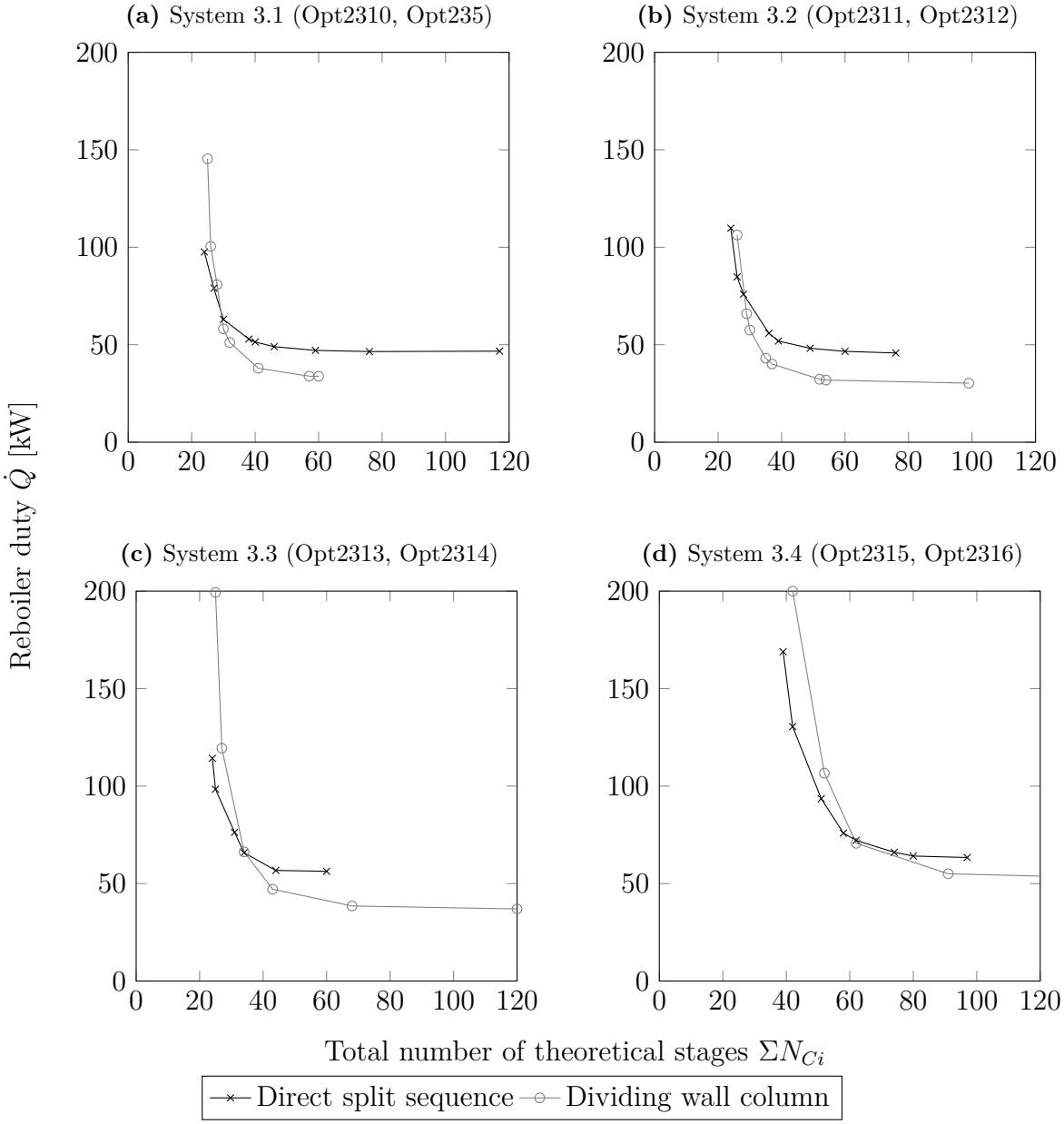

Figure 4.13: $N\dot{Q}$ optima of the four ternary systems in a dividing wall column and direct split sequence to reach 95 mol % pure products obtained by optimization.

4.4.1 Quantification by Decision Number DN and relative intersection variables

The task of the Decision Number DN is to map which of two process options i and j is superior in terms of energy demand considering the entire set of the Pareto-optimal solutions if the curves intersect. In the context of distillation, it determines the relative location of the point, at which the lowest energy demand is shifted from one process option to another. Its calculation is based on the area between the two convex Pareto-fronts of the two distillation options before and after their intersection as indicated in Figure 4.14. In the area A_1 Option j dominates option i and vice versa for area

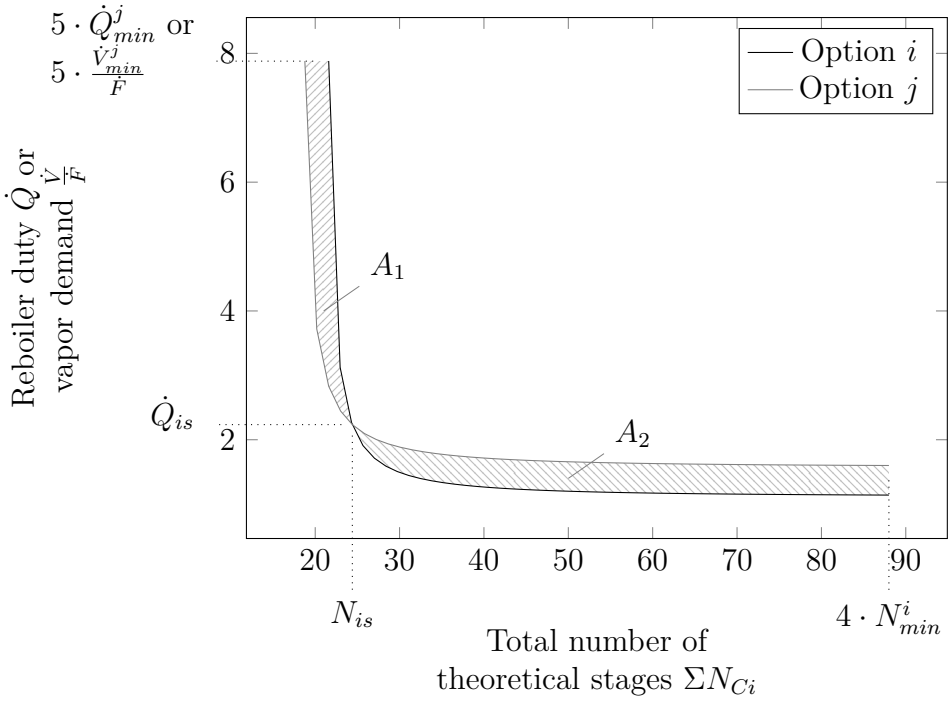

Figure 4.14: Explanation of integrals used for the calculation of the Decision Number.

A_2. The upper limit of the integration is set to be at $4 \cdot N^i_{min}$, since this total stage number approximates an infinite stage number. The lower limit is set to $5 \cdot \dot{Q}^j_{min}$, since most optimizations showed approximately this reboiler duty at the minimum stage number. However, it should be kept in mind that the setting of these ranges can affect the resulting areas. Accordingly, the Decision Number rather evaluates trends than absolute values.

The calculation of the Decision Number is shown in Equation 4.8. By its definition the number is in the range between -1 and 1. For positive values option i is more beneficial and for negative values option j. If DN is around zero, both options are equally suitable, thus half area is dominated by option i and half by j. In this work usually the dividing wall column is option i and a conventional column sequence is option j. Correspondingly, a DN of zero means, that the minimum energy savings of

the dividing wall column equal the savings of the minimum stage number of the column sequence.

$$DN = \frac{A_2 - A_1}{A_1 + A_2} \tag{4.8}$$

The areas between the curves can be calculated analytically, if the approximation method for the $N\dot{Q}$ curves from Equation 4.3 in Section 4.3 is applied. For the detailed calculation see Section A.5.1 in the appendix. However, this calculation procedure is quite elaborate and has to be adapted for actual optimization results, since no functional correlation is available. Accordingly, a simplified method to determine the Decision Number has been developed. First the stage ratio intersection N_{is} and energy demand intersection $\dot{Q}_{is}$ are introduced for the coordinated of the stage number and reboiler duty, at which the curves intersect (Index is = intersection). This intersection can either be read from optimization data or calculated from the approximation equations of the $N\dot{Q}$ optima of the two options. For the calculation based on the approximation equation (Equation 4.3) $\dot{Q}^{DSS} = \dot{Q}^{DWC}$ is assumed. Consequently, Equation 4.9 has to be solved to find the number of stages at which the curves intersect N_{is}.

$$\frac{0.27 \cdot \dot{Q}_{min}^{DSS}}{\left(\frac{N_{is}}{0.97 \cdot N_{min}^{DSS}}\right)^2 - 1} + \dot{Q}_{min}^{DSS} = \frac{0.27 \cdot \dot{Q}_{min}^{DWC}}{\left(\frac{N_{is}}{0.97 \cdot N_{min}^{DWC}}\right)^2 - 1} + \dot{Q}_{min}^{DWC} \tag{4.9}$$

The corresponding reboiler duty at the intersection $\dot{Q}_{is}$ is then calculated by inserting N_{is} in Equation 4.3. Afterwards the relative stage number and reboiler duty can be calculated for each column option with Equation 4.10.

$$\begin{aligned} N_{rel,is} &= \frac{N_{is}}{0.97 \cdot \Sigma N_{min,Ci}} \\ \dot{Q}_{rel,is} &= \frac{\dot{Q}_{is}}{\dot{Q}_{min}} \end{aligned} \tag{4.10}$$

It is found that the simplified Equation 4.11 to calculate the Decision Number results in an almost identical results as the calculation based on the integration between the two curves followed by applying Equation 4.8. For a comparison of the two methods see Figure 4.17 in Section 4.4.2.1.

$$DN \approx \frac{\ln\left(\left|\frac{\dot{Q}_{rel,is}^{DSS} - \dot{Q}_{rel,is}^{DWC}}{N_{rel,is}^{DSS} - N_{rel,is}^{DWC}}\right|\right) - 0.35}{2.7} \tag{4.11}$$

With this simplified equation the Decision Number can be calculated only on the basis of the feed stream composition, its liquid fraction, the relative volatilities of the components and the product purity specifications. With this knowledge, first the $\dot{V}_{min}$ diagram (for the equations see supporting material on [62]) and the minimum stage number of the column (Section 4.3.3 by Fenske) can be calculated. This data is

then combined with the approximation of $N\dot{Q}$ optima from Section 4.3. Consequently the equations 4.9 and 4.10 have to be applied to calculate the intersection of the optima of two distillation options. These parameters are then inserted into Equation 4.11 and the Decision number can be estimated.
Note that also on the basis of the standardized values tendencies can be read. The dividing wall column is advantageous for cases at low ratios of N_{is}/N_{min}^{DWC} and high ratios of $\dot{Q}_{is}/\dot{Q}_{min}^{DWC}$. In that case, the minimum stage number of the dividing wall column and direct split sequence are close to each other and thus the intersection of the curves is close to the minimum stage number of the dividing wall column. Correspondingly, the range of the theoretical stages in which the direct split sequence is the only possible option is relatively small. Note in this context that the operating point of a column is usually chosen close to the strongest curvature of the $N\dot{Q}$ curve at around $N = 1.2 \cdot N_{min}$.
The lower border of the stage ratio is one. In this case the minimum stage number of the dividing wall column is only slightly above the one of the direct split sequence. If both require the same minimum stage number or the one of the dividing wall column is lower, there is no intersection of the curves anymore. Accordingly, the dividing wall column would be the most beneficial solution in the whole solution space and not only in part of it. Consequently also the Decision Number is one. The difference between N_{is}/N_{min}^{DWC} and N_{is}/N_{min}^{DSS} basically indicates the difference between the minimum stage number of the two options. The ratio $\dot{Q}_{is}/\dot{Q}_{min}^{i}$ is partly related to the ones at N_{is}/N_{min}^{i}, if one of them is lower the other one is higher. At high energy demand ratios the intersection of the curves is located closer to the minimum stage number and thus energy savings can be expected for the dividing wall column in a large range of the solution space. The lower border of the ratio $\dot{Q}_{is}/\dot{Q}_{min}^{DWC}$ is around 1.3, since in most cases the minimum energy demand of the dividing wall column is approximately 30 % below the one of the direct split sequence.

4.4.2 Simple dividing wall column

The energy saving potential of a dividing wall column is investigated in this section based on the Decision Number and standardized intersection variables. First the impact of the product purity specification is discussed in Section 4.4.2.1. In this context, also the correspondence between the full (Equation 4.8) and simplified model (Equation 4.11) of the Decision Number is investigated. Afterwards, the impact of the mixture on the energy saving potential is investigated in more detail in Section 4.4.2.2. Note here that the actual optimization results have already been shown in Figure 4.13. Afterwards, the effect of the feed stream composition is presented in Section 4.4.2.3.

4.4.2.1 Impact of product purity specifications

The impact of the product purity specification is investigated for system 3.1, which is optimized for minimum purities of 90 mol %, 95 mol % and 98 mol % in the dividing wall

column (Opt2318, Opt235, Opt2320) and direct split sequence (Opt2317, Opt 2310, Opt2319). Additionally, an approximation according to Section 4.3.1 is performed to increase the significance of the results at 90 mol %, 95 mol %, 96.5 mol %, 98 mol % and 99.9 mol %. Figure 4.15 shows the $N\dot{Q}$ optima for all cases based on the approximation approach.
The $N\dot{Q}$ optima shift to higher stage numbers and energy demands with increasing

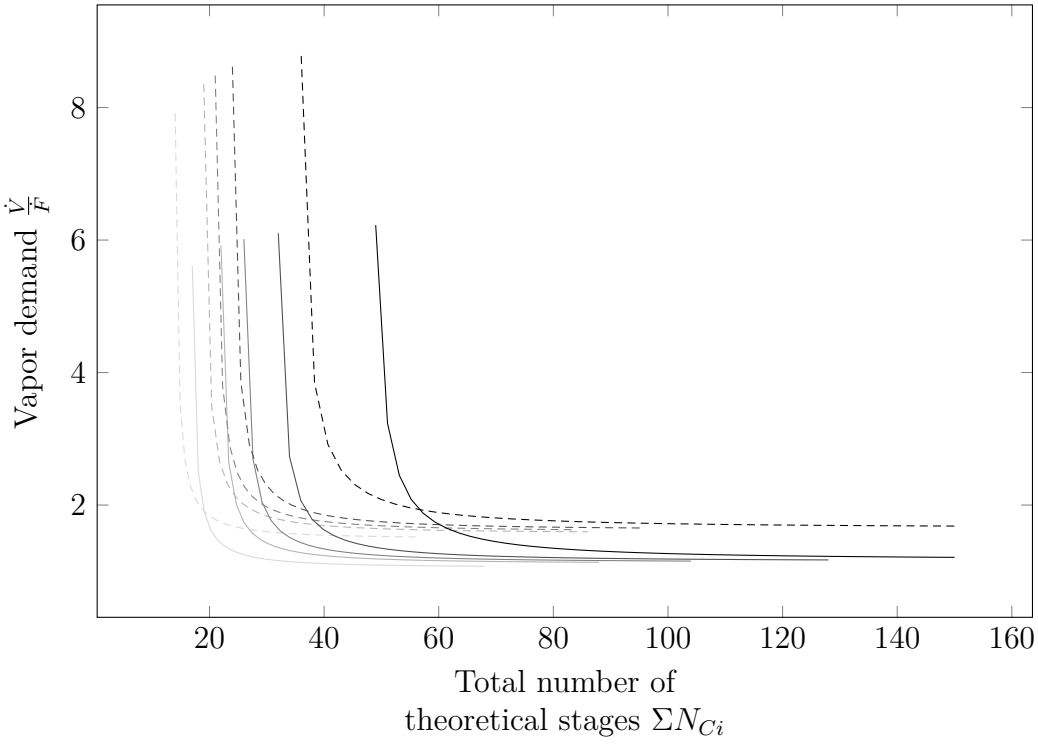

Dividing wall column & 90.0 mol %	Direct split sequence & 90.0 mol %
Dividing wall column & 95.0 mol %	Direct split sequence & 95.0 mol %
Dividing wall column & 96.5 mol %	Direct split sequence & 96.5 mol %
Dividing wall column & 98.0 mol %	Direct split sequence & 98.0 mol %
Dividing wall column & 99.9 mol %	Direct split sequence & 99.9 mol %

Figure 4.15: Resulting $N\dot{Q}$ optima of system 3.1 in dividing wall column and direct split sequence for different product purities based on new approximation approach (for method see Section 4.3). Data sets Approx12 - Approx16.

purity requirenents. However, the impact on the stage number is much more pronounced than the one of the energy demand. Thus, the relative location of the intersection of the curve from the dividing wall column compared to the direct split sequence could also shift. In order to simplify this investigation, Figure 4.16 presents the resulting impact of the product specifications on the intersection location. According to the approximation the stage intersection ratio of the dividing wall column is almost independent of the product purity specifications at around 1.2. For the direct split sequence this ratio is only constant at lower product purities below 95 mol %, above it increases with increasing product specifications. This behavior can be explained with the development

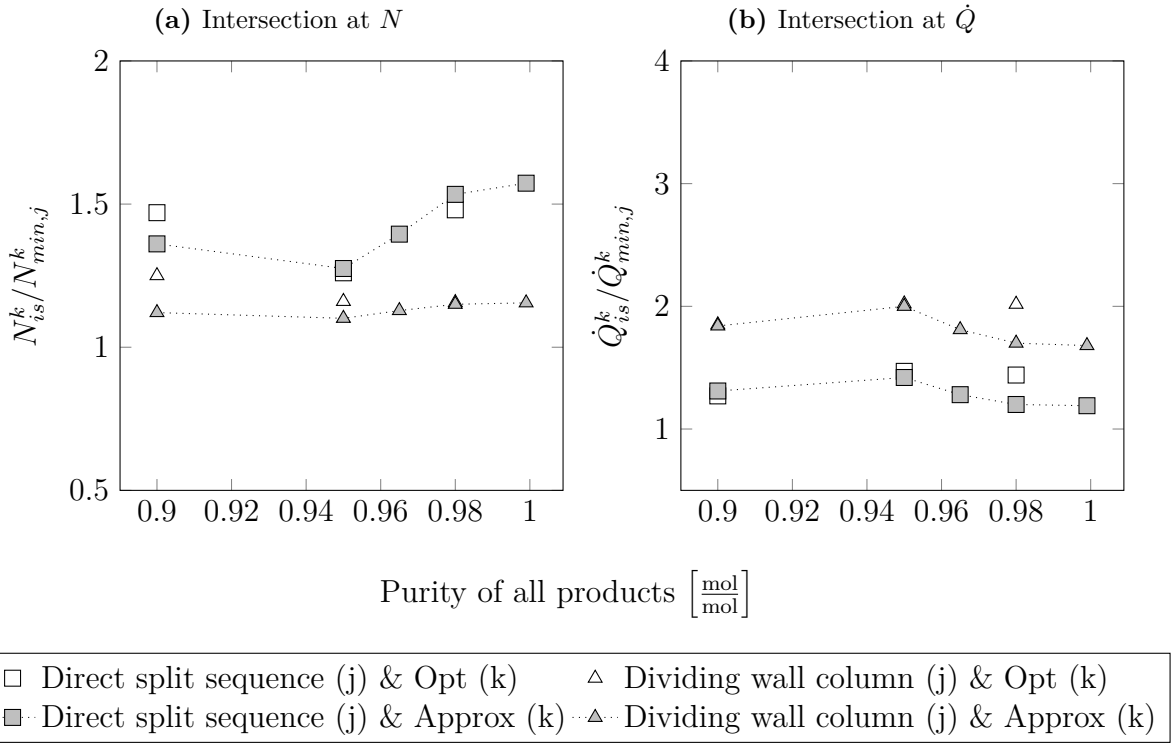

Figure 4.16: Location of the intersections of the $N\dot{Q}$ optima of system 3.1 with different product purities from optimization (Opt) and approximation (Approx, for method see Section 4.3). Data sets Approx12 - Approx16, note that the dotted line is only a visual aid.

of the minimum stage number of the columns depending on the product specifications from Figure 4.8a in Section 4.2.1. For the dividing wall column it was found that the minimum stage number increases stronger than the necessary reboiler duty for higher product purities. Probably, the increase in minimum stage numbers is less pronounced for the direct split sequence resulting in the $N\dot{Q}$ optima to drift apart at lower stage numbers. As a consequence, the stage intersection factor of the direct split sequence increases strong while the one of the dividing wall column is relatively stable. This also matches the results in Figure 4.16b, which show that the product specifications have low impact on the energy demand intersection. Only a slight decrease is observable for increasing product purities, however the difference between direct split and dividing wall column is almost constant. Again the optimization results show a similar trend.
Based on these results the Decision Number is calculated and plotted in Figure 4.17 depending on the purity specifications of the products. Three approaches are compared. First, the actual results from the optimization in combination with the simplified equation of the Decision Number (Equation 4.11), second the approximation of the $N\dot{Q}$ optima and a full integration to calculate the Decision Number (Equation 4.8) and third an approximation in combination with the simplified equation to calculate the Decision Number (Equation 4.11).

First of all, it is observable that the full and simplified model of the Decision Numbers are in good agreement, accordingly in all following calculations only the simplified model

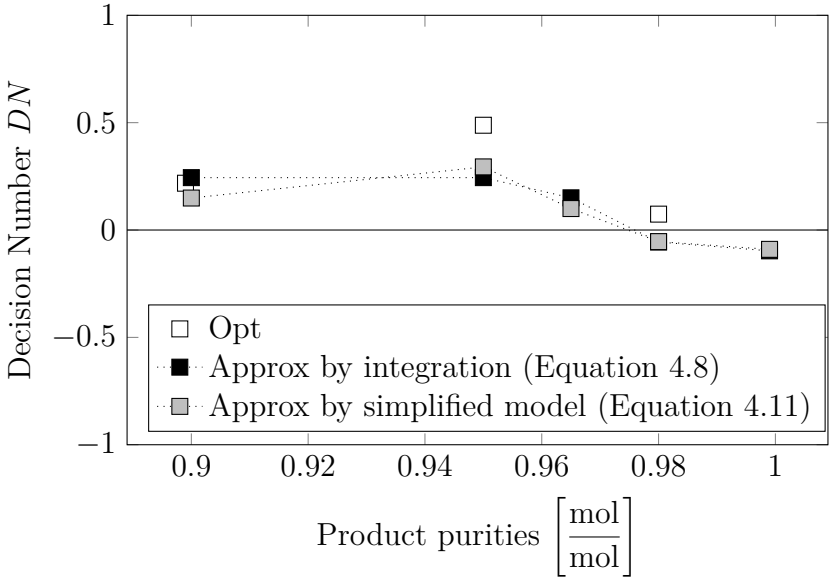

Figure 4.17: Decision Number of dividing wall column in comparison to direct split sequence for system 3.1 ($ESI = 1.08$) at different product purities and equimolar feed (Approx12 - Approx16).

from Equation 4.11 is used. The results from approximation and optimization show a similar trend, at low product purities of 90 mol % the Decision Number is positive and thus the dividing wall column is more advantageous than the direct split sequence. For increasing product purities it is slightly increasing but decreases again for purities above 95 mol %. This behavior is caused by the significant increase in the stage intersection ratio of the direct split sequence in Figure 4.16a. Thus, for high product purities of system 3.1 the options dividing wall column and direct split sequence are almost equally suited with a slight advantage of the direct split sequence. This is in contrast to the widespread opinion in the literature that dividing wall columns are always the better column choice. However, it should also be kept in mind that the total stage number of dividing wall columns could also be counted in a way neglecting parallel sections (discussed in Section 2.1.1). Then, the minimum total stage number of the dividing wall column would be reduced and the Decision Number increased.
Summarizing, the product purity specifications only have a pronounced impact on the stage intersection factor of the direct split sequence. The stage ratio related to the minimum stage number of the dividing wall column is almost constant at 1.15 in the investigated product purity range and the energy demand ratio is almost unaffected. As a consequence, for high purity products the distillation options dividing wall column and direct split sequence are equally suited.

4.4.2.2 Impact of feed mixture

In this section, the impact of the components in the feed mixture on the saving potential is analyzed. For this purpose, the dividing wall column is compared to the direct and indirect split sequence for various mixtures. First, the results for the direct split

sequence are shown, followed by the ones for the indirect split.
In Figure 4.13 bi-objective optimization results for four systems in a dividing wall column in comparison to the direct split sequence were already shown but not analyzed in detail. Thus, these are studied in this section. For this purpose, the results are standardized according to Equation 4.10, similar as presented in the previous Section 4.4.2.1. The resulting relative locations of the Pareto-front intersections over the ESIs of the systems are shown in Figure 4.18. Additionally, the approximation method is applied in order to determine more data points without the need of additional optimization runs. Note that these results are valid for an equimolar feed stream composition with a liquid fraction of $q = 1$ and 95 mol % pure products.
The data from the approximation method (gray filled markers) predicts a clear trend.

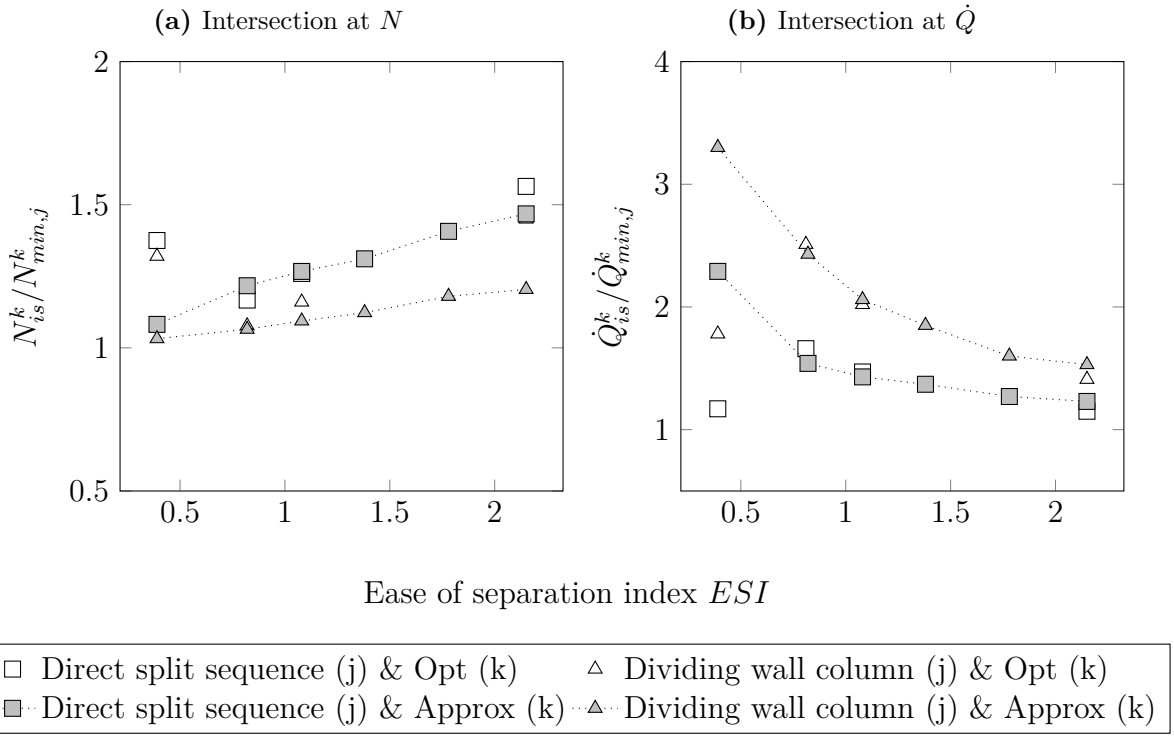

Figure 4.18: Location of the intersections of the $N\dot{Q}$ optima of dividing wall column in comparison to direct split sequence of all ternary systems with 95 mol % pure products based on optimization (Opt) and approximation method (Approx, for method see Section 4.3). Note that the dotted line is only a visual aid. Corresponding data sets Approx1 - Approx6.

The stage ratio of the intersection for systems with ESIs below 0.4 is close to one (Figure 4.18a), correspondingly the energy demand intersection is high (Figure 4.18b). For lower ESIs there is no intersection of the curves anymore. If the ESI is increased, the ratios of the stage intersections increase while the energy demand intersection decreases. Considering the difference between the values of the direct split compared to the dividing wall column, it is observable that the differences also change. For increasing stage numbers the difference between direct split sequence and dividing wall column increases with the ESI while the opposite trend is observable for the energy demand

ratios. The results from the optimization runs (white filled markers) validate these observations. Only for the system at an ESI of 0.38 (system 3.3) stronger deviations can be seen. Probably this behavior can be explained with the real behavior of the system.
It should also be kept in mind that usually a column is designed at stage numbers around $N = 1.2 \cdot N_{min}$. Accordingly, one column option is more beneficial than another if the stage intersection factor of a column option is below 1.2. As the stage intersection factor of the dividing wall column is below 1.2 for ESIs lower than 1.8, it can be guaranteed that its energy consumption for a standard design is below the one of a direct split sequence with the same total stage number. For higher ESIs it is possible that the intersection is very close to this design point and thus the energy savings can be expected to be below 30 %. On the other hand, if a direct split sequence is designed at $N = 1.2 \cdot N_{min}^{DSS}$ its corresponding energy consumption is only lower than the one of a dividing wall column with the same total stage number for systems with an ESI below one.
In order to evaluate which setup is best suited considering the two-dimensional solution range, the Decision Numbers are calculated for the optimization and approximation results (method according to Equation 4.11) from Figure 4.18. Also, similar calculation are performed for several systems obtained at a higher purity of 98 mol %. The results are shown in Figure 4.19.

The observations for the data set of 95 mol % matches the ones derived from the

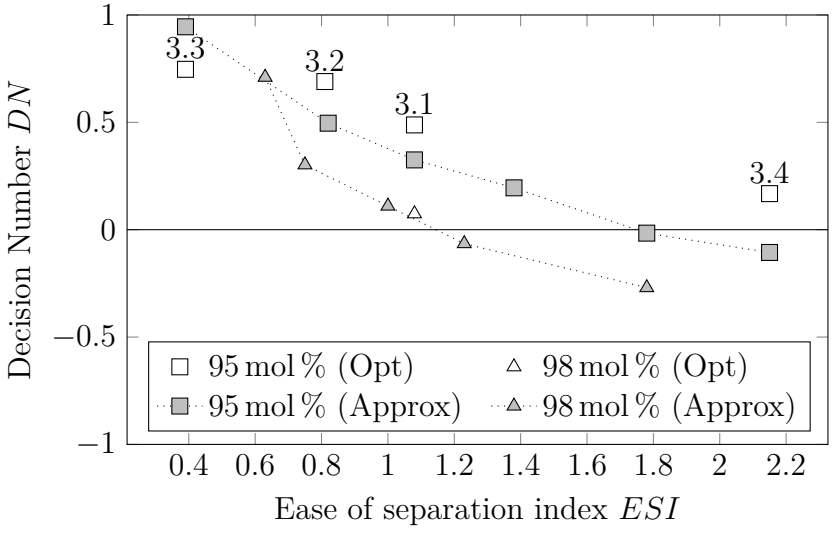

Figure 4.19: Decision Number of dividing wall column in comparison to direct split sequence for different systems (indicated by the labels) and product purities (similar for all product flows) (Approx1 - Approx6 for 95 mol %, Approx7 - Approx11 for 98 mol %).

intersection values in Figure 4.18. For low ESIs the dividing wall column is the more beneficial option. If the ESI is increased, the location of the intersection shifts to the disadvantage of the dividing wall column. However, up to ESIs of around 1.8, the dividing wall column is overall still better suited than the direct split sequence. This

border shifts to lower ESIs if higher product purities are necessary. The approximation shows, that the direct split sequence gets more beneficial for 98 mol % pure products and ESIs above 1.1. The impact of the product purity specification on the $N\dot{Q}$ optima intersection has already been discussed in more detail in Section 4.4.2.1.
A similar calculation procedure is applied in order to compare the dividing wall column with the indirect split sequence. The resulting Decision Numbers for different mixtures split into 95 mol % and 98 mol % pure products in both distillation options is shown in Figure 4.20. In comparison to the indirect split sequence, the dividing wall column gets

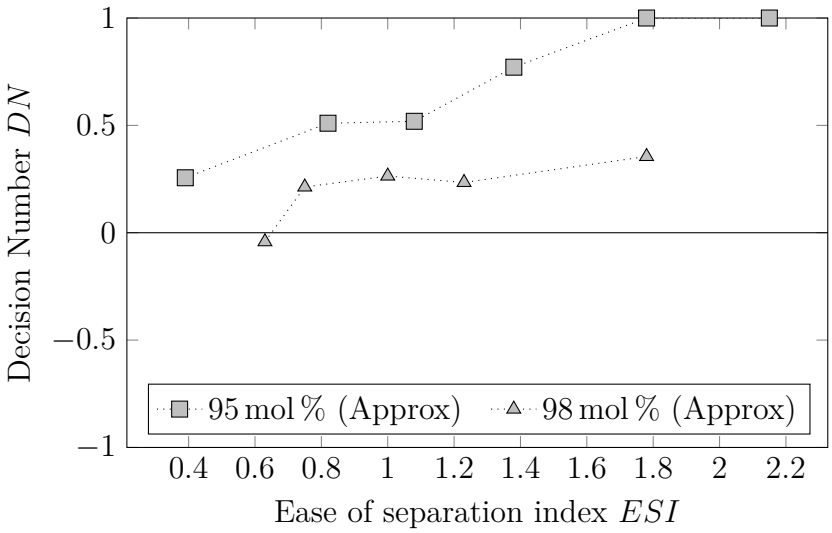

Figure 4.20: Decision Number of dividing wall column in comparison to indirect split sequence for different systems and product purities (similar for all product flows) (Approx1 - Approx6 for 95 mol %, Approx7 - Approx11 for 98 mol %).

more beneficial for systems with higher ESIs. At ESIs above 1.8, the Pareto-fronts do not even intersect anymore. This development is reversed in comparison to the direct split sequence from Figure 4.19. However, the observation that the DN decreases for increasing product purities still applies.
Summarizing, the dividing wall column is more beneficial compared to the direct split sequence in a broad range, especially for low ESIs. At very low ESI values, it may even happen that there is no longer an intersection of the $N\dot{Q}$ curves and thus the dividing wall column is more suitable in the entire operating range. For very high ESIs the direct split sequence is advantageous, the exact ESI of the transition mainly depends on the product purity specification. An opposite effect is found in comparison to the indirect split sequence. Then, the dividing wall column gains suitability for systems with higher ESIs.

4.4.2.3 Impact of feed stream composition

Last, the impact of the feed stream composition on the Decision Number of the dividing wall column in comparison to the direct and indirect split sequence is investigated. As it

additionally depends on the system, whether one or another column sequence is better suited, a comparison between the direct and indirect sequence is performed as a first step. For the study the systems 3.1 and 3.3 are chosen at 95 mol % product purities. The feed stream composition is varied according to Approx17-28 and Approx29-40 from Table A.14 in the appendix (Section A.5). The investigation is performed in a composition ranges down to 10 % of each component. Below, the mixtures are close to be binary and thus a dividing wall column is not recommended.
First, the results for system 3.1 are shown. This system has a higher BC than AB peak in the $\dot{V}_{min}$ diagram (see Section 3.5). In order to evaluate, whether the direct or indirect split sequence is the better option for a column sequence in the whole feed composition range, Figure 4.21 shows the Decision Number of these options depending on the initial molar fractions of the components (indicated by black dots) in a ternary diagram. In the case DN equals one, the direct split sequence totally dominates the indirect sequence. Thus, the Pareto-fronts do not intersect. The opposite applies for a DN of -1.
In a large feed composition range the DN is one, thus the direct split totally dominates

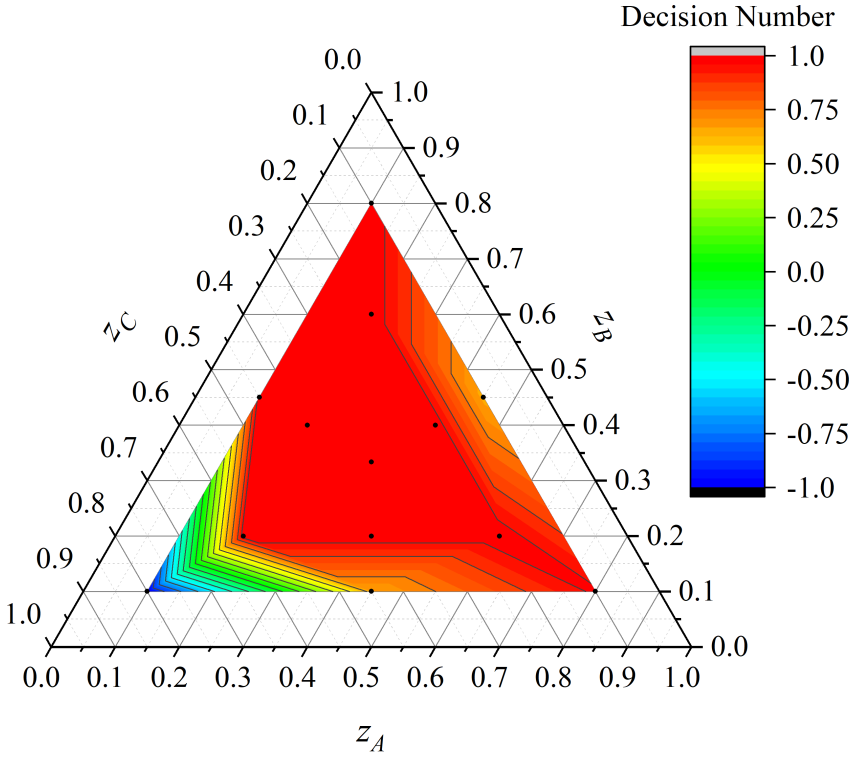

Figure 4.21: Decision Number of systems 3.1 in a direct vs. indirect split sequence for product purities of 95 mol % and different feed stream compositions from approximation (for method see Section 4.3). Data sets Approx3 and Approx17 - Approx28.

the indirect split sequence. However, for large fractions of component C, the Pareto-fronts intersect and thus the DN is below one. For component C with 80 mol % in the feed stream, the indirect split sequence totally dominates. Nevertheless, for

the comparison with the dividing wall column, the direct split sequence is chosen. Figure 4.22 shows the Decision Number of system 3.1 in the dividing wall column in comparison to the direct split sequence.

In a relative broad range the Decision Number is at around 0.3, thus the Pareto-fronts

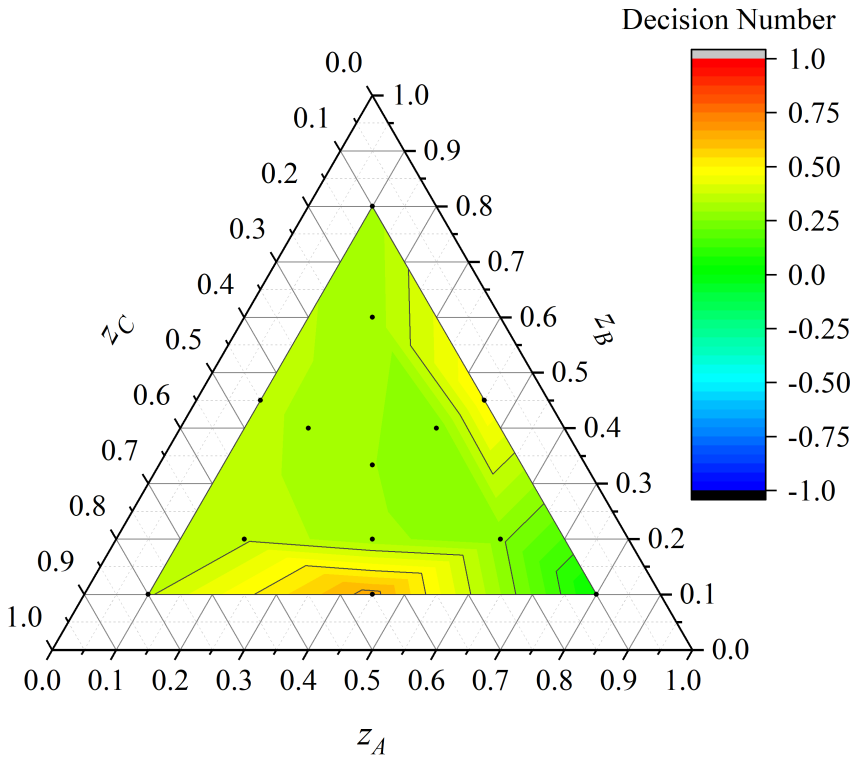

Figure 4.22: Decision Number of systems 3.1 in a dividing wall column vs. direct split sequence for product purities of 95 mol % and different feed stream compositions from approximation (for method see Section 4.3). Data sets Approx3 and Approx17 - Approx28.

intersect but the range in which the dividing wall column is more advantageous is larger than the one of the direct split sequence. A slight decrease is observable for high molar fractions of component A. In contrast to that the Decision Number increases slightly for low amounts of B in an equimolar mixture of A and C or low fractions of C in equimolar mixtures of A and B. However, it can be concluded that there is no significant effect of the feed stream composition on the Decision Number of the dividing wall column in comparison to the direct split sequence for system 3.1.

Similar calculations are repeated with system 3.3. For the mixture the AB split requires more energy than BC according to the $\dot{V}_{min}$ diagram (see Section 3.5). Again, as a first step the direct and indirect split sequence are compared for the whole feed composition range. Again the DN is defined in a way, that positive values denote the advantage of the direct and negative of the indirect split sequence.

For this system negative DNs dominate. Especially for low fractions of component A the indirect split clearly is better suited than the direct one. With increasing amount of component A in the feed stream, the direct split gains suitability up to the point where

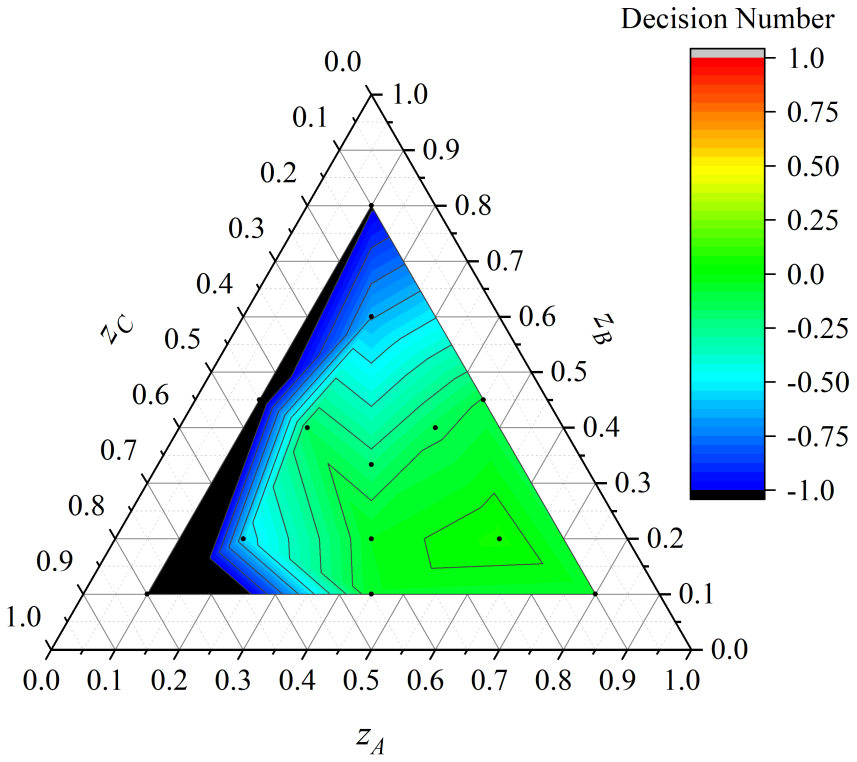

Figure 4.23: Decision Number of systems 3.3 of direct vs. indirect split sequence for product purities of 95 mol % and different feed stream compositions from approximation (for method see Section 4.3). Data sets Approx1 and Approx29 - Approx40.

both options are equally appropriate. Even though the indirect split sequence does not dominate as strong as the direct one for system 3.1, it is chosen for a comparison to the dividing wall column. Figure 4.24 shows the DN of the DWC in comparison to the ISS for system 3.3.

Similar as in Figure 4.22 the DN is relatively constant at 0.3 with a slight decrease for high fractions of component A. Correspondingly, only a very low increase of the suitability of the dividing wall column for increasing molar fraction of component B is found. This observation is not in line with the statement that dividing wall columns are increasingly more suitable with a higher fraction of middle boiling component in the feed stream. However, this statement is often based on the assumption of an infinite stage number [7]. In this work, the stage number was considered as additional dimension for the quantification of the energy saving potential. Correspondingly, it can be concluded that not all observations from an operation at an infinite stage number also apply for the minimum stage operation.

Summarizing, dividing wall columns are the more beneficial process option in a broad operating range of feed compositions. However, even though the Decision Number is positive in most cases it should be kept in mind that the Pareto-optimal $N\dot{Q}$ curves of the column sequences and dividing wall column intersect resulting in the DNs below

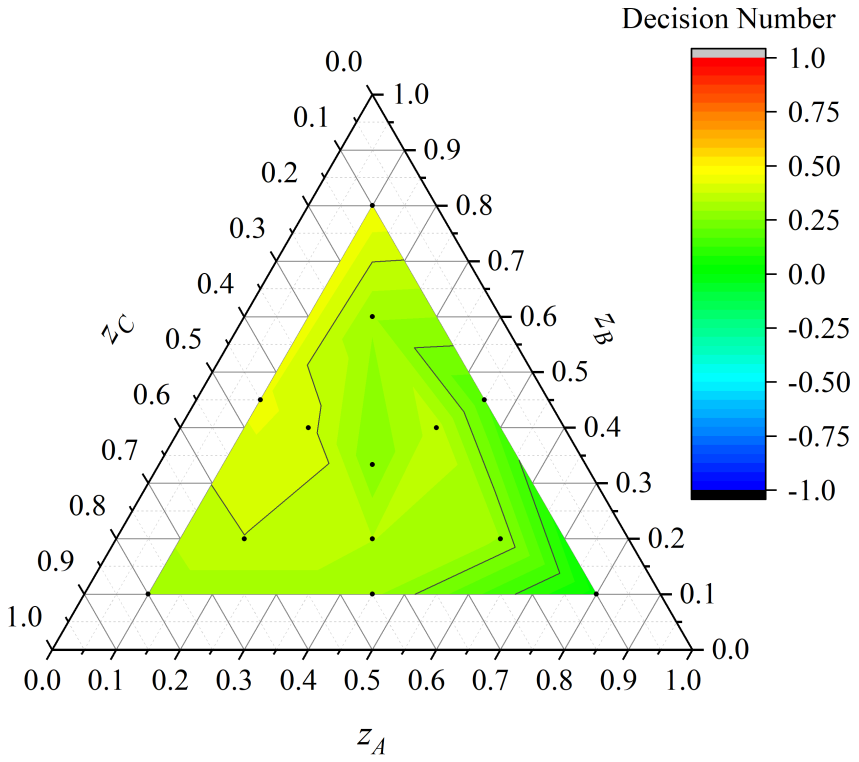

Figure 4.24: Decision Number of systems 3.3 in a dividing wall column vs. indirect split sequence for product purities of 95 mol % and different feed stream compositions from approximation (for method see Section 4.3). Data sets Approx1 and Approx29 - Approx40.

one. Thus, for strong limitations of the number of theoretical stages conventional column sequences are in most cases the better option.

4.4.3 Simplified multiple dividing wall column

Also for the quaternary system 4.1, a conventional column sequence should be compared to the simplified multiple dividing wall column. For a conventional column sequence there are four options since three columns are used one after another. The suited combinations are direct-direct, direct-indirect, indirect-direct or indirect-indirect. All have the a similar minimum stage number according to Fenske but the minimum energy demand is different, which can be estimated with the help of $\dot{V}_{min}$ diagram. The calculation results in the sequence direct-direct to require least energy. Thus this sequence is used for an $N\dot{Q}$ optimization for at least 98 mol % pure products. The results are compared to the ones for the simplified multiple dividing wall column in Figure 4.25. Note that the results for the smDWC are the same as in Figure 4.9.
The differences between the two extreme points minimum stage number and minimum energy demand are significantly larger compared to the conventional three product dividing wall column and the direct split. The intersection factor is reduced to $1.08 \cdot N_{min}^{mDWC}$ of the multiple dividing wall column or $1.51 \cdot N_{min}^{DSS}$ of the column sequence. The Decision Number is at 0.3 and thus the multiple dividing wall column is overall better suited than the split sequence. This validates the high potential of multiple dividing wall columns to reduce energy consumption over a broad operating range.
In this context note that the multiple dividing wall column with three dividing walls most likely has a higher total minimum stage number than the smDWC while the same minimum energy demand is needed. A higher minimum stage number results from the fact that additional stages have to be provided for the AD split. A similar minimum energy demand is predicted by the $\dot{V}_{min}$ diagram. Consequently, it can be expected that for this kind of column the intersection is located at higher total stage numbers. Consequently, the Decision Number would be lower.

For higher product purity constraints, the intersection can be assumed to be shifted to higher total stage numbers. Additionally, the observation from Section 4.4.2, that the intersection factor of the curves stays same, can also be assumed to be valid. Note that the full optimization like the one of the mDWC in Figure 4.25 are very time intensive (two to three weeks) and thus those are only performed for one system.

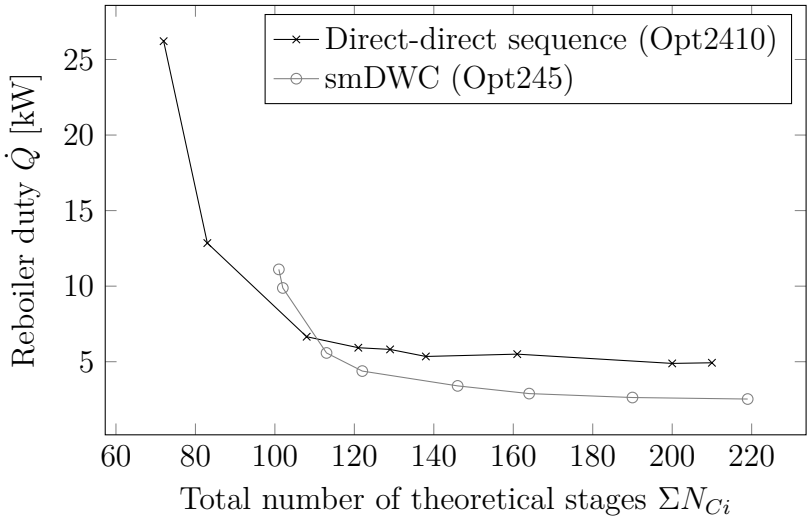

Figure 4.25: $N\dot{Q}$ optima for the quaternary system 4.1 in a simplified multiple dividing wall column and direct split sequence to reach 98 mol % pure products.

4.4.4 Pilot plant of simplified multiple dividing wall column

In this section the energy saving potential of the multiple dividing wall column pilot plant at Ulm University (see Section 2.1.2) is investigated for all quaternary systems presented in Section 3.5. From Figure 4.10 in Section 4.2.2.2 it gets clear that the overall energetic minimum might not reachable for all systems due to a non-optimal uniform stage allocation in the column sections. Accordingly, also the energy saving potential stated in the previous section cannot be totally exploited. The suitability of the stage allocation in the pilot plant for all systems is summarized in Table 4.2. First, the total minimum stage number for all systems to reach 98 mol % pure product is shown, for system 4.1 also for higher purities. Additionally, the ratio n, describing the relation of the actual stage number divided by the minimum one is shown for the whole column and all product splits. Note that the minimum stage number is estimated with the Fenkse equation as described in Section 4.3.3.

For all systems at 98 mol % the total stage number of 220 set in the pilot plant is relatively high ($n_{column,i} \geq 1.6$) and thus energy savings can still be expected. However, it also gets clear that the stage allocation is not equally suited for all systems, which is illustrated by the standard deviation σ of all n_i. The lowest standard deviation is observable for systems 4.1 and 4.4, closely followed by 4.3. Higher deviations are found for the systems 4.6, 4.5 and 4.2, where the last one shows the highest value. This is an important fact which should be kept in mind for the following evaluations. It should also be noted that while higher purity requirements result in a higher minimum number of stages, the optimum stage allocation and thus also the standard deviation of the pilot plant remains almost the same.

Again bi-objective optimizations are performed to determine the $N\dot{Q}$ optima of all systems in the pilot plant. Even though a uniform stage allocation is set, the chosen packings inside the column could be replaced resulting in another total stage number.

Table 4.2: Minimum stage number for quaternary systems calculated with Fenske equation (all products at 98 mol %), n_i of product splits in pilot plant and their standard deviation σ.

System	Product purities [mol %]	N_{min}	n_{column}	n_{BD}	n_{AC}	n_{AB}	n_{BC}	n_{CD}	$\sigma(n_i)$
4.1	98	99	2.2	2.5	2.4	3.3	1.7	1.8	0.7
4.1	99	115	1.9	2.1	2.0	2.9	1.5	1.6	0.5
4.1	99.8	141	1.6	1.9	1.8	2.2	1.1	1.2	0.5
4.2	98	77	2.9	2.9	4.0	6.7	1.9	2.1	1.9
4.3	98	122	1.8	1.9	2.2	3.3	1.3	1.4	0.8
4.4	98	58	3.8	5.0	3.3	3.6	3.3	3.6	0.7
4.5	98	82	2.7	3.5	3.3	3.6	3.6	1.3	1.0
4.6	98	71	3.1	3.8	3.3	4.0	3.6	1.8	0.9

Accordingly, the total stage number is considered as optimization variable even though the allocation is set. Additional optimization variables are the estimated vapor and liquid splits, product flows and reboiler duty. All results for systems 4.1 to 4.6 are summarized in Table 4.3. Additionally, energy saving E_i^j (Equation 3.4 in Section 3.4) of the pilot plant compared to a direct-direct split sequence at 220 optimally allocated stages is also shown in the table. Note that the energy savings are partly based on linear interpolation. This is caused by the optimization routine, which calculates only the minimum required number of Pareto-optimal compromises between the objectives, here N and $\dot{Q}$ (see Section 3.2). Thus, in some cases no energy demand is available for 220 stages of the pilot plant. In this case, the corresponding energy demand is determined by an linear interpolation between the two compromises closest to this stage number. Note also that the data for system 4.1 has already been presented in Figure 4.10 (data set "N_{Ci} all same and N_{C32} double") and Figure 4.25 (data set "Direct-direct sequence").

All tested mixtures can be separated in the pilot plant according to the specified product purities. It should be noted that the overall Decision Number of the pilot plant for system 4.1 is reduced to -0.04 compared to 0.3 for an optimized stage allocation (Section 4.4.3), accordingly considering the whole feasible operating range, the direct-direct split sequence and the multiple dividing wall column pilot plant are equally suited. This behavior is caused by the non-optimal allocation of the theoretical stages in the column sections.

For system 4.1 the impact of the product purity specifications can be seen. For increasing product purity specifications the location of the $N\dot{Q}$ optima intersection is shifted towards higher total stage numbers, additionally it is observable that the Decision Number decreases, similar as in Figure 4.17 for the simple dividing wall column. Correspondingly, the energy savings of the pilot plant in comparison to a conventional split sequence decreases for increasing product purities. For high purities around 99.8 mol %, no more savings can be expected since the intersection is located at

Table 4.3: Bi-objective optimization results of several systems in the multiple dividing wall column pilot plant (PP). *Based on linear interpolation.

System	Product purities [mol %]	$N\dot{Q}$ intersection			Properties of PP		Run number Opt...
		N_{is} [−]	$\dot{Q}_{is}$ [kW]	DN [−]	$\dot{Q}_{opt}^{PP}$ [kW]	E_{DSS}^{PP} [%]	
4.1	98.0	141	5.35	-0.04	2.68	45.6	2410 & 246
4.1	99.0	180	5.22	-0.34	3.13*	35.8*	2411 & 2412
4.1	99.8	265	5.59	-0.35	5.79*	-103.8*	2413 & 2414
4.2	98.0	160	4.3 3	-0.37	2.56	37.6*	2415 & 2416
4.3	98.0	144	5.14	-0.12	2.74	40.0*	2417 & 2418
4.4	98.0	87	2.67	-0.12	1.32*	42.8*	2419 & 2420
4.5	98.0	144	3.07	-0.56	2.30	22.4*	2421 & 2422
4.6	98.0	136	3.19	-0.41	2.10*	28*	2423 & 2424

a stage number higher than 220.
All other systems are only optimized at 98 mol % pure products. Even though all Decision Numbers are negative, thus considering the whole solution range the direct split sequence is more beneficial, the pilot plant still saves significant amounts of energy. This can be explained with the fact, that the total stage number of the pilot plant is significantly higher than the stage number, at which the Pareto-optimal solutions of the pilot plant and the column sequence intersect. However, for all systems different total energy savings are found, which can mainly be explained with the thermodynamic properties of the mixtures. Figure 4.26 presents the total energy saving from Table 4.3 in dependence on the ESI differences (Equation 2.11 in Section 2.1.3.2) of the systems. This plot is chosen since the difference in the two ESIs of quaternary systems gives information about their optimal stage allocation inside the column. The corresponding stage relations are also indicated in the diagram. The systems at negative difference of the ESI in the upper part of the column minus the one in the lower part require similar stage numbers for the AB and BC splits and significantly less for CD. These show relatively low savings due to the fact, that the equal stage allocation provides "too much" stages in the upper part of the column for the AB and BC split, which has already been presented in Table 4.2. Correspondingly, the column has much more stages than required and the saving compared to a totally optimized direct split sequence is reduced. Systems with an ESI difference in the range 0 to 0.5 show higher savings above 40 %. If the stage requirements for AB is below the one of BC and CD, which are almost equal, the ESI difference is positive. Consequently, for differences above 0.5 the saving decreases again but less pronounced than for negative differences. This arises from the fact that only two sections instead of four have too many theoretical stages. However, it should be noted that for all tested systems one of the ESIs is close to one, thus two of the three sharp product splits require almost the same stage numbers. Nevertheless, there could also be systems, for which this does not apply and thus the

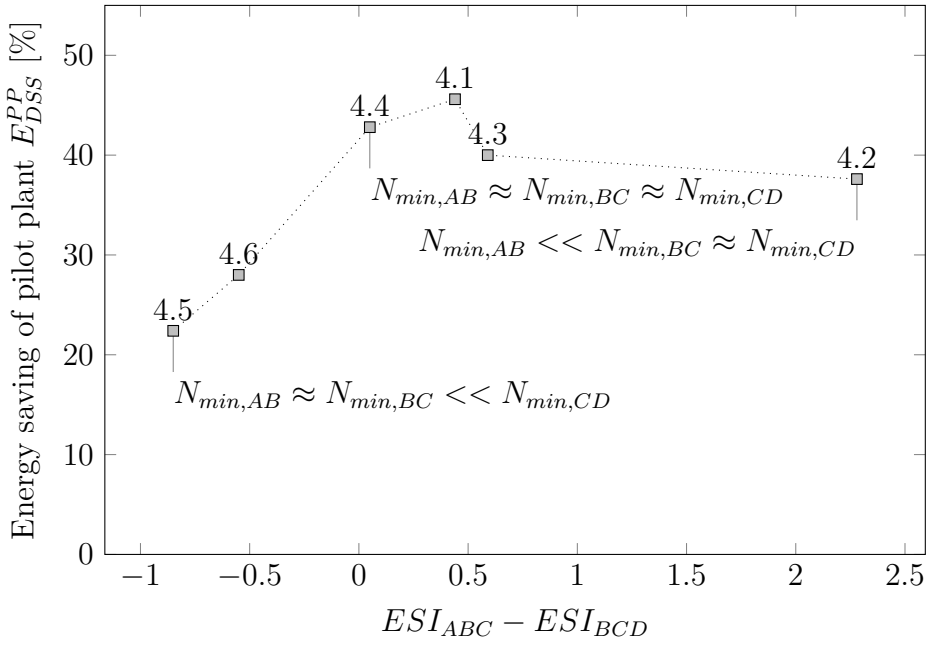

Figure 4.26: Development of energy saving of the pilot plant compared to the direct-direct split sequence depending on ESIs of systems for 98 mol % pure products. A similar development is observable plotting the Decision Number instead of the energy savings.

trend could be different from the one in Figure 4.26. Additionally, the simplified version of the multiple dividing wall column which is used for the pilot plant is not suited for all quaternary systems and thus some are neglected in the analysis. These are systems requiring $N_{min,AB} > N_{min,BC} \leq N_{min,CD}$ ($ESI_{ABC} < 1$ and $ESI_{BCD} \leq 1$).
Summarizing, due to the high total stage number the pilot plant offers high energy savings for a broad range of systems and purities. Highest savings can be expected if the second ESI is around one and the first ESI in the range of 1 to 1.5. Then, the uniform stage allocation is almost optimal for the system. If the stage allocation deviates strongly from the optimum one, the saving potential is reduced.

5 Results part II: Operational flexibility close to the optimum

As already discussed in section 2.2, several combinations of the liquid and vapor split can be expected to result in exactly the same product quality for one energy input and thus the same optimally operated column. This can also be read from $\dot{V}_{min}$ diagrams (Section 2.1.3.1). Assuming that the requirement of a column is to reach a minimum and no exact product purity, depending on the systems a relatively large range of the vapor and liquid split could be used in operation. This behavior is in this work denoted as flexibility. If a column is operated outside this flexibility range, the product specifications are not reachable anymore. However, to the best of the authors knowledge no study was published investigating this flexibility close to the energetic optimum of the column in the context of the chosen column design in depth. Note that the term "close to" the optimum is used instead of "at". This can be explained with the fact that distillation columns are usually not operated at the energetic minimum but with slightly higher energy input. Correspondingly, "close to" the energetic optimum can be described with a factor above one being multiplied with the optimal value. This factor is always given for the following calculations.
The objective of this section is to evaluate the effect of several column variables on the shape and size of the flexibility region of the liquid and vapor split. These investigations are partly performed for a simple and partly for the multiple dividing wall column pilot plant (see Section 2.1.2). However, all results also apply for other versions of dividing wall columns.
All calculations in this chapter are based on the method from Section 3.3. The following sections are organized as follows. First, the impact of the distance from the energetic minimum is investigated in Section 5.1. Afterwards, the impact of the total stage number and a non-optimal stage allocation in the column sections is studied in depth in Section 5.2. Here, additionally a new shortcut approach is introduced to enable the estimation of suitable vapor and liquid splits for dividing wall columns with finite stage numbers (Section 5.2.3). Then, the effect ofthe specified product flows (Section 5.3) and feed composition disturbances on suited split ranges is studied in Section 5.4. Last, the flexibility of different systems in the multiple dividing wall column pilot plant at Ulm University is presented in Section 5.5.
A list of all performed screenings can be found in the supporting material [62], the corresponding loop number can be found next to each diagram. Note that the notation is according to the principle "Scr31", Scr stands for screening, the first number for the number of components and the following ones are loop numbers.

5.1 Impact of distance to energetic minimum

In this section the impact of the distance to the energetic minimum is evaluated. Section 5.1.1 focuses on simple dividing wall columns. Afterwards, in Section 5.1.2 a similar but much more detailed analysis is performed for a smDWC. The second section is described more extensively, since most of the contend has not yet been published in detail elsewhere.

5.1.1 Simple dividing wall column

Suited vapor and liquid split ranges of system 3.1 to reach 95 mol % pure products in a simple dividing wall column are investigated at 40 stages in total ($n = 1.8 \cdot N_{min}$) and an optimal stage allocation in the column sections (from Figure 4.13c). The resulting split ranges for different distances to the corresponding energetic minimum are shown in Figure 5.1. The corresponding energetic optimum ($\dot{Q} = 1.0 \cdot \dot{Q}_{opt}$) can already be

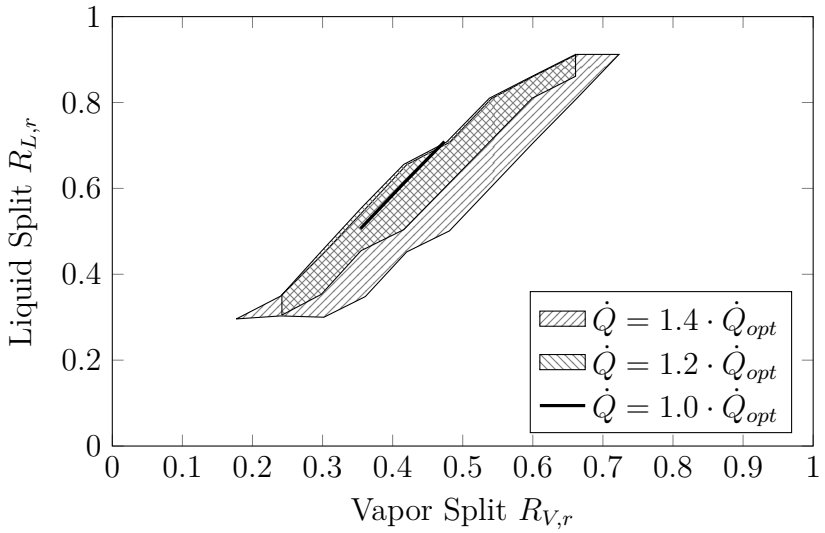

Figure 5.1: Split flexibility of system 3.3 in optimally designed dividing wall column (95 mol % pure products, $\Sigma N_{Ci} = 40$) (Scr31).

reached with several combinations of the liquid and vapor split which are located on a straight line with positive slope. This behavior can be understood imagining the prefractionator of the dividing wall column as normal distillation column with a reboiler and condenser. If in that case a certain amount of vapor is produced, the resulting reflux stream is set for the product specifications. This theoretically needed reflux stream also has to be provided in the dividing wall column, which is adjusted by the liquid split to the prefractionator. Thus, there is one optimum liquid split for every vapor split and the relation is linear with a positive slope. If more vapor (energy) than necessary is provided, the linear dependency widens into a field, in which several liquid splits are suited for one vapor split. This behavior is also stated in literature for an infinite stage number [36].

5.1.2 Multiple dividing wall column pilot plant

A similar investigation is performed for the simplified multiple dividing wall column pilot plant at Ulm University (for a description of the pilot plant see Section 2.1.2). First of all it should be noted that the pilot plant is designed to be flexible for different mixtures. Thus the stage number in all column sections is equal (despite section C32). Accordingly, the stage allocation in the column sections is non-optimal for some systems, and the following Section 5.2 should also be considered.
There is little literature on the flexibility of multiple dividing wall columns. Accordingly, in this paragraph first the flexibility in such a column is explained on the basis of $\dot{V}_{min}$ diagrams. The vapor and liquid split ranges resulting from the $\dot{V}_{min}$ diagram are valid for columns fulfilling the considered assumptions, namely an infinite stage number, constant relative volatilities and molar flows, sharp product splits and an operation at the corresponding minimum energy demand. Afterwards, the knowledge is applied to analyze screening results of rigorous flow-sheet simulations neglecting these assumptions.
As already stated, the first step to understand the flexibility in a multiple dividing wall columns is understanding the $\dot{V}_{min}$ diagram. In contrast to the simple dividing wall column for ternary feeds, the diagram for quaternary feeds shows not just one peak that can be shifted to the value of the highest one but two. Accordingly, the behavior is more complex than for three component systems. In Figure 5.2 the possible peak shifts of system 4.1 are shown [130].

The first option in Figure 5.2a is the original $\dot{V}_{min}$ diagram as already presented in Figure 3.5, which limits the split ranges in one dimension. Starting from here, several options are available changing the vapor and liquid splits without increasing one peak above the highest one of CD and thus also the total vapor demand of the split. Either only the AB peak can be increased (Figure 5.2b) or only the BC peak (Figure 5.2c). Last, both peaks can be shifted to the minimum vapor demand of the CD split (Figure 5.2d). Note that obviously during operation of such a column AB, BC and CD are always at the same height. However, the sharp splits with intermediate boiling components, thus AC and BD, can be operated at all intermediate solutions from option 1 to 4 resulting in a relatively broad operating window. This is indicated by the dark areas in Figure 5.2d. It can be concluded, that the vapor and liquid split ranges for the column C2, in which the AC separation is performed, are relatively broad since the optimality region is an area and not only a line. Especially the vapor split can be operated in a relatively wide range which is advantageous for a stable operation. The optimality region for column C3 performing the BD split is significantly smaller and only located on a line.
The pilot plant is also suited for systems having the BC peak in the middle of the $\dot{V}_{min}$ diagram as the highest one. In that case the AC split also has an optimality region lying on a line and no more in an area. Accordingly, for these systems the flexibility can be expected to be lower than for systems with the CD peak as highest one.
However, it should still be kept in mind that these observations based on the $\dot{V}_{min}$ diagrams only approximate the real behavior of a system sufficiently, if the relative

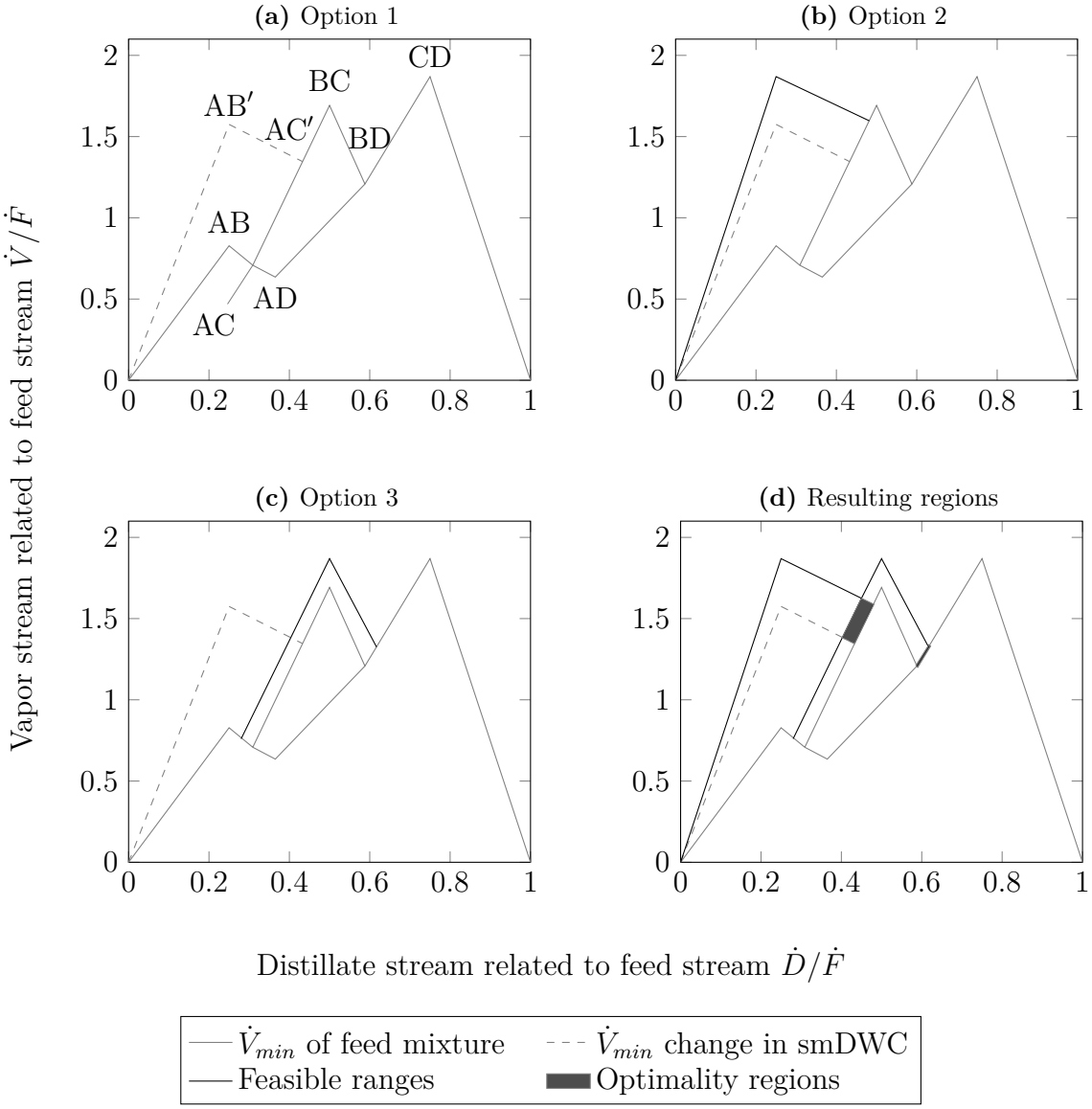

Figure 5.2: Derivation of optimality regions of system 4.1. [130]

volatilities of the components inside the column are almost constant and the stage number approximates an infinite one. Thus, for strongly non-ideal behavior, performing a rigorous screening with a flow-sheet simulator is unavoidable. For the quaternary systems investigated in this work stronger non-ideal behavior is observable in the presence of butanal and methyl acetate. The behavior of system 4.1 is relatively ideal, accordingly to validate the knowledge from the $\dot{V}_{min}$ diagram it is chosen for a screening run.

The minimum energy of the system in the pilot plant is around 2.7 kW (see Section 4.1.2). Three screening runs are performed at $\dot{Q} = 2.8\,\text{kW} = 1.04 \cdot \dot{Q}_{opt}$, $\dot{Q} = 3\,\text{kW} = 1.12 \cdot \dot{Q}_{opt}$ and $\dot{Q} = 3.2\,\text{kW} = 1.19 \cdot \dot{Q}_{opt}$. Figure 5.3 shows the full screening results of the second

run in SOPPs. Note that for C3 an adapted liquid split is shown, which results from Equation 5.1.

$$R_{L,C2C3ad,l} = R_{L,C2C3,l} \cdot R_{L,C1C2,l} \tag{5.1}$$

The adapted liquid split shows how much vapor is fed from the main column C1 to the prefractionating column C3. From the plots it gets clear that the purity of component C

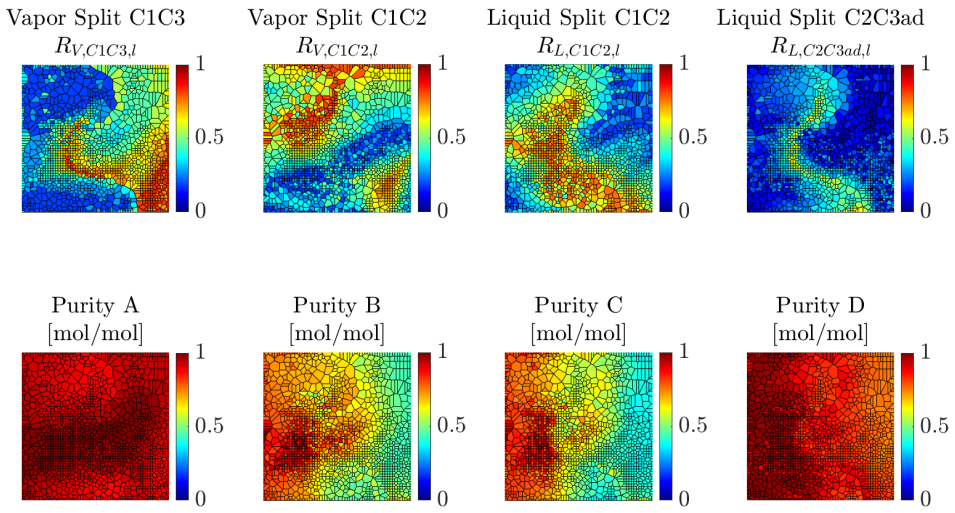

Figure 5.3: Full screening results for system 4.1 in the pilot plant at $\dot{Q} = 3\,\text{kW} = 1.09 \cdot \dot{Q}_{opt}$ for 98 mol % pure products (Scr42).

is limiting the flexibility, followed by component B. However, still there is a relatively large area in which all components can be obtained in high purities above 98 mol %. Similar trends are observable for the two other runs.

In order to get a better overview on suited split combinations, Figure 5.4 shows a two-dimensional projection of the results obtaining at least 98 mol % purity of all products for the three considered cases of different reboiler duties. This kind of projection which consists of two plots will also be used in the following sections. The first diagram (Figure 5.4a) shows the connection between the vapor and liquid splits to the prefractionating columns C2 and C3. Note again that the adapted liquid split is shown for column C3 (Equation 5.1). If the original liquid split $R_{L,C2C3,l}$ is shown instead, there is no such clear dependency. This again illustrates, that all four liquid and vapor splits inside the smDWC are correlated with each other. Thus, also the "vapor over liquid split"-fields for the columns C2 and C3 (from Figure 5.4a) are related to each other. For this reason, a second diagram is needed (Figure 5.4b) that shows another projection of the four-dimensional space. There, the corresponding required combination of the two vapor splits $R_{V,l,C1C2}$ and $R_{V,l,C1C3}$ is shown. Again, these two diagrams have to be read in combination and are not independent of each other. They just show different projections of the same solution space.

It can be seen that column C2 is more flexible in terms of liquid and vapor splits

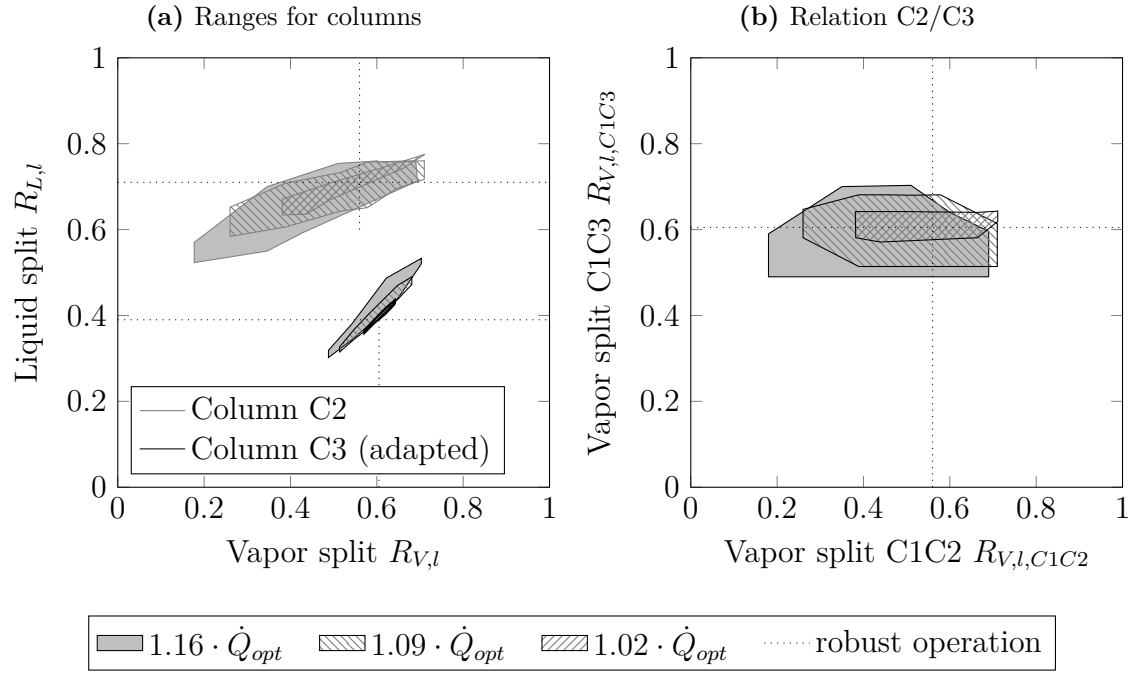

Figure 5.4: Suited vapor and liquid split ranges for system 4.1 in the pilot plant at $\dot{Q} = 3\,\mathrm{kW} = 1.1 \cdot \dot{Q}_{opt}$ and at least 98 mol % pure products (Scr41 - Scr43).

than column C3. This matches the theoretical observations from the $\dot{V}_{min}$ diagram of the system. Similar as for the simple dividing wall column the operation ranges of the split increase with increasing energy input and thus distance from the energetic optimum. Note that slight non-overlapping regions of the fields are probably resulting from the step size during the screenings. An interesting fact is in which direction the fields grow when the energy input is increased since this does not happen uniformly in all dimensions. The vapor split between the columns C1 and C2 only increases in the direction of lower split ratios to the left side of the dividing wall, while the vapor split between C1 and C3 increases in both directions. Similar observations are valid for the liquid splits. The adapted liquid split C2C3ad (Equation 5.1) is only extended to higher split ratios, while C1C2 increases uniformly. Based on this knowledge it can be concluded where the most stable operating point of such a column is located, which is indicated by the intersections of the black dotted lines in the diagram.

5.2 Impact of total stage number and allocation

In the following section, the correlation between the total stage number and the stage allocation in the column sections and the flexibility of a dividing wall column is investigated. This behavior has not been discussed in literature yet. For this purpose, first a relation is derived based on theoretical knowledge of $\dot{V}_{min}$ diagrams and optimal column designs in Section 5.2.1. Afterwards, the statements are validated with a rigorous flow-sheet simulation in Section 5.2.2. Last, based on the findings a new

shortcut approach to determine the vapor and liquid split flexibility for dividing wall columns with finite stage numbers is presented in Section 5.2.3.

5.2.1 Correlation on an theoretical basis

In order to derive a relation between the vapor and liquid split flexibility and the theoretical stage number in the column sections, the idea of $\dot{V}_{min}$ diagrams can be combined with knowledge about Pareto-optimal $N\dot{Q}$ compromises of distillation columns [131]. As already discussed in Section 2.1.3.1 the original $\dot{V}_{min}$ diagram, which can be used to determine the vapor and liquid split flexibility, is only valid at an infinite stage number inside the column and is applicable for dividing wall columns. Thus, the diagram is basically one extreme compromise of the $N\dot{Q}$ curve of such a column. Correspondingly, the $\dot{V}_{min}$ diagram could be expanded to a third dimension which represents the relative stage number n_i of each column region performing a certain product split. The result is a three dimensional version of the $\dot{V}_{min}$ diagram. Based on this diagram and the actual stage number in a column with finite stages, a projection back to the axis of the original $\dot{V}_{min}$ diagram can be performed. For this, the available stage numbers in the column regions performing a product split are divided by the corresponding minimum stage number resulting in the available n_i. The corresponding vapor demand for this split can then be determined and plotted similar to the original $\dot{V}_{min}$ diagram. In this stage-adapted $\dot{V}_{min}$ diagram adjusted vapor and liquid splits can be determined for finite stage numbers. In order to clarify the procedure, it is calculated in the following using an example system.
For the following calculations system 3.1 is used as feed to a simple distillation column. In the column three kinds of product splits can be performed which are either the AB, AC or BC split. For all three splits, the total number of theoretical stages N and the vapor demand $\dot{V}/\dot{F}$ are minimized by varying the feed stage location. As a constraint the recovery of the key distillate component is set to be above 99.9 mol %. The results are then plotted in a three dimensional version of the $\dot{V}_{min}$ diagram in Figure 5.5 on the left side. As already discussed above, the diagram also considers the dimension n_i which is the ratio of the stage number to the minimum one of each column region. Note that the Pareto-front ($\dot{V}/\dot{F}$ over n_i) of each product separation is continuous, but for clarity reasons only some cases of n_i the corresponding relation of $\dot{V}/\dot{F}$ over $\dot{D}/\dot{F}$ is shown. For the calculation of n_i the minimum stage number is estimated with the Fenske equation according to Section 4.3.3, resulting in 15 stages for AC, 16 for AB and 18 for BC. The original $\dot{V}_{min}$ diagram can be found at one end of the resulting Pareto-optimal curve at $n_i = 4$, which approximates an infinite stage number.
The general shape of the original $\dot{V}_{min}$ diagram, which is indicated by gray square markers at $n_i = 4$ in the left diagram from Figure 5.5, stays the same if the stage number is reduced optimally towards $N_{min,i}$, thus for $n_{AB} = n_{AC} = n_{BC} = n_{column}$. The only difference is that the total vapor demand increases with n_i for all splits. From the diagram the development of the liquid and vapor split flexibility to lower stage numbers can be calculated for an optimally stage allocation in the column regions

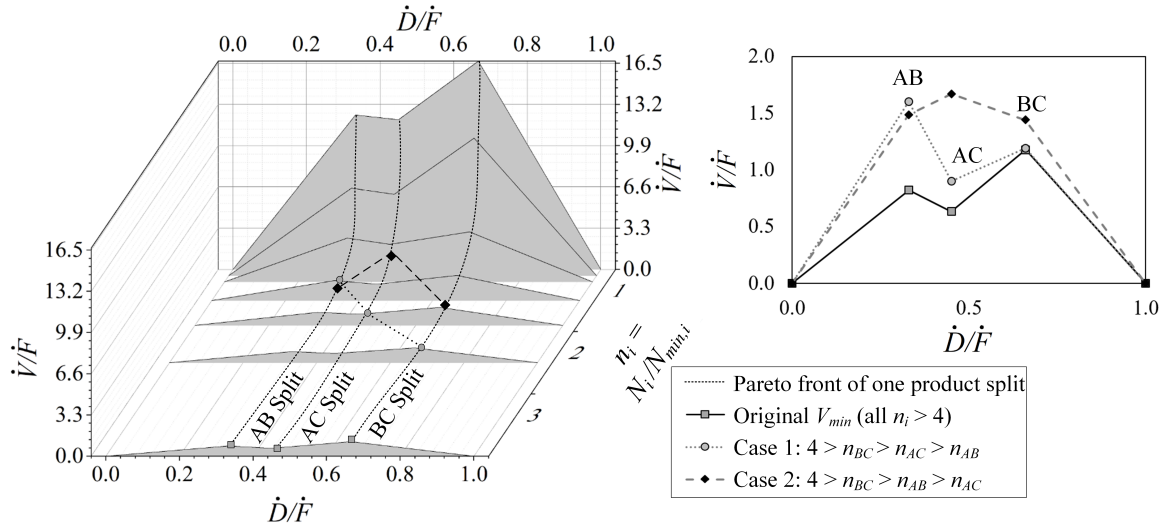

Figure 5.5: Three dimensional version of the $\dot{V}_{min}$ diagram and projection of three cases to the conventional two-dimensional plot. Note that the cases are indicated in the legend which is valid for both diagrams. [131]

($n_{AB} = n_{AC} = n_{BC} = n_{column}$). The results are shown in Figure 5.6. As already stated

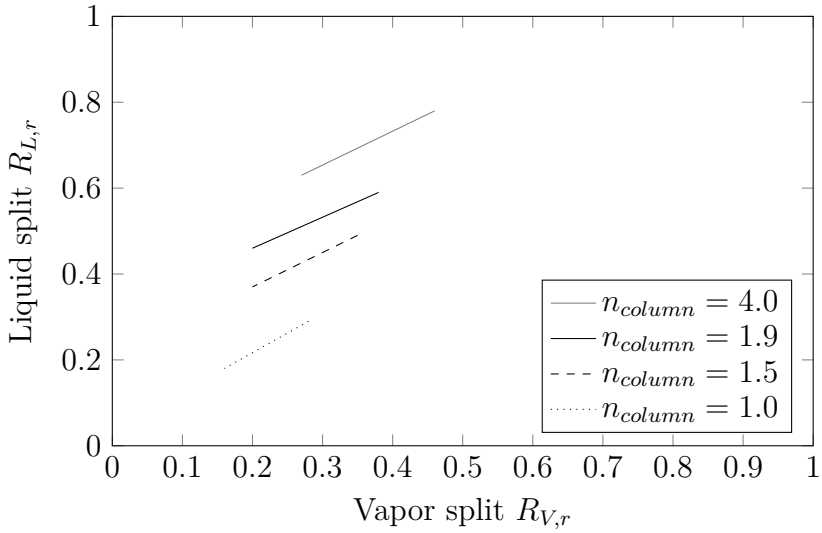

Figure 5.6: Development of split flexibility towards lower total stage numbers according to extended $\dot{V}_{min}$ diagram for $n_{AB} = n_{AC} = n_{BC} = n_{column}$.

in Section 2.1.3.1 a linear dependence of the liquid and vapor split is found with a positive slope. Proceeding to lower stage numbers and thus lower n_i results in the liquid split to decrease significantly while the vapor split has to be reduced only slightly. Thus, the optimal range of the liquid split is strongly dependent on the total stage number, even when an optimal stage allocation is used. Additionally, the slope of the lines changes where the slope is lower for higher n_{column}. Note that the development of the slope can be the opposite, if the AB peak is higher instead of the BC peak in the $\dot{V}_{min}$diagram. At this point it can already be concluded that the optimal range of liquid

and vapor splits of a column with optimally allocated stages depends on the total stage number of the column, or more precisely on the relative distance to the minimum total stage number.
An even more interesting aspect is, how the original $\dot{V}_{min}$ diagram changes for non-optimally allocated stages in the column regions responsible for certain product splits ($n_{AB} \neq n_{AC} \neq n_{BC}$), because this also gives information about corresponding changes in the vapor and liquid split flexibility. In order to emphasize this, two cases are indicated in Figure 5.5 in the left diagram. The corresponding projection of these points to a conventional visualization in a 2D-plot analogue to the $\dot{V}_{min}$ diagram (stage-adapted $\dot{V}_{min}$ diagrams) can be found in the diagram on the right side. Note that the same line types and symbols are used in both diagrams.
The first case (gray circles) assumes that n_{BC} has the highest value, followed by n_{AC} and n_{AB}. Accordingly, the number of theoretical stages for the AB split are closer to the minimum one than for BC. As a result, the vapor demand of AB increases to a higher value than the one of BC. If the stages are allocated in such a non-optimal way, an operation close to the minimum vapor demand of the totally used stage number is not possible, because the stages are basically located at the wrong location. However, considering the vapor and liquid split flexibility this is no big issue since again there is a significant difference in height between the AB and BC peak. Even though they lie in a different range than before, there is a relatively large flexibility of the splits. However, this operation is not the most energy efficient one for the total stage number.
The second case (black rhombus) represents a worst case scenario in a certain way, even though it is very unlikely that this will occur in a real plant for fluid dynamic reasons. BC still has the highest n_i, but now AC has a smaller n_i than AB. This results in all three splits having almost the same energy demand. This is problematic from several points of view. First, neglecting AC, it can be seen that the vapor demand of AB and BC is equal. This means that the splits would have to be run strictly at the optimum, there would be no multiple steady states and thus no flexibility in operation. Correspondingly, the flexibility has to be gained by additional energy input. Second, the AC split being the highest one would mean that the vapor split has to be at a fraction of zero since all produced vapor is needed in the prefractionator. Accordingly, such an operation is not realizable close to the stage related energetic optimum. An excess of vapor would be needed just to enable a stable operation also on the right side of the dividing wall.
Summarizing, the total number and distribution of theoretical stages within the different sections of a dividing wall column has an impact on the range of the optimality region. Especially if the total stage number comes close to the minimum one, slight deviations of n_i can cause strong changes in the vapor demand in each section and thus also on the flexibility of the liquid and vapor splits. Additionally, it is found that the optimal range of the liquid split is strongly dependent on the total stage number, it decreases with decreasing stage numbers while the suited interval width stays almost same. In order to validate this theoretically developed ideas, they are validated with rigorous flow-sheet simulation in the following section.

5.2.2 Validation with rigorous flow-sheet simulation

To validate the statements from the previous section a suited system has to be chosen. For system 3.1 and 3.3 a relatively high flexibility of the liquid and vapor split can be assumed from the $\dot{V}_{min}$ diagrams (see Section 3.5 and Figure 3.4) at an infinite stage number. Nevertheless, real columns have to be operated at a lower total stage number and thus the question is, whether the originally high flexibility can be maintained in any case. Mainly the impact of a stage allocation different to the optimum one should be evaluated. The optimized stage allocation for system 3.1 is almost uniformly distributed on column sections, while system 3.3 requires rather different stage numbers in the sections (see supporting material in [62]). As the objective of this section is to investigate the flexibility of a system in a non-optimally designed column, system 3.3 is chosen to be split in a dividing wall column with similar stages in all column sections, which could occur for a separation in a multi-purpose plant. Accordingly, it applies that $n_{AB} \neq n_{AC} \neq n_{BC}$ and the impact of a non-optimal stage allocation on the flexibility range can be evaluated.
The flexibility of the vapor and liquid splits are determined as described in Section 3.3, the product purities are afterwards set to be at least 95 mol %. Two cases for the stage allocation are compared. First, the optimum one resulting in the data points in Figure 4.13c (optimal stage allocation). Second, the stages in all column sections are the same (uniform stage allocation), which can be denoted as non-optimal for the system. In both cases, the product streams are fixed to the optimum ones at $\frac{\dot{D}}{\dot{F}_A} = 1.01$ and $\frac{\dot{S}}{\dot{F}_B} = 0.94$. The lowest energy demand for the screened stage numbers and allocations at which the product purities are reached are plotted in Figure 5.7 [131].

As expected for the optimum stage allocation almost the same result is found as

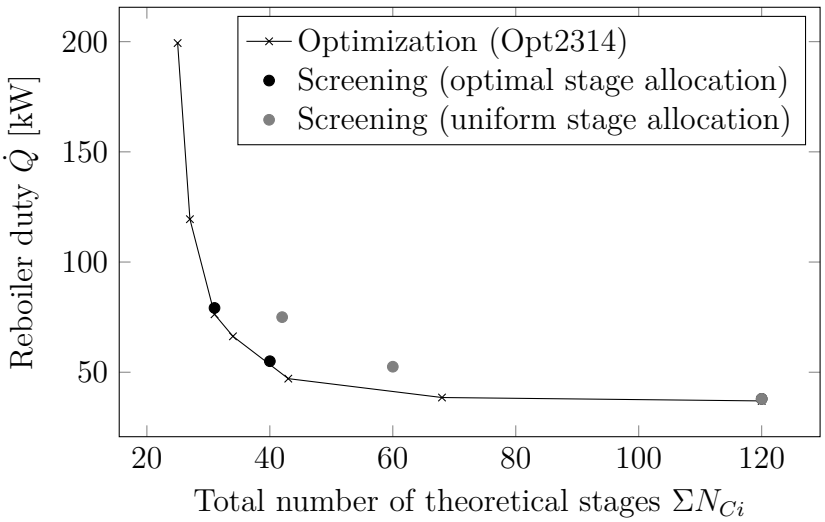

Figure 5.7: Minimum energy demand found during screening (determined by the step width) to reach 95 mol % pure products compared to optimization results from Figure 4.13c.

during the optimization, the results of the screening are only slightly higher due to the step width during screening. For the non-optimal uniform stage allocation the

energy demand increases. The reboiler duties from this diagram will in the following be denoted as $\dot{Q}_{opt}$ for a certain stage allocation. For the evaluation of the screenings, first the vapor and liquid split ranges at $\dot{Q} = 1.2 \cdot \dot{Q}_{opt}$ resulting in at least 95 mol % are plotted in Figure 5.8. Figure 5.8a shows the results for the optimum stage allocation

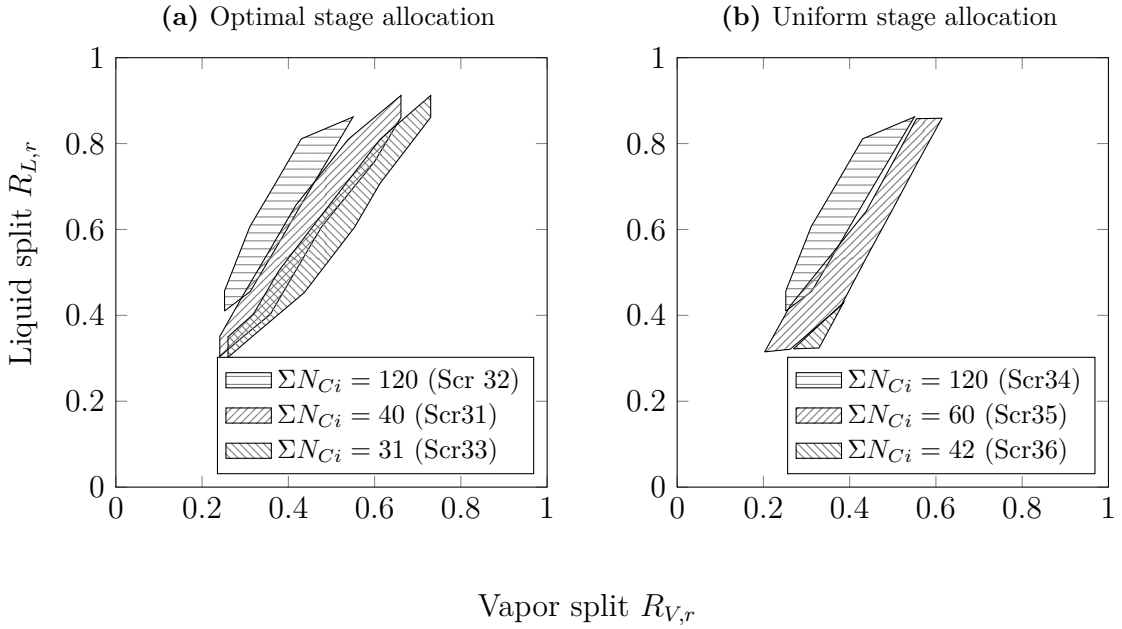

Figure 5.8: Correlation between liquid and vapor split for system 3.3 (at least 95 mol % pure products) at $\dot{Q} = 1.2 \cdot \dot{Q}_{opt}$.

inside the column. At 120 stages in total several suited combinations of the vapor and liquid split are found resulting in a field of flexibility. The dependency can be described with a positive slope. Proceeding to lower optimally allocated stage numbers results in an enlargement of the field which is slightly tilted resulting in a lower slope. Accordingly, the corresponding liquid split for one vapor split decreases compared to higher stage numbers. However, generally it is possible to maintain the flexibility of the liquid and vapor split at lower total stage numbers, assuming that the stage allocation is optimal. These screening results match the theoretical considerations from the previous Section 5.2.1, where it is observed that the liquid split will decrease with increasing stage number. Also, the slope change of the fields fits the expectations for systems with a higher AB peak. Only the development of the vapor split deviates. However, only small changes are expected which could probably not be described with the used step size of the screening. Also no simulations could be run at sufficient high liquid splits due to convergence problems of the flow sheet simulations. Since most of these observations can also be found in literature (see Section 2.2) the interesting question is, how this behavior changes, if the theoretical stages are not located optimally inside the column.

To answer this question, one can have a closer look on Figure 5.8b, which shows the vapor and liquid split ranges at a uniform and thus non-optimal stage allocation. Decreasing the stages from 120 to 60 results in a slight increase of the vapor split range, similar as for the optimal stage allocation. However, if the stages are reduced further

to 42, the flexibility range is shrunk significantly. For a better understanding of this behavior the data set at 40 stages and optimal allocation from the previous section in Figure 5.1 can be compared with the one at 42 stages and uniform allocation at different energy inputs, which is shown in Figure 5.9. First of all, the energetic minimum can

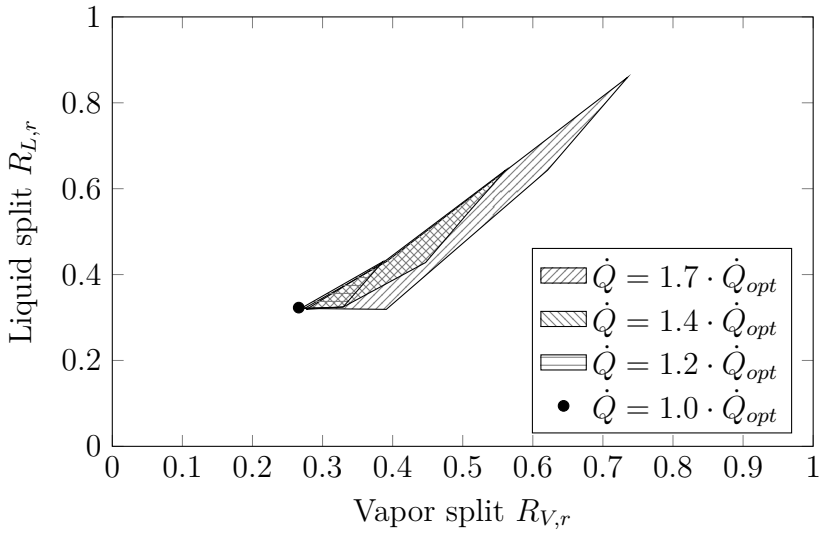

Figure 5.9: Correlation between liquid and vapor split for system 3.3 (at least 95 mol % pure products at uniform (non-optimal) stage allocation and $\Sigma N_{Ci} = 42$). Note in comparison Figure 5.1 in Section 5.1 for optimal stage allocation. $\dot{Q}_{opt}$ is defined as the optimum energy demand for the set stage allocations (Scr36).

no more be reached with a broad range of liquid and vapor splits but only in a very narrow region. Even though increasing the energy input also broadens the operating window, still the range is much smaller than for the optimal stage allocation. In order to reach a comparable flexibility range of the splits as for an optimal allocation at $\dot{Q} = 1.2 \cdot \dot{Q}_{opt}$, the reboiler duty has to be increased to 1.7 times of the minimum energy demand. This factor does not yet include the additional increase in energy demand found in Figure 5.7. All in all, the column with a non-optimal stage allocation but the same operating flexibility of the splits needs 229 % of the energy input that is required for the optimal allocation.

Summarizing, the flexibility of the liquid and vapor split can be maintained at lower stage numbers but are shifted, if the stages are allocated optimal in the column sections. However, the optimal range of the flow splits is shifted with a more pronounced effect on the liquid than on the vapor split. An non-optimal stage allocation can result in significant restrictions of the operating ranges with increasing effect for decreasing stage number. This restriction can only be compensated by a considerable increase in energy demand. Even though these observations are based on calculations in a simple dividing wall column they are assumed to be also valid for multiple dividing wall columns.

5.2.3 Shortcut approach to estimate flexibility ranges for finite stage numbers

In the previous sections it got clear that optimal vapor and liquid split ranges are shifting for lower total stage numbers. Correspondingly, the suitability of $\dot{V}_{min}$ diagrams to estimate internal streams to initialize flow-sheet simulations is reduced for non-optimal stage allocations and lower total stage numbers. The extent of the reduced suitability is shown with an example considering system 4.1 in a simplified multiple dividing wall column with 13 stages in all sections and 26 in section C32. The overall minimum stage number of the column to obtain all products in 98 mol % is 99, thus the assumed column has a stage factor of $n_{column} = 1.44$, which represents a usual column design. A flow sheet simulation of such a column is initialized with the vapor and liquid split ranges suggested by the original $\dot{V}_{min}$ diagram, which is shown in Figure 5.2 in Section 5.1. The resulting product purities for the four options are presented in Table 5.1. For all options the purities of the side draw products C and D are between $55-66$mol %. These low purities indicate that the $\dot{V}_{min}$ predicted liquid and vapor splits are not well suited as initial guesses for simulations. Consequently, an adapted method to estimate split ranges of column with finite stage numbers which can also be non-optimally allocated is presented in this section [130]. Note that the same example system and column is used in the following to explain the procedure.
The new method is based on the extended $\dot{V}_{min}$ diagram from Section 5.2.1. However, the diagram in the latter cited section is originally developed in combination with an optimization. In order to calculate the diagram without the need of a flow-sheet simulator and optimizer, the original $\dot{V}_{min}$ calculation can be combined with the $N\dot{Q}$ approximation method presented in Section 4.3. For the calculation, the following steps have to be followed. First of all, the original $\dot{V}_{min}$ diagram has to be calculated (see supporting material for the procedure [62]). Afterwards, for all splits i Equation 5.2 is applied, which is based on the approximation method from Equation 4.3 in Section 4.3.1. For this purpose also the minimum stage number of all splits has to be calculated according to Section 4.3.3. The minimum vapor demand of a product split, its minimum stage number and the available one in the corresponding column section are then inserted into Equation 5.2.

$$\frac{\dot{V}_i}{\dot{F}} = \frac{\dot{V}_{min,i}}{\dot{F}} \cdot \left(\frac{0.27}{\left(\frac{N_i}{0.97 \cdot N_{min,i}}\right)^2 - 1} + 1 \right) \tag{5.2}$$

As a result, the vapor demand in all column sections can be approximated with the knowledge of the relative volatilities of the feed stream, its composition and liquid fraction. The resulting stage-adapted $\dot{V}_{min}$ diagram of the column for the previously presented example is shown in Figure 5.10a. Due to the fact, that the BC and CD Peak are operated closer to their minimum stage number than the AB split, these peaks are increased much more pronounced. This also causes the BC peak to become the highest one for the operation in the considered column setup.

Based on this adapted $\dot{V}_{min}$ diagram of the system inside the column with set finite

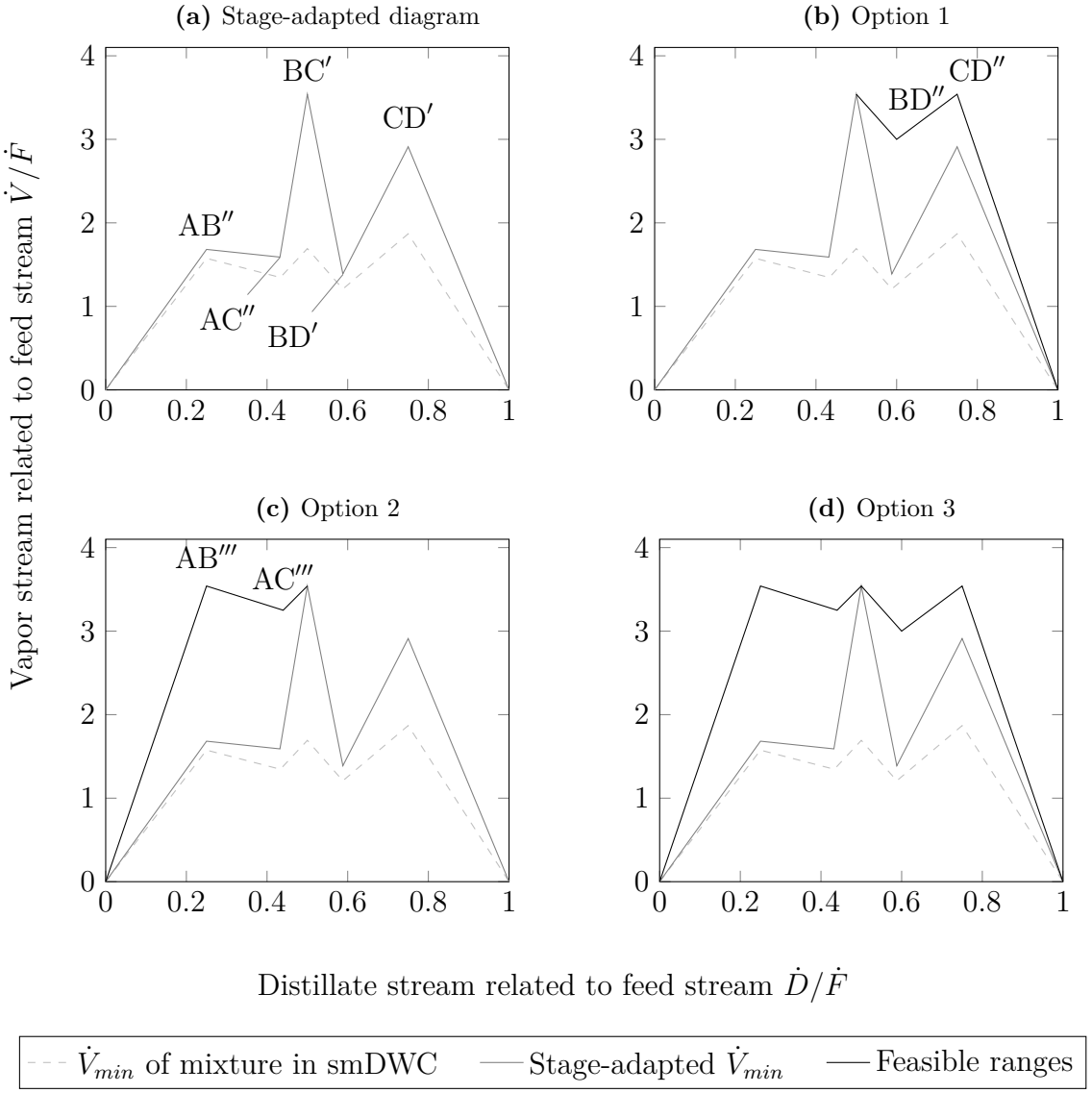

Figure 5.10: New approach to determine optimality regions of system 4.1 at a finite stage number of 143 and a similar allocation as in the pilot plant. [130]

stage numbers, the vapor and liquid split flexibility ranges can be determined optically. The principle is similar to the one in Figure 5.2. However, since the BC peak is now the highest one AB and CD can be increased. The AC and BC splits in between the maxima have to be estimated. It is found that the best results are obtained when both minima are shifted in a way that the slope on on the left and right of it stay similar to the one in the original $\dot{V}_{min}$ diagram. The suitable extreme cases of shifted peaks are shown in Figure 5.10b, 5.10c and 5.10d. Again all intermediate solutions are also possible. However, the option in Figure 5.10b cannot be realized inside a column. A higher BD than AC peak means, that column section C22 would have to be operated at a negative amount of vapor. Consequently, BD can only be increased further if AC is also increased.

Based on these stage-adapted $\dot{V}_{min}$ diagrams, the vapor and liquid split ranges can be read similarly as described in Section 2.1.3.1. Figure 5.11 shows the resulting ranges for the column derived by the new method in comparison to the original $\dot{V}_{min}$ ranges and the ones obtained from flow-sheet screenings as described in Section 3.3. For the screening $\dot{Q} = 1.1 \cdot \dot{Q}_{opt}$, optimal product flows and 97 mol % pure products are assumed.

From the diagram it gets clear why the simulation initialized with the split ranges

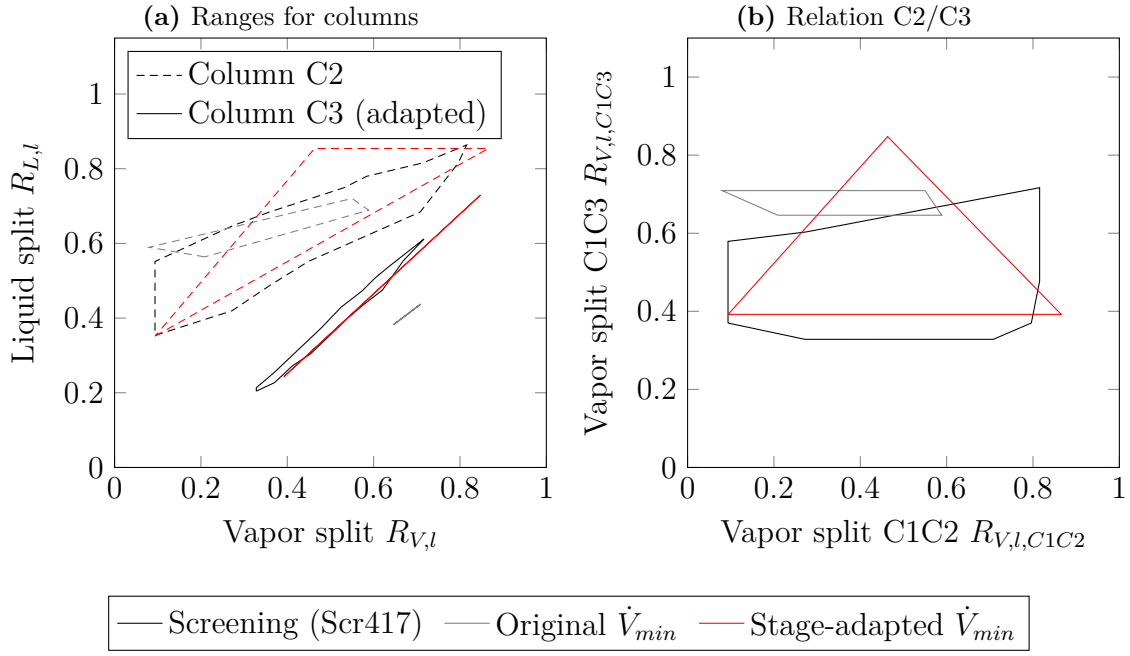

Figure 5.11: Flexibility range of system 4.1 in Pilot Plant with 13 stages in all sections and 26 in C32 (97 mol % at $\dot{Q} = 5.1$ kW) in comparison to approximation with original and adapted $\dot{V}_{min}$ method. For better clearance suited areas of each case are not filled. [130]

of the original $\dot{V}_{min}$ diagram result in such low purities. The liquid and vapor splits predicted for column C3 are no more located in the suited range resulting from the screening. Nevertheless, the split ranges for column C2 are located inside the suited range but are significantly smaller. The new prediction method covers a large range of the actually feasible operating range. However, it should be noted that certain regions are even overestimated. This mainly concerns C2 and C3 at higher liquid and vapor split ratios. Nevertheless, the extreme values resulting from the stage-adapted $\dot{V}_{min}$ diagram are used to initialize a flow-sheet simulation of a smDWC. The resulting product purities are also shown in Table 5.1. From the first two cases all products are obtained at purities above 96.9 mol %, for the last case the purities are slightly lower. This case is the one which overestimates the actual split range for column C3 most. Nevertheless, the purities are significantly higher than for the ranges predicted by the original $\dot{V}_{min}$ diagram.

Summarizing, this new method avoids the drawbacks of $\dot{V}_{min}$ diagrams to estimate split ranges for multiple dividing wall columns with finite stage numbers. High product purities are reached when applying the method to estimate suited liquid and vapor split

Table 5.1: Product purities [mol %] resulting from original and adapted $\dot{V}_{min}$ method in a smDWC with 13 stages in all sections and 26 in C32, $\dot{Q} = \dot{Q}_{opt} = 4.63\,\text{kW}$ and optimal product flows.

Comp. i	Original $\dot{V}_{min}$ method [63]				Adapted $\dot{V}_{min}$ method		
	Figure 5.2a	Figure 5.2b	Figure 5.2c	Figure 5.2d	Figure 5.10a	Figure 5.10c	Figure 5.10d
A	98.3	97	98	98.1	98.4	98.0	98.1
B	66.2	66.2	61.6	63.3	96.6	97.8	94.7
C	59.9	61.5	55.9	57.7	95.7	97.1	93.9
D	92.4	92.6	92.7	93	97.5	97.3	97.3

ranges. For the method no additional feed properties have to be known, thus it can be declared as a shortcut approach.

5.3 Impact of product flows

Figure 5.12 shows the impact of the product flows on the split ranges in the multiple dividing wall column pilot plant (see Section 2.1.2) for a similar distance from the energetic optimum of the corresponding column setup. In the investigated range product

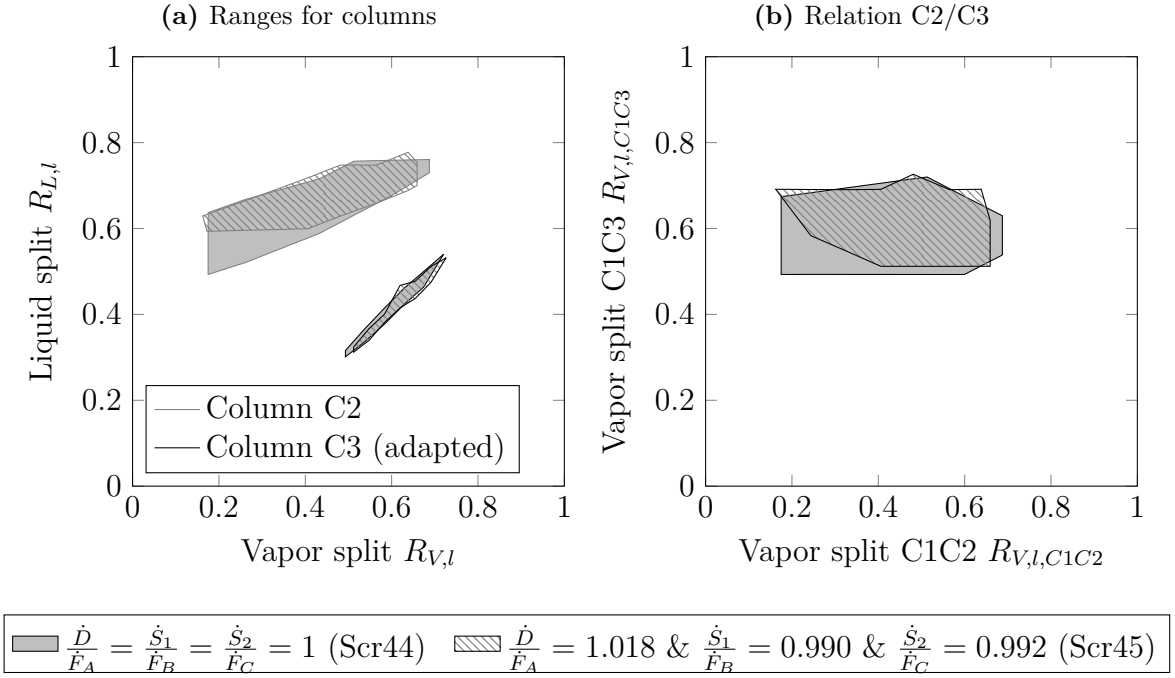

Figure 5.12: Flexibility range of system 4.1 in pilot plant for different product flows at $\dot{Q} = 1.12 \cdot \dot{Q}_{Opt,i}$.

flows have no significant effect on suited split ranges. Only the lower border of the liquid split to C2 is slightly increased. Nevertheless, it should be noted that the energy demand depends on the set product flows (see Figure 4.9). Accordingly, if the energy input is kept constant while varying the product flows, the split ranges can change according to the distance from the corresponding energetic minimum (see Section 5.1). Also there are lower and upper ranges of the product flows in which still the product purity requirements can be fulfilled.

5.4 Impact of feed stream composition

In this section the impact of feed composition disturbances on the split flexibility is investigated. For this purpose, system 4.3 is chosen to be split in the pilot plant (see Section 2.1.2). This mixture is chosen as it showed problems during dynamic simulations. After feed stream disturbances the product specifications were not reached anymore. Note that these dynamic simulations are carried out in the research group of the author but were not part of this work.
To better understand the problem a screening is performed. Six feed disturbances are

considered that are shown in Table 5.2, for each the molar fraction of one component is reduced by 0.05 and increased correspondingly for another close boiling component. The cases are similar to the ones presented by Preißinger *et al.* [132]. Note that one difference to the latter cited paper is that not the total mass flow but the total molar flow is kept constant. The K-values of the feed stream and the resulting minimum energy demand according to the $\dot{V}_{min}$ diagram are also shown in Table 5.2. Note that Case0 is the base case at an equimolar composition.

Overall the energy demand of the different feed compositions is in a range of ±4 % of

Table 5.2: Feed composition cases for system 4.3, feed flow rate $\dot{F} = 100\,\mathrm{mol \cdot h^{-1}}$ and $q = 1$.

Name	z_A [mol %]	z_B [mol %]	z_C [mol %]	z_D [mol %]	K_A [−]	K_B [−]	K_C [−]	K_D [−]	$\dot{V}_{min}$ $\left[\mathrm{mol \cdot h^{-1}}\right]$
Case0	0.25	0.25	0.25	0.25	1.93	0.9	0.67	0.5	236.42
Case1	0.3	0.2	0.25	0.25	1.88	0.81	0.63	0.47	238.08
Case2	0.2	0.3	0.25	0.25	1.98	0.99	0.71	0.52	233.43
Case3	0.25	0.3	0.2	0.25	1.89	0.91	0.65	0.49	227.2
Case4	0.25	0.2	0.3	0.25	1.98	0.88	0.68	0.5	246.2
Case5	0.25	0.25	0.3	0.2	1.91	0.9	0.67	0.49	241.28
Case6	0.25	0.25	0.2	0.3	1.96	0.91	0.67	0.5	230.08

the base case scenario (calculated with the $\dot{V}_{min}$ diagram). The highest energy demand is observable for Case4 and the lowest for Case3. During dynamic simulations it is observed that the control loop of the reboiler is not affected by feed stream disturbances and thus the energy input for all cases is constant. It is set according to the energy demand of the base case at $\dot{Q} = 3.226\,\mathrm{kW} = 1.18 \cdot \dot{Q}_{opt,Case0}$, considering the energy demand of the other splits the distance from the optimum is approximately in the range of $1.14 - 1.22 \cdot \dot{Q}_{opt}$.

For all cases screenings are performed according to Section 3.3 assuming the product flows to equal the feed flow of the corresponding main product. Figure 5.13 shows the resulting split ranges to reach 98 mol % pure products. The regions of suited split combinations shift for different feed stream compositions. On the one hand this results from distances of the cases from their corresponding energetic optimum. Accordingly Case4 is more limited in terms of flexibility than Case3. On the other hand, the energy demand of the AC and BD splits performed in the prefractionating columns C2 and C3 are affected by the feed stream composition. Consequently, also suited split ranges are shifted for feed stream disturbances. However, there are regions in which suited splits for all feed cases overlap, which is indicated by a filled gray area in Figure 5.13. For the column C2 this range is relatively large while for column C3 the area is rather narrow. Nevertheless, both cover a broad range of the vapor splits and the narrow character of the field of C3 occurs from the very limited range of suited liquid splits. However, it should be kept in mind that the adapted liquid split of C3 is shown, which

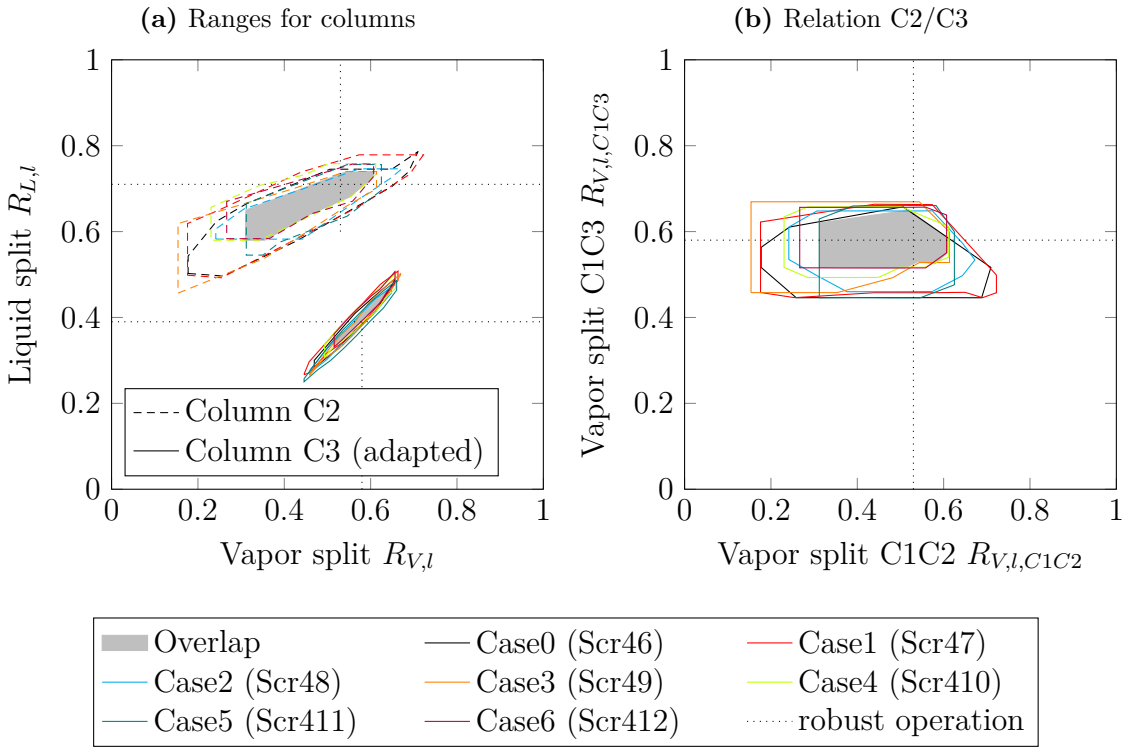

Figure 5.13: Flexibility range of system 4.3 in pilot plant for several feed stream compositions at $\dot{Q} = 1.18 \cdot \dot{Q}_{opt,Case0}$. For better clearance suited areas of each case are not filled.

is a multiplication of the liquid split from C1 to C2 and C2 to C3. Accordingly, the range is probably larger as it appears in the diagram. Suited stable operating values of the splits, indicated by the intersection of the black dotted lines in Figure 5.13, can be determined in accordance with the development of the fields for different distances from the energetic optimum (Figure 5.4 in Section 5.1). Additionally, sufficient distance from the border of the fields should be considered in order to guarantee a stable operation. From the results it can be concluded that controlled vapor splits are not necessarily required in order to operate a multiple dividing wall column pilot plant, also if feed disturbances occur. Interestingly, not even the liquid split has to be controlled if it can be guaranteed that is set to the value corresponding to the present vapor splits. However, most likely fluctuation occur during the operation that could disturb the vapor split. Thus, the liquid split should be adapted correspondingly. In order to reach a stable operation, the overlapping regions of the splits for the considered feed stream compositions can be determined. Nevertheless, it should be kept in mind that the corresponding product flows also have to be regulated in a suited range (see Section 5.3), otherwise the product specifications cannot be met.

5.5 Flexibility of different systems in pilot plant

The flexibility of all quaternary systems from Section 3.5 in the pilot plant (see Section 2.1.2) are analyzed in this section. In this context, several overlapping effects can occur. First, obviously the systems have different $\dot{V}_{min}$ diagrams (Section 3.5), which results in different initial flexibility ranges at infinite stage numbers. Second, the stage allocation in the column is non-optimal for all systems (see Table 4.2 in Section 4.4.4) resulting in a distortion of the $\dot{V}_{min}$ diagram and correspondingly also suited split ranges (Figure 5.8b in Section 5.2.2). Third, the ratio n describing the distance to the minimum stage number is different for all systems (see Table 4.2 in Section 4.4.4), which mainly affects the suited liquid split ranges (see Figure 5.6 in Section 5.2.1 and Figure 5.8a in Section 5.2.2).
Figure 5.14 shows the ranges for systems 4.1 to 4.4 at $\dot{Q} = 1.1 - 1.2 \cdot \dot{Q}_{opt}$. Systems 4.1,

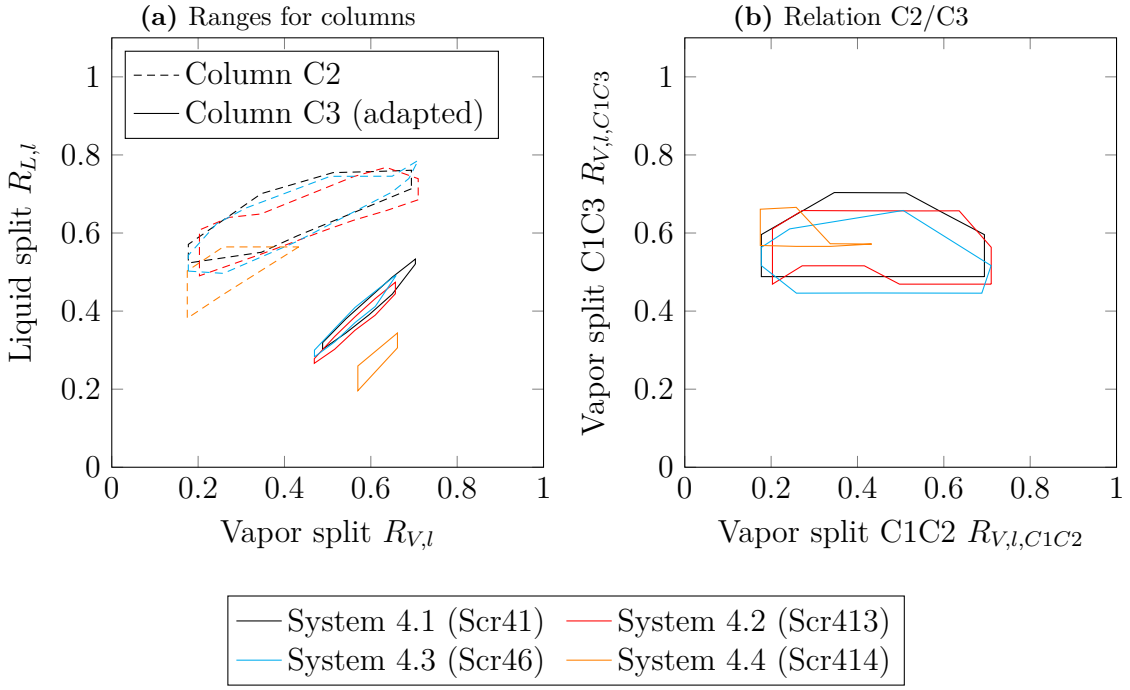

Figure 5.14: Flexibility range of system 4.1 to 4.4 (equimolar feed) in pilot plant at $\dot{Q} = 1.1 - 1.2 \cdot \dot{Q}_{opt}$. For better clearance suited areas of each case are not filled.

4.2 and 4.3 have quite similar $\dot{V}_{min}$ diagrams and also similar energy demands due to the fact that the components C and D are identical. All diagrams suggest a moderate split flexibility. However, while the stage allocation is well suited for systems 4.1 and 4.3, for system 4.2 significantly too many stages are provided for the AB and AC split. In Section 4.4.4 it was observed that this causes a reduced energy saving potential of this system in the pilot plant compared to column sequences. However, for the split ranges this has a rather beneficial effect. The highest BC peak is slightly increased causing a higher flexibility of the splits. Consequently, all three systems have almost the same flexibility ranges of the liquid and vapor splits. In contrast to this, system 4.4

requires less energy input and theoretical stages, correspondingly the stage number in the column can almost be approximated as infinite. Also the stage allocation is well suited for the system. However, the $\dot{V}_{min}$ diagram suggests a low flexibility since the shifted AB peak is almost at the same height as the CD split, only for the BC split some flexibility can be expected. Due to the fact that the stage allocation is rather optimal, this limited flexibility can be assumed to be maintained in the pilot plant, which fits the split ranges shown in Figure 5.14. However, it should be noted that all four systems can hardly reach product purities at 98 mol % if the vapor split to column C3 is 0.5, which can be expected to be approximately the vapor split that sets in the column. The vapor split should be higher at around 0.6 to reach a stable operation. For systems 4.4 also the vapor split to column C2 is an issue and should be lower at around 0.25. Accordingly, to enable a flexible character of the pilot plant it is recommended to have the opportunity to roughly adjust the vapor split inside the column, for example by an aperture to roughly adjust the pressure drop in certain column sections. Like that, it can be guaranteed that all four systems can be split to the desired purity inside the pilot plant.

Figure 5.15 shows suited vapor and liquid split ranges for systems 4.5 and 4.6. Both $\dot{V}_{min}$ diagrams in Figure 3.5 suggested a significant flexibility due to a very high CD peak compared to AB and BC. Also the ratio n_{column} is similar for both systems at around three and the stage allocation is rather inappropriate. This arises from the fact that the stage number n_{CD} is significantly lower than n for all other splits. Correspondingly, the adapted $\dot{V}_{min}$ diagram for the column shows an even higher flexibility than originally predicted.

The theoretical considerations about the flexibility of systems 4.5 and 4.6 match the results shown in Figure 5.15. Both have a very broad operating range of the splits. Different than the systems 4.1 to 4.4, they are also operable at both vapor splits around 0.5. Accordingly, for these two systems no additional adjustment of the vapor splits is needed for a stable operation close to the corresponding energetic optimum of the column.

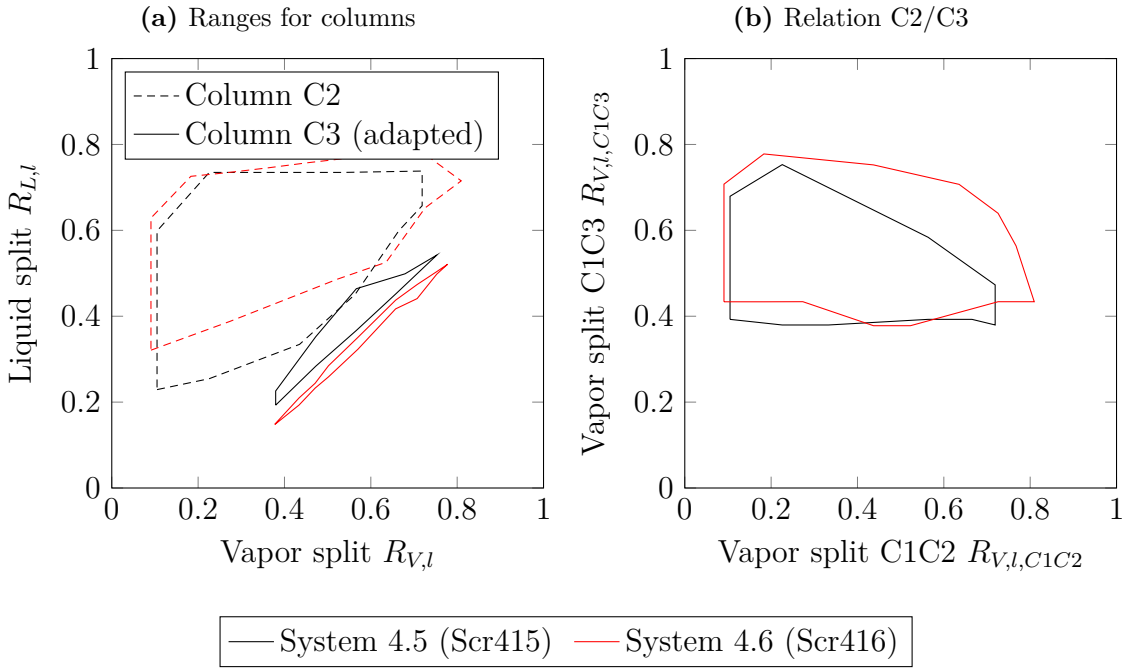

Figure 5.15: Flexibility range of system 4.5 and 4.6 (equimolar feed) in pilot plant at $\dot{Q} = 1.1 - 1.2 \cdot \dot{Q}_{opt}$. For better clearance suited areas of each case are not filled.

6 Summary

The objective of this work is to create a deep insight into the high-dimensional optimal space of simple and multiple dividing wall columns, highlight the relation of the results to the defined optimization problem and focusing on the importance of vapor and liquid split flexibility in this context. Overall, complex mathematical methods are applied in order to gain a deep understanding of optimally designed dividing wall columns. This knowledge could afterwards be translated back to develop shortcut methods predicting the found relations in a simple way. For this purpose, the work is separated into two main parts: optimization and operational flexibility.

In the optimization part, first a new kind of multi-objective optimization is introduced for dividing wall columns. In addition to the total stage number and energy demand of the column, it also includes the product purities as objectives. Consequently, a large part of the optimal space can be calculated. In order to visualize the results, self-organizing patch plots are applied. Both approaches in combination are a powerful tool for an *a posteriori* investigation of the high-dimensional objective space. Only one calculation run is required, then the results can be evaluated several times with regard to various points of view. This approach is applicable for all kinds of distillation columns.

The following section focuses on investigating the impact of the optimization problem definition of the results. For this purpose, simplified optimizations considering only two objectives are performed. For a simple dividing wall columns it is found that each component has different $N\dot{Q}$ optima for set product flows. However, these optimal curves are shifted for different product purity constraints and product flows. Consequently, for the product flows set to the one of each component in the feed stream, the intermediate boiling component limits the process while the low- and high boiling components are obtained in a higher purity then required. Thus it is recommended to include the the product flows as optimization variables. Then, the side draw flow is reduced and all products can be obtained in the same purity. Nevertheless, this is only relevant, if the product purities are below one, otherwise an adjustment of the product flows is not useful. Generally, it is found that the outcome of the optimization is strongly affected by the *a priori* defined input.

For a simplified multiple dividing wall column calculations are then performed for all products to have the same purity of 98 mol %. Due to the high complexity, a simplification of the optimization problem is reasonable and suited variables for simplification are searched. For this purpose several optimizations with reduced variable sets are performed. It is found, that not only the product purities but also the overall energy demand is very sensitive to the product flows. Accordingly, in the operation of such a column, their control structure is crucial to reach the desired product specifications, especially for lower total stage numbers. Also the choice of the theoretical stage allocation influences the energy demand. However, here the Fenske equation can be applied to reduce the optimization problem significantly by

nine variables without increasing the energy demand of the column notably.
Based on all results a new approach to approximate $N\dot{Q}$ optima of distillation columns or sequences is developed. For its calculation only feed stream properties are required which are the composition, liquid fraction and relative volatilities of all components. The Fenske equation is applied to estimate the minimum stage number and the $\dot{V}_{min}$ diagram is used to determine the minimum energy demand. For a new standardization of the stage number and energy demand it is shown that all Pareto-optimal solutions are located on an almost identical curve. This approach maps the results much better than the standardization method of Gilliland and Molakanov, which especially shows weaknesses for column sequences. Thus a new simple equation is provided for the calculation of Pareto-optimal solutions.
The next section focuses on the energy saving potential of dividing wall columns. Compared to conventional column sequences, the dividing wall column has a higher minimum stage number. On the other hand, the minimum energy demand of dividing wall columns is lower and thus the Pareto-optimal $N\dot{Q}$ curves have an intersection. For a quantification which distillation option is better suited considering the whole operating window a new dimensionless number called Decision Number is introduced. It is defined in the range of -1 to 1, where a positive value means that the dividing wall column is more beneficial and vice versa for column sequences. The Decision Number can either be calculated based on optimization results or estimated with the previously presented $N\dot{Q}$ optima approximation. Several variables are then examined for their influence on which distillation variant is the more superior one. For the tested mixtures it is found that the dividing wall column is more advantageous in comparison to the direct split sequences for systems with a low Ease of Separation Index. If the index increases the advantage of the dividing wall column decreases. An opposite trend is observed comparing the dividing wall column with an indirect split sequence. The transition from one option to another is affected by the specified product purities. For low to moderate purities the effect is rather small while at high purity products column sequences gain more virtues. The feed stream composition does not affect the Decision Number and thus the relative location of the intersection of Pareto-optimal compromises. However, it should be kept in mind that this will of course affect the energy and stage requirements.
Afterwards, the saving potential of multiple dividing wall columns is investigated focusing on the flexible designed pilot plant planned at Ulm University. Six suited systems are optimized and the results are compared the ones of conventional column sequences. It is found that the pilot plant offers significant amounts of energy savings for 98 mol % pure products in any case, being in the range of $25 - 45\%$. However, for higher product purities the savings are reduced. Also it is observed that the energy savings are lower for systems requiring significantly different stage allocations in the column sections.
Overall, in the first part of this work a detailed study about the optimal space of distillation columns is presented. These studies have resulted in a comprehensive understanding of the relations that lead to optimal column designs. Based on this knowledge, new empirical shortcut methods could be introduced. These enable the

estimation of optimal column designs without the need of an optimizer. Additionally, it can be evaluated whether a column sequence or an intensified dividing wall column is the better suited option for a given separation task without an optimization.
In the second part of this work the operational flexibility close to the energetic optimum is investigated in depth. Its importance arises from the fact that one optimal operation point cannot only be reached by one combination of the liquid and vapor split but by a set of them which leads to the flexibility in operation already mentioned. In other words, the robustness of the optimum is investigated. This relation is also important the other way around. It is found that the flexibility can severely be limited if non-optimal stages are chosen in some column sections, consequently operating such a column can become challenging. This observation can be explained with an extended version of the $\dot{V}_{min}$ diagram developed in this work which also considers the ratio of the stages for one split related to the minimum one n_i. Also the distance to the minimum stage number affects the location of suited liquid and vapor split ranges. Especially suited liquid split ranges are strongly affected by the total stage number. Correspondingly, the suitability of the $\dot{V}_{min}$ diagrams to initialize flow-sheet simulations is reduced at lower stage numbers. Thus, based on the stage-adapted version of the $\dot{V}_{min}$ diagram in combination with the approximation approach for $N\dot{Q}$ optima a method is developed to estimate the vapor and liquid split ranges in dividing wall columns with finite stage numbers. An example simulation proves that the new approach guarantees high-purity products, which are not reached with the values predicted by the original $\dot{V}_{min}$ method. Further, the presented screenings can also be used to enhance the dynamic behavior of the pilot plant in Ulm University. For this purpose, the impact of feed stream disturbances on the vapor and liquid split ranges are evaluated. Even though the ranges are shifted there are overlapping regions for all feed cases. In this overlapping region the column should be operated to reliably reach the desired product specifications. Additionally, the split flexibility of several systems suited for the pilot plant is evaluated. The resulting split ranges can be explained with the knowledge gained in the preceding sections.
Summarizing, also the second part of this work makes a significant contribution to making the behavior of dividing wall columns more comprehensible. Flexibility ranges of the liquid and vapor splits can be calculated and then be used to enable a more stable operation. This could be a first step towards establishing also multiple dividing wall columns in the chemical industry.

Bibliography

[1] Y. K. Molokanov, T. P. Korablina, N. I. Mazurina and G. A. Nikiforov: *An approximate method of calculating the basic parameters of a multicomponent fractionation.* Chemistry and Technology of Fuels and Oils, 7(2):129–133, 1971.

[2] BCS Incorporated and Oak Ridge National Laboratory: *Materials for Separation Technologies: Energy and Emission Reduction Opportunities.*

[3] J. L. Humphrey and G. E. Keller: *Separation process technology.* Chemical engineering books. McGraw Hill, New York, 1997.

[4] Energy Information Administration, National Energy Information Center: *Annual Energy Review 2001.*

[5] D. S. Sholl and R. P. Lively: *Seven chemical separations to change the world.* Nature (London, United Kingdom), 532(7600):435–437, 2016.

[6] T. Grützner, D. Ziegenbalg and R. Güttel: *Process Intensification - An Unbroken Trend in Chemical Engineering.* Chemie Ingenieur Technik, 90(11):1823–1831, 2018.

[7] A. Mersmann, M. Kind and J. Stichlmair: *Thermische Verfahrenstechnik: Grundlagen und Methoden.* Chemische Technik/Verfahrenstechnik. Springer, Berlin, 2., wesentlich erw. and aktualisierte Aufl. edition, 2005.

[8] A. A. Kiss: *Advanced distillation technologies: Design, control, and applications.* Wiley, Chichester, West Sussex, United Kingdom, First edition edition, 2013.

[9] N. Asprion and G. Kaibel: *Dividing wall columns: Fundamentals and recent advances.* Chemical Engineering and Processing: Process Intensification, 49(2):139–146, 2010.

[10] Ö. Yildirim, A. A. Kiss and E. Y. Kenig: *Dividing wall columns in chemical process industry: A review on current activities.* Separation and Purification Technology, 80(3):403–417, 2011.

[11] I. Dejanović, L. Matijašević and Ž. Olujić: *Dividing wall column—A breakthrough towards sustainable distilling.* Chemical Engineering and Processing: Process Intensification, 49(6):559–580, 2010.

[12] Ž. Olujić, M. Jödecke, A. Shilkin, G. Schuch and B. Kaibel: *Equipment improvement trends in distillation.* Chemical Engineering and Processing: Process Intensification, 48(6):1089–1104, 2009.

[13] C. Triantafyllou and R. Smith: *The Design and Optimisation of Fully Thermally Coupled Distillation Columns.* Chemical Engineering Research and Design, 70:118–132, 1992.

[14] C. Li, Q. Zhang, J. Xie, J. Fang and H. Li: *Design, optimization, and industrial-scale experimental study of a high-efficiency dividing wall column.* Separation and Purification Technology, 247:116891, 2020.

[15] M. A. Schultz, D. G. Stewart, J. M. Harris, S. P. Rosenblum, M. S. Shakur and D. E. O'Brien: *Reduce costs with dividing-wall columns.* Chemical Engineering Progress, 98:64–71, 2002.

[16] T. Waltermann, S. Sibbing and M. Skiborowski: *Optimization-based design of dividing wall columns with extended and multiple dividing walls for three- and four-product separations.* Chemical Engineering and Processing: Process Intensification, 146:107688, 2019.

[17] A. A. Kiss: *Distillation technology - still young and full of breakthrough opportunities.* Journal of Chemical Technology & Biotechnology, 89(4):479–498, 2014.

[18] R. O. Wright: *Fractionation apparatus*, 1949.

[19] G. Kaibel, C. Miller, M. Stroezel, R. von Watzdorf and H. Jansen: *Industrieller Einsatz von Trennwandkolonnen und thermisch gekoppelten Destillationskolonnen.* Chemie Ingenieur Technik, 76(3):258–263, 2004.

[20] I. Dejanović, L. Matijašević, I. J. Halvorsen, S. Skogestad, H. Jansen, B. Kaibel and Ž. Olujić: *Designing four-product dividing wall columns for separation of a multicomponent aromatics mixture.* Chemical Engineering Research and Design, 89(8):1155–1167, 2011.

[21] I. Dejanović, I. J. Halvorsen, S. Skogestad, H. Jansen and Ž. Olujić: *Hydraulic design, technical challenges and comparison of alternative configurations of a four-product dividing wall column.* Chemical Engineering and Processing: Process Intensification, 84:71–81, 2014.

[22] U. Preissinger, L.-M. Ränger and T. Grützner: *Design Considerations of a Simplified Multiple Dividing Wall Column Pilot Plant.* ChemEngineering, 3(2):34, 2019.

[23] M. Bortz, J. Burger, N. Asprion, S. Blagov, R. Böttcher, U. Nowak, A. Scheithauer, R. Welke, K.-H. Küfer and H. Hasse: *Multi-criteria optimization in chemical process design and decision support by navigation on Pareto sets.* Computers & Chemical Engineering, 60:354–363, 2014.

[24] R. T. Marler and J. S. Arora: *Survey of multi-objective optimization methods for engineering.* Structural and Multidisciplinary Optimization, 26(6):369–395, 2004.

[25] W. L. Luyben (editor): *Distillation design and control using Aspen Simulation.* Wiley and AIChE, Hoboken, NJ and New York, NY, 2. ed., [elektronische Ressource] edition, 2013.

[26] N. Ramírez-Corona, A. Jiménez-Gutiérrez, A. Castro-Agüero and V. Rico-Ramírez: *Optimum design of Petlyuk and divided-wall distillation systems using a shortcut model.* Chemical Engineering Research and Design, 88(10):1405–1418, 2010.

[27] G. P. Rangaiah: *Multi-objective optimization: Techniques and applications in chemical engineering*, volume v. 5 of *Advances in Process Systems Engineering.* World Scientific Publishing Co. Pte. Ltd, Singapore, 2nd ed. edition, 2017.

[28] C. Gutiérrez-Antonio and A. Briones-Ramírez: *Pareto front of ideal Petlyuk sequences using a multiobjective genetic algorithm with constraints.* Computers & Chemical Engineering, 33(2):454–464, 2009.

[29] N. Asprion, R. Böttcher, J. Höller, P. Schwartz, J. Schwientek and M. Bortz: *From Single Process Simulation and Optimization to Decision Making Based on a Multitude of Solutions.* In *29th European Symposium on Computer Aided Process Engineering*, volume 46 of *Computer Aided Chemical Engineering*, pages 7–12. Elsevier, Amsterdam, 2019.

[30] H. Alcocer-García, J. G. Segovia-Hernández, O. A. Prado-Rubio, E. Sánchez-Ramírez and J. J. Quiroz-Ramírez: *Multi-objective optimization of intensified processes for the purification of levulinic acid involving economic and environmental objectives.* Chemical Engineering and Processing: Process Intensification, 136:123–137, 2019.

[31] M. von Kurnatowski, M. Bortz, A. Scherrer, A. Hoffmann, H.-M. Lorenz, M. Caraucan, T. Grützner, N. Künzle and K.-H. Küfer: *Multi-criteria Optimization of an Industrial World-Scale Process.* Chemie Ingenieur Technik, 89(11):1471–1478, 2017.

[32] F. I. Gómez-Castro, J. G. Segovia-Hernández, S. Hernández, C. Gutiérrez-Antonio and A. Briones-Ramírez: *Dividing Wall Distillation Columns: Optimization and Control Properties.* Chemical Engineering & Technology, 31(9):1246–1260, 2008.

[33] R. Chavez C., J. D. Seader and T. L. Wayburn: *Multiple steady-state solutions for interlinked separation systems.* Industrial & Engineering Chemistry Fundamentals, 25(4):566–576, 1986.

[34] E. Song, S. Li and E. Wang: *Dynamic Analysis for the Multi-Steady States in the Dividing Wall Column.* Process Integration and Optimization for Sustainability, 3(2):179–187, 2019.

[35] S. Erwei, Q. Lijuan and W. Erqiang: *Prediction for Multi-Steady-State Solutions in the Thermal-Coupled Distillation.* Process Integration and Optimization for Sustainability, 3(4):505–514, 2019.

[36] I. J. Halvorsen and S. Skogestad: *Optimal operation of Petlyuk distillation: Steady-state behavior.* Journal of Process Control, 9(5):407–424, 1999.

[37] E. Song and E. Wang: *Design of a Dividing-Wall Column Considering its Multiple Steady State Characteristic.* Chemical Engineering & Technology, 41(3):517–523, 2018.

[38] D. Staak, T. Grützner, B. Schwegler and D. Roederer: *Dividing wall column for industrial multi purpose use.* Chemical Engineering and Processing: Process Intensification, 75:48–57, 2014.

[39] L. T. Maralani, X. Yuan, Y. Luo, C. GONG and G. YU: *Numerical Investigation on Effect of Vapor Split Ratio to Performance and Operability for Dividing Wall Column.* Chinese Journal of Chemical Engineering, 21(1):72–78, 2013.

[40] A. Górak and H. Schoenmakers: *Distillation: Operation and applications / edited by Andrzej Gorak, Hartmut Schoenmakers.* Academic Press, Amsterdam, 2014.

[41] Z. Lei, B. Chen and Z. Ding: *Special distillation processes.* Elsevier, Amsterdam and Oxford, 2005.

[42] F. B. Petlyuk, V. Platonov and D. M. Slavinskii: *Thermodynamically optimal method for separating multicomponent mixtures.* International Chemical Engineering, 5(3):555–561, 1965.

[43] N. Saxena, N. Mali and S. Satpute: *Study of thermally coupled distillation systems for energy-efficient distillation.* Sadhana: Academy Proceedings in Engineering Sciences, 42(1):119–128, 2017.

[44] A. A. Kiss and C. S. Bildea: *A control perspective on process intensification in dividing-wall columns.* Chemical Engineering and Processing: Process Intensification, 50(3):281–292, 2011.

[45] G. Dünnebier and C. C. Pantelides: *Optimal Design of Thermally Coupled Distillation Columns.* Industrial & Engineering Chemistry Research, 38(1):162–176, 1999.

[46] G. Kaibel: *Distillation columns with vertical partitions.* Chemical Engineering & Technology, 10(1):92–98, 1987.

[47] I. J. Halvorsen, I. Dejanović, S. Skogestad and Ž. Olujić: *Internal configurations for a multi-product dividing wall column.* Chemical Engineering Research and Design, 91(10):1954–1965, 2013.

[48] Ž. Olujić, I. Dejanović, B. Kaibel and H. Jansen: *Dimensioning Multipartition Dividing Wall Columns.* Chemical Engineering & Technology, 35(8):1392–1404, 2012.

[49] C. A. Villegas-Uribe, J. R. Alcántara-Avila, N. Medina-Herrera, R. Gómez-González and S. Tututi-Avila: *Temperature control of a Kaibel, Agrawal and Sargent dividing-wall distillation columns.* Chemical Engineering and Processing: Process Intensification, 159:108248, 2021.

[50] F. Jing, C. Xiaomin, L. Xiaochun, Ning. Xiang and L. Chunli: *Shortcut Method of Design and Energy-Saving Analysis of Sargent Dividing Wall Column.* China Petroleum Processing and Petrochemical Technology, 20(4):99–108, 2018.

[51] I. J. Halvorsen and S. Skogestad: *Energy efficient distillation.* Journal of Natural Gas Science and Engineering, 3(4):571–580, 2011.

[52] L.-M. Ränger, U. Preissinger and T. Grützner: *Multiple Dividing-Wall Columns - Current Status and Future Prospects.* Chemie Ingenieur Technik, 91(4):420–428, 2019.

[53] G. Madenoor Ramapriya, M. Tawarmalani and R. Agrawal: *Thermal coupling links to liquid-only transfer streams: A path for new dividing wall columns.* AIChE Journal, 60(8):2949–2961, 2014.

[54] X. Ge, B. Liu, X. Yuan and B. Liu: *Simplifying and synthesizing practical four-product dividing wall column configurations.* Chemical Engineering Research and Design, 125:433–448, 2017.

[55] Sulzer Chemtech Ltd: *Structured Packings: Energy-efficient, innovative and profitable.*

[56] N. D. van Long and M. Lee: *Advances in Distillation Retrofit.* Springer, Singapore, 2017.

[57] A. J. V. Underwood: *Fractional Distillation of Ternary Mixtures Part I.* Journal of the Institute of Petroleum, pages 111–118, 1945.

[58] A. J. V. Underwood: *Fractional Diatillation of Ternary Mixtures Part II.* Journal of the Institute of Petroleum, pages 198–613, 1946.

[59] I. J. Halvorsen and S. Skogestad: *Minimum Energy Consumption in Multicomponent Distillation. 1. Vmin Diagram for a Two-Product Column.* Industrial & Engineering Chemistry Research, 42(3):596–604, 2003.

[60] I. J. Halvorsen and S. Skogestad: *Minimum Energy Consumption in Multicomponent Distillation. 2. Three-Product Petlyuk Arrangements.* Industrial & Engineering Chemistry Research, 42(3):605–615, 2003.

[61] I. J. Halvorsen and S. Skogestad: *Minimum Energy Consumption in Multicomponent Distillation. 3. More Than Three Products and Generalized Petlyuk Arrangements.* Industrial & Engineering Chemistry Research, 42(3):616–629, 2003.

[62] L.-M. Ränger: *Multi-Objective Optimization of Simple and Multiple Dividing Wall Columns and their Operational Flexibility Close to the Optimum: Supplementary Information for Dissertation.* http://dx.doi.org/10.18725/OPARU-39802, 2021.

[63] L.-M. Ränger, U. Preissinger and T. Grützner: *Robust Initialization of Rigorous Process Simulations of Multiple Dividing Wall Columns via Vmin Diagrams.* ChemEngineering, 2(2):25, 2018.

[64] M. R. Fenske: *Fractionation of Straight-Run Pennsylvania Gasoline.* Industrial & Engineering Chemistry, 24(5):482–485, 1932.

[65] K. Muralikrishna, V. Madhavan and S. S. Shah: *Development of Dividing Wall Distillation Column Design Space for a Specified Separation.* Chemical Engineering Research and Design, 80(2):155–166, 2002.

[66] N. Sotudeh and B. Hashemi Shahraki: *A Method for the Design of Divided Wall Columns.* Chemical Engineering & Technology, 30(9):1284–1291, 2007.

[67] D. W. Tedder and D. F. Rudd: *Parametric studies in industrial distillation: Part I. Design comparisons.* AIChE Journal, 24(2):303–315, 1978.

[68] E. R. Gilliland: *Multicomponent Rectification Estimation of the Number of Theoretical Plates as a Function of the Reflux Ratio.* Industrial & Engineering Chemistry, 32(9):1220–1223, 1940.

[69] C. G. Kirkbride: *Process design procedure for multicomponent fractionators.* Petroleum Refinery, 9(23):321–336, 1944.

[70] E. Wang: *Simulation and analysis of multiple steady states in dividing wall column.* Asia-Pacific Journal of Chemical Engineering, 10(1):75–83, 2015.

[71] X. Ge, X. Yuan, C. Ao and K.-K. Yu: *Simulation based approach to optimal design of dividing wall column using random search method.* Computers & Chemical Engineering, 68:38–46, 2014.

[72] D. Dwivedi, J. P. Strandberg, I. J. Halvorsen, H. A. Preisig and S. Skogestad: *Active Vapor Split Control for Dividing-Wall Columns.* Industrial & Engineering Chemistry Research, 51(46):15176–15183, 2012.

[73] X. Ge, C. Ao, X. Yuan and Y. Luo: *Investigation of the Effect of the Vapor Split Ratio Decision in Design on Operability for DWC by Numerical Simulation.* Industrial & Engineering Chemistry Research, 53(34):13383–13390, 2014.

[74] X. Ge, B. Liu, B. Liu, H. Wang and X. Yuan: *Investigation of the operability for four-product dividing wall column with two partition walls.* Chinese Journal of Chemical Engineering, 26(8):1670–1676, 2018.

[75] L. T. Biegler and I. E. Grossmann: *Retrospective on optimization.* Computers & Chemical Engineering, 28(8):1169–1192, 2004.

[76] T. Waltermann and M. Skiborowski: *Conceptual Design of Highly Integrated Processes - Optimization of Dividing Wall Columns.* Chemie Ingenieur Technik, 89(5):562–581, 2017.

[77] C. M. Fonseca and P. J. Fleming: *Multiobjective optimization and multiple constraint handling with evolutionary algorithms. I. A unified formulation.* IEEE Transactions on Systems, Man, and Cybernetics - Part A: Systems and Humans, 28(1):26–37, 1998.

[78] D. E. Grierson: *Pareto multi-criteria decision making.* Advanced Engineering Informatics, 22(3):371–384, 2008.

[79] J. Horn, N. Nafpliotis and D. E. Goldberg: *A niched Pareto genetic algorithm for multiobjective optimization.* In *Proceedings of the First IEEE Conference on Evolutionary Computation*, pages 82–87, Piscataway, NJ and s.l., 1994. IEEE Neural Networks Council.

[80] C. M. Fonseca and P. J. Fleming: *Genetic Algorithms for Multiobjective Optimization: Formulation, Discussion and Generalization.* In S. Forrest (editor): *Proceedings of the Fifth International Conference on Genetic Algorithms.* Kaufmann, San Mateo, Calif., 1993.

[81] M. Ehrgott: *Multicriteria Optimization.* 10717, Berlin, Heidelberg, 2005.

[82] N. Asprion, R. Böttcher, R. Pack, M.-E. Stavrou, J. Höller, J. Schwientek and M. Bortz: *Gray-Box Modeling for the Optimization of Chemical Processes.* Chemie Ingenieur Technik, 91(3):305–313, 2019.

[83] J. Burger, N. Asprion, S. Blagov, R. Böttcher, U. Nowak, M. Bortz, R. Welke, K.-H. Küfer and H. Hasse: *Multi-Objective Optimization and Decision Support in Process Engineering - Implementation and Application.* Chemie Ingenieur Technik, 86(7):1065–1072, 2014.

[84] V. K. Sangal, V. Kumar and I. M. Mishra: *Optimization of structural and operational variables for the energy efficiency of a divided wall distillation column.* Computers & Chemical Engineering, 40:33–40, 2012.

[85] N. Khalili, N. Kasiri, J. Ivakpour, A. Khalili-Garakani and M. H. Khanof: *Optimal configuration of ternary distillation columns using heat integration with external heat exchangers.* Energy (Oxford, United Kingdom), 191:116479, 2020.

[86] M. Khalifa and M. Emtir: *Rigorous optimization of heat-integrated and Petlyuk column distillation configurations based on feed conditions.* Clean Technologies and Environmental Policy, 11(1):107–113, 2009.

[87] I. Dejanović, L. Matijašević and Ž. Olujić: *An Effective Method for Establishing the Stage and Reflux Requirement of Three-product DividingWall Columns.* Chemical and Biochemical Engineering Quarterly, 25(2):147–157, 2011.

[88] N. van Duc Long and M. Lee: *Dividing wall column structure design using response surface methodology.* Computers & Chemical Engineering, 37:119–124, 2012.

[89] C. Gutiérrez-Antonio: *Multiobjective Stochastic Optimization of Dividing-wall Distillation Columns Using a Surrogate Model Based on Neural Networks.* Chemical and Biochemical Engineering Quarterly, 29(4):491–504, 2016.

[90] S. Jia, X. Qian and X. Yuan: *Optimal design for dividing wall column using support vector machine and particle swarm optimization.* Chemical Engineering Research and Design, 125:422–432, 2017.

[91] M. J. D. Powell: *A fast algorithm for nonlinearly constrained optimization calculations.* In G. A. Watson (editor): *Numerical Analysis*, volume 630 of *Lecture Notes in Mathematics*, pages 144–157. Springer Berlin Heidelberg, Berlin, Heidelberg, 1978.

[92] A. Wächter and L. T. Biegler: *On the implementation of an interior-point filter line-search algorithm for large-scale nonlinear programming.* Mathematical Programming, 106(1):25–57, 2006.

[93] K. Mueller: *Optimization.* EDTECH, 2019.

[94] J. F. Bonnans, J. C. Gilbert, C. Lemaréchal and C. A. Sagastizábal: *Numerical Optimization: Theoretical and Practical Aspects.* Mathematics and Statistics (Springer-11649. Springer and Springer e-books, Berlin, Heidelberg, 2006.

[95] D. J. Reid: *Genetic algorithms in constrained optimization.* Mathematical and Computer Modelling, 23(5):87–111, 1996.

[96] G. Mavrotas: *Effective implementation of the ϵ-constraint method in Multi-Objective Mathematical Programming problems.* Applied Mathematics and Computation, 213(2):455–465, 2009.

[97] G. Eichfelder: *Scalarizations for adaptively solving multi-objective optimization problems.* Computational Optimization and Applications, 44(2):249–273, 2009.

[98] S. L. Faulkenberg and M. M. Wiecek: *Generating equidistant representations in biobjective programming.* Computational Optimization and Applications, 51(3):1173–1210, 2012.

[99] K. Klamroth, J. Tind and M. M. Wiecek: *Unbiased approximation in multicriteria optimization.* Mathematical Methods of Operations Research, 56(3):413–437, 2003.

[100] J. I. Serna Hernández: *Multi-objective optimization in mixed integer problems: With application to the beam selection optimization problem in IMRT.* Mathematics. mbv, Mensch-und-Buch-Verl., Berlin, 2011.

[101] K. A. Amminudin, R. Smith, D.-C. Thong and G. P. Towler: *Design and Optimization of Fully Thermally Coupled Distillation Columns.* Chemical Engineering Research and Design, 79(7):701–715, 2001.

[102] M. B. Franke: *Design of Dividing-Wall Columns by Mixed-Integer Nonlinear Programming Optimization.* Chemie Ingenieur Technik, 89(5):582–597, 2017.

[103] M. Errico, B.-G. Rong, J. G. Segovia-Hernández and P. Pirellas: *Design and Optimization of Intensified Quaternary Petlyuk Configuration.* In K. V. Gernaey, J. K. Huusom and R. Gani (editors): *12th International Symposium on Process Systems Engineering and 25th European Symposium on Computer Aided Process Engineering*, volume 37 of *Computer aided chemical engineering, 1570-7946*, pages 1367–1372. Elsevier, Amsterdam, 2015.

[104] J. A. Vázquez-Castillo, J. G. Segovia-Hernández and J. M. Ponce-Ortega: *Multiobjective Optimization Approach for Integrating Design and Control in Multicomponent Distillation Sequences.* Industrial & Engineering Chemistry Research, 54(49):12320–12330, 2015.

[105] F. I. Gómez-Castro, N. E. Ramírez-Vallejo, J. G. Segovia-Hernández, C. Gutiérrez-Antonio, M. Errico, A. Briones-Ramírez and J. Sánchez-Aguilar: *Energy consumption maps for quaternary distillation sequences.* In *26th European Symposium on Computer Aided Process Engineering*, volume 38 of *Computer Aided Chemical Engineering*, pages 121–126. Elsevier, 2016.

[106] J. Koehler, P. Poellmann and E. Blass: *A Review on Minimum Energy Calculations for Ideal and Nonideal Distillations.* Industrial & Engineering Chemistry Research, 34(4):1003–1020, 1995.

[107] L.-M. Ränger, M. von Kurnatowski, M. Bortz and T. Grützner: *Multi-Objective Optimization of Dividing Wall Columns and Visualization of the High-Dimensional Results.* Computers & Chemical Engineering, 142:107059, 2020.

[108] N. Asprion: *Modeling, Simulation, and Optimization 4.0 for a Distillation Column.* Chemie Ingenieur Technik, 92(7):879–889, 2020.

[109] S. Liu, D. Maljovec, B. Wang, P.-T. Bremer and V. Pascucci: *Visualizing High-Dimensional Data: Advances in the Past Decade.* IEEE Transactions on Visualization and Computer Graphics, 23(3):1249–1268, 2017.

[110] M. de Oliveira and H. Levkowitz: *From visual data exploration to visual data mining: A survey.* IEEE Transactions on Visualization and Computer Graphics, 9(3):378–394, 2003.

[111] J. Zhang, M. L. Huang, W. B. Wang, L. F. Lu and Z.-P. Meng: *Big Data Density Analytics Using Parallel Coordinate Visualization.* In *2014 IEEE 17th International Conference on Computational Science and Engineering*, pages 1115–1120. IEEE, 2014.

[112] A. O. Artero, de Oliveira, M. C. F. and H. Levkowitz: *Uncovering Clusters in Crowded Parallel Coordinates Visualizations: IEEE Symposium on Information Visualization, Austin, TX, 2004, pp. 81-88.* In *IEEE Symposium on Information Visualization*, pages 81–88. IEEE, 10/10/2004 - 12/10/2004.

[113] H. Zhou, X. Yuan, H. Qu, W. Cui and B. Chen: *Visual Clustering in Parallel Coordinates.* Computer Graphics Forum, 27(3):1047–1054, 2008.

[114] F. Masseglia, M. Teisseire and P. Poncelet (editors): *Successes and new directions in data mining.* IGI Global (701 E. Chocolate Avenue Hershey Pennsylvania 17033 USA), Hershey, Pa, 2008.

[115] J. G. Dy and C. E. Brodley: *Visualization and interactive feature selection for unsupervised data.* In R. Ramakrishnan, S. Stolfo, R. Bayardo and I. Parsa (editors): *Proceedings of the sixth ACM SIGKDD international conference on Knowledge discovery and data mining - KDD '00*, pages 360–364, New York, New York, USA, 2000. ACM Press.

[116] P. Cunningham: *Dimension Reduction.* In M. Cord and P. Cunningham (editors): *Machine Learning Techniques for Multimedia: Case Studies on Organization and Retrieval*, pages 91–112. Springer Berlin Heidelberg, Berlin, Heidelberg, 2008.

[117] A. K. Jain, M. N. Murty and P. J. Flynn: *Data clustering.* ACM Computing Surveys (CSUR), 31(3):264–323, 1999.

[118] S. Wold, K. Esbensen and P. Geladi: *Principal component analysis.* Chemometrics and Intelligent Laboratory Systems, 2(1-3):37–52, 1987.

[119] J. B. Tenenbaum: *A Global Geometric Framework for Nonlinear Dimensionality Reduction.* Science (Washington, DC, United States), 290(5500):2319–2323, 2000.

[120] L. van der Maaten and G. E. Hinton: *Visualizing High-Dimensional Data Using t-SNE.* Journal of Machine Learning Research, 9(nov):2579–2605, 2008.

[121] T. Kohonen: *The self-organizing map.* Proceedings of the IEEE, 78(9):1464–1480, 1990.

[122] T. Kohonen: *Essentials of the self-organizing map.* Neural Networks, 37:52–65, 2013.

[123] C. A. Astudillo and B. J. Oommen: *Topology-oriented self-organizing maps: A survey.* Pattern Analysis and Applications, 17(2):223–248, 2014.

[124] J. Vesanto: *SOM-based data visualization methods.* Intelligent Data Analysis, 3(2):111–126, 1999.

[125] K. Stöbener, P. Klein, M. Horsch, K.-H. Küfer and H. Hasse: *Parametrization of two-center Lennard-Jones plus point-quadrupole force field models by multicriteria optimization.* Fluid Phase Equilibria, 411:33–42, 2016.

[126] R. Klein: *Concrete and abstract Voronoi diagrams: Zugl.: Freiburg (Breisgau), Univ., Habil.-Schr., 1989 u.d.T.: Klein, Rolf: On a generalization of planar Voronoi diagrams*, volume 400 of *Lecture Notes in Computer Science.* Springer, Berlin, 1989.

[127] K. Schittkowski: *MISQP: A Fortran Subroutine of a Trust Region SQP Algorithm for Mixed-Integer Nonlinear Programming: User 's Guide.*

[128] K. Schittkowski: *NLPQLP: A Fortran Implementation of a Sequential Quadratic Programming Algorithm with Distributed and Non-Monotone Line Search: User's Guide, Version 4.2.*

[129] G. Azzopardi: *Self-Organizing Map - Simple demonstration*, 2013.

[130] L.-M. Ränger and T. Grützner: *Shortcut Method for Initialization of Dividing–Wall Columns and Estimating Pareto–Optimal NQ –Curves.* Chemical Engineering & Technology, 44(10):1919–1928, 2021.

[131] L.-M. Ränger, L. Trescher, M. von Kurnatowski, M. Bortz and T. Grützner: *Vapor and liquid split flexibility in dividing wall columns in relation to the theoretical stage allocation.* Chemical Engineering and Processing: Process Intensification, 163, 2021.

[132] U. Preissinger, G. Lukač, I. Dejanović and T. Grützner: *Investigation of Control Structures for a Four–Product Laboratory Multiple Dividing–Wall Column Using Dynamic Simulation.* Chemical Engineering & Technology, 44(2):223–237, 2021.

[133] P. M. Heertjes: *Determination of Vapour-Liquid Equilibria of Binary Mixtures.* Chemical and Process Engineering, 41:385–386, 1960.

[134] S. Saito: *Separation of Hydrocarbons.* Asahi-Garasu-Kogyo-Gijutsu-Shoreikai-Kenkyu-Hokuku, 15:397–407, 1969.

[135] A. Hu, K. Liu and Jin Z.: *Vapor-Liquid Equilibrium Data for Toluene-p-Xylene System.* Shiyou Huagong, 19(5):306–308, 1990.

[136] Z. Jin, A. Hu and K. Liu: *Vapor-Liquid Equilibrium for Ternary Mixtures of Benzene,Toluene, and p-Xylene.* Chinese Journal of Chemical Engineering, 1(1):47–51, 1993.

[137] D.-S. Jan, H.-Y. Shiau and F.-N. Tsai: *Vapor-Liquid Equilibria of n-Hexane + Cyclohexane + n-Heptane and the Three Constituent Binary Systems at 101.0 kPa.* Journal of Chemical & Engineering Data, 39(3):438–440, 1994.

[138] C. Ihmels, 2014.

[139] J. Wisniak, G. Embon, R. Shafir, H. Segura and R. Reich: *Isobaric Vapor−Liquid Equilibria in the Systems Methyl 1,1-Dimethylethyl Ether + Octane and Heptane + Octane.* Journal of Chemical & Engineering Data, 42(6):1191–1194, 1997.

[140] H. H. Amer, R. R. Paxton and M. van Winkle: *Methanol-Ethanol-Acetone.* Industrial & Engineering Chemistry, 48(1):142–146, 1956.

[141] A. Arce, J. Martínez-Ageitos, E. Rodil and A. Soto: *Phase equilibria involved in extractive distillation of 2-methoxy-2-methylpropane+methanol using 1-butanol as entrainer.* Fluid Phase Equilibria, 171(1-2):207–218, 2000.

[142] A. S. Brunjes and M. J. P. Bogart: *Vapor-Liquid Equilibria for Commercially Important Systems of Organic Solvents: The Binary Systems Ethanol-n-Butanol, Acetone-Water and Isopropanol-Water.* Industrial & Engineering Chemistry, 35(2):255–260, 1943.

[143] R. G. Shakirzyanov, M. G. Ibragimov, E. S. Telyakov and A. K. Safiullina: *Untersuchung des Dampf-Flüssig-Gleichgewichtes im System Isopentan-n-Pentan.* pages 3–4, 1989.

[144] G. Calingaert and L. B. Hitchcock: *The Application of the Phase Rule to the Calculation of Liquid and Vapor Compositions in Binary Systems. Deviations from Raoult's Law for Hydrocarbon Mixtures.* Journal of the American Chemical Society, 49(3):750–765, 1927.

[145] K. Ochi and K. Kojima: *On the Vapor -Liquid Equilibria for Ternary System consisting of Alcohols and Water.* Kagaku Kogaku, 33(4):352–357,a1, 1969.

[146] J. Suska, R. Holub, P. Vonka and J. Pick: *Liquid-Vapor Equilibrium XLII. Systems: Ethyl, Alcohol Water Tert Butyl Alcohol and Ethyl Alcohol Water Isobutyl Alcohol.* Collection of Czechoslovak Chemical Communications, 35:385–395, 1970.

[147] V. G. Artyukhov and D. S. Bereznikova: *Dampf-Flüssig-Gleichgewicht im System n-Propanol-Isobutanol bei Atmosphärendruck.* 15:139–145, 1973.

[148] L. Gay: *Distillation et rectification des mélanges complexes. (Deuxième mémoire).* Chimie & Industrie, Genie Chimique, 18(2):187–203, 1927.

[149] A. Tamir and J. Wisniak: *Vapor-liquid equilibriums of isobutanol-n-butanol and isopropanol-sec-butanol systems.* Journal of Chemical & Engineering Data, 20(4):391–392, 1975.

[150] V. P. Patlasov, A. V. Grishunin, M. I. Balashov, T. S. Rudakovskaya and L. A. Serafimov: *Untersuchung und Berechnung des Dampf-Flüssig-Gleichgewichts im System Methylacetat-Methanol-Propanol.* Osnovnoi Organicheskii Sintez i Neftekhimiya, 8:103–107, 1977.

[151] J. Ortega and P. Susial: *Vapor-Liquid Equilibria of Binary Mixtures of Methyl Alkanoates + Isomeric Butanols.* ELDATA: The International Electronic Journal of Physico-Chemical Data, 1(1):1–11, 1995.

[152] C.-L. Peng and K.-C. Chao: *Vapor-Liquid Equilibrium in Binary Mixtures of Ethyl Tert-Butyl Ether + Ethanol and n-Butyraldehyde + n-Propanol.* In *DIPPR Data Series*, pages 23–27. 1994.

[153] L. A. Serafimov, V. S. Timofeev and S. V. Lvov: *Liquid-vapour phase equilibria in certain binary mixtures contained in the products of oxo synthesis from propene at atmospheric pressure.* Zhurnal Fizicheskoi Khimii, 48(8):1890–1894, 1965.

[154] G. Radnai, P. Rasmussen and A. Fredenslund: *Vapor-Liquid Equilibrium Data for Binary Mixtures Containing Aldehydes and Esters and for the Mixture 1,1,2 Tricholoro-1,1,2 Trifluoroethane Plus N-Hexane.* AIChE Symposium Series, 83(256):70–79, 1987.

[155] B. N. Raju, R. Ranganathan and M. N. Rao: *Thermodynamics of Vapor-Liquid Equilibria. System: (1) Benzene-Cumene, (2) Iso-Amyl Alcohol, Cumene (3) Methanol-Methylcyclohexane.* Indian Chemical Engineer, 5:82–94, 1963.

[156] B. Tyminski and A. Klepanska: *Vapor-Liquid Equilibrium in Some Two- and Three-Component Fields.* Inzynieria Chemiczna, 9(1):259–271, 1979.

A Supporting information

A.1 Supplements to theoretical background

Figure A.1 shows a scheme of the multiple dividing wall column pilot plant planned at Ulm University by Preißinger *et al.* [22].

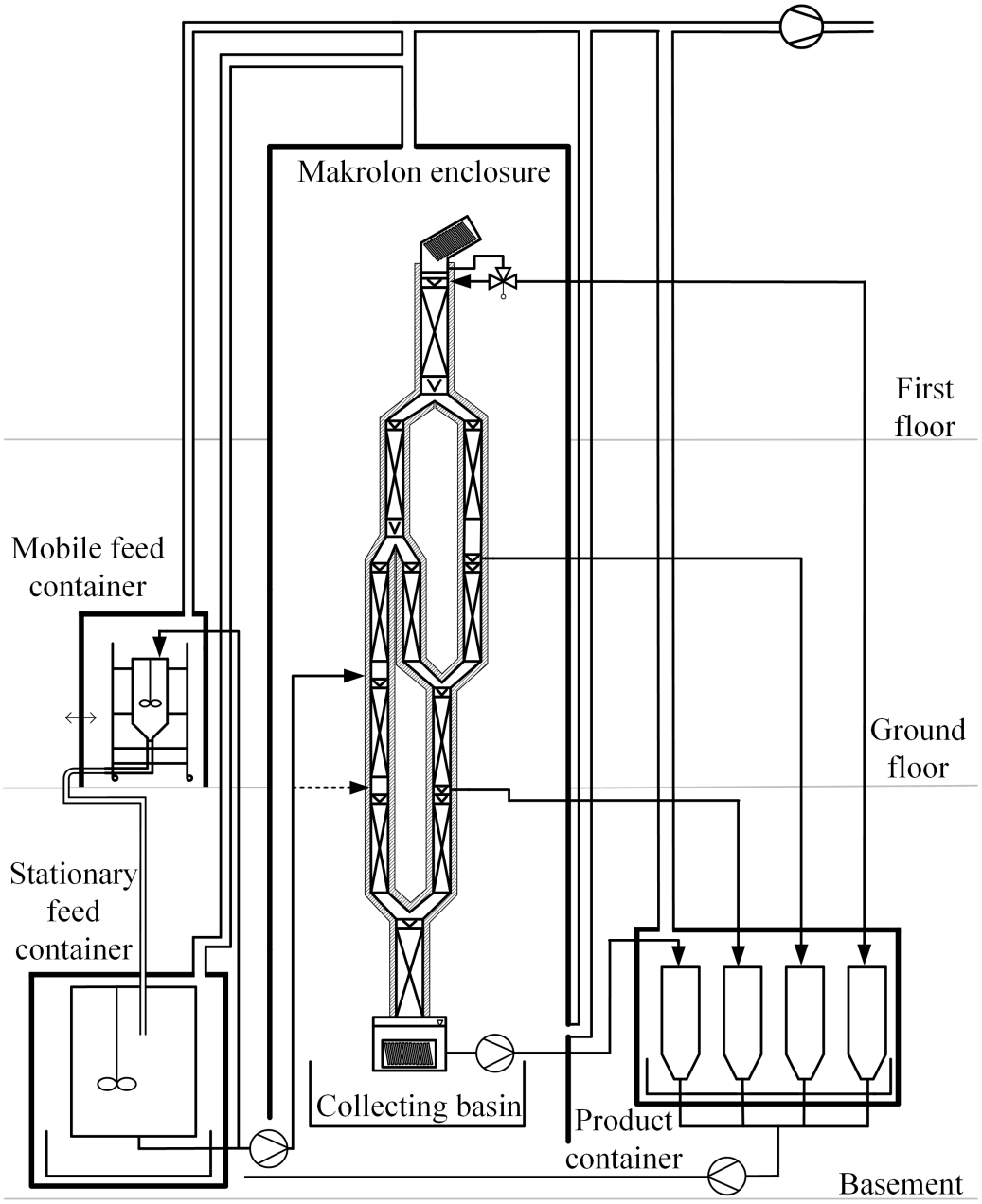

Figure A.1: Scheme of the multiple dividing wall column pilot plant planned at Ulm University.

A.2 Supplements to Aspen Plus simulations

This section first focuses on the thermodynamic modeling of the Aspen Plus simulations in Section A.2.1. Afterwards, implementation options of the dividing wall column that are tested are shown in Section A.2.2.

A.2.1 Thermodynamic modeling

The activity coefficients of all components in mixtures (Aspen Plus internal name GAMMA) are calculated with the non-random two liquid model (NRTL), as shown in equation A.1.

$$\begin{aligned}\ln\left(\mathrm{GAMMA}_i\right) =& \frac{\sum_j x_j \tau_{ji} G_{ji}}{\sum_k x_k G_{ki}} \\ &+ \sum_j \frac{x_j G_{ij}}{\sum_k x_k G_{kj}} \left(\tau_{ij} - \frac{\sum_m x_m \tau_{mj} G_{mj}}{\sum_k x_k G_{kj}}\right)\end{aligned} \tag{A.1}$$

$$G_{ij} = \exp(-\alpha_{ij}\tau_{ij})$$
$$\tau_{ij} = a_{ij} + \frac{b_{ij}}{T} + e_{ij}\ln T + f_{ij}T$$
$$\alpha_{ij} = c_{ij} + d_{ij}\left(T - 273.15\,\mathrm{K}\right)$$
$$\tau_{ii} = 0$$
$$G_{ii} = 1$$

The parameters used for the calculation of the ternary and quaternary systems are listed in Table A.1 and A.2, respectively.

Table A.1: NRTL parameters for ternary systems, $d_{ij} = e_{ij} = f_{ij} = 0$. Sources: * APV110VLE-IG (data base), ** NISTV110 NIST-IG (data base), *** Estimated with UNIFAC.

System	i	j	a_{ij}	a_{ji}	b_{ij}	b_{ji}	c_{ij}	Source	Valid. with
	A	B	-2.885	2.191	1123.950	-863.731	0.3	*	[133]
3.1	A	C	0	0	122.685	-136.481	0.3	*	[134]
	B	C	0	0	-91.146	75.898	0.3	*	[135, 136]
	A	B	0	0	48.073	-56.201	0.3	*	[137]
3.2	A	C	-0.345	-1.029	270.441	149.524	0.3	*	[138]
	B	C	-0.471	-0.484	421.264	-28.486	0.3	*	[139]

Continued on next page

Table A.1: NRTL parameters for ternary systems, $d_{ij} = e_{ij} = f_{ij} = 0$. Sources: * APV110VLE-IG (data base), ** NISTV110 NIST-IG (data base), *** Estimated with UNIFAC.

Continued from previous page

System	i	j	a_{ij}	a_{ji}	b_{ij}	b_{ji}	c_{ij}	Source	Valid. with
3.3	A	B	4.712	-2.313	-1162.295	483.844	0.3	*	[140]
	A	C	2.22	-1.517	-337.712	242.624	0.3	*	[141]
	B	C	0	0	-85.219	128.502	0.3	*	[142]
3.4	A	B	0	0	-116.614	126.490	0.3	***	N/A
	A	C	0	0	-264.293	413.763	0.3	*	[143]
	B	C	0	0	128.824	-114.771	0.3	***	[144]

Table A.2: NRTL parameters for quaternary systems, $d_{ij} = e_{ij} = f_{ij} = 0$. Sources: * APV110VLE-IG (data base), ** NISTV110 NIST-IG (data base), *** Estimated with UNIFAC, **** Regression.

System	i	j	a_{ij}	a_{ji}	b_{ij}	b_{ji}	c_{ij}	Source	Valid. with
4.1	A	B	8.2606	-9.721	-2846.6829	3409.6863	0.3	*	[145]
	A	C	-0.347	-0.833	167.914	252.533	0.3	*	[146]
	B	C	-0.991	0.725	110.275	69.232	0.3	*	[147]
	A	D	0	0	-85.219	128.502	0.3	*	[142]
	B	D	0	0	112.946	-88.318	0.3	*	[148]
	C	D	-5.775	5.649	1959.376	-1817.563	0.3	*	[149]
4.2	A	B	-5.498	3.615	2150.979	-1222.160	0.3	*	[150]
	A	C	-4.101	1.992	1482.18	-510.19	0.5	**	[151]
	B	C	-0.991	0.725	110.275	69.232	0.3	*	[147]
	A	D	7.451	-6.891	-2197.741	2244.387	0.3	*	[151]
	B	D	0	0	112.946	-88.318	0.3	*	[148]
	C	D	-5.775	5.649	1959.376	-1817.563	0.3	*	[149]

Continued on next page

Table A.2: NRTL parameters for quaternary systems, $d_{ij} = e_{ij} = f_{ij} = 0$. Sources: * APV110VLE-IG (data base), ** NISTV110 NIST-IG (data base), *** Estimated with UNIFAC, **** Regression.

Continued from previous page

System	i	j	a_{ij}	a_{ji}	b_{ij}	b_{ji}	c_{ij}	Source	Valid. with
4.3	A	B	0	0	291.165	-315.794	0.3	****	[152]
	A	C	0	0	750.5039	-425.543	0.3	****	[153]
	B	C	-0.991	0.725	110.275	69.232	0.3	*	[147]
	A	D	0	0	147.134	-50.032	0.3	*	[153]
	B	D	0	0	112.946	-88.318	0.3	*	[148]
	C	D	-5.7751	5.649	1959.376	-1817.563	0.3	*	[149]
4.4	A	B	0	0	243.553	-186.215	0.3	*	[154]
	A	C	-5.498	3.615	2150.979	-1222.156	0.3	*	[150]
	B	C	-0.120	-0.0429	0	0	0.1	**	[152]
	A	D	7.451	-6.891	-2197.741	2244.387	0.3	*	[151]
	B	D	0	0	147.134	-50.032	0.3	*	[153]
	C	D	0	0	112.946	-88.318	0.3	*	[148]
4.5	A	B	0	0	243.553	-186.2151	0.3	*	[154]
	A	C	-5.498	3.6145	2150.979	-1222.16	0.3	*	[150]
	B	C	-0.120	-0.043	0	0	0.1	**	[152]
	A	D	-4.101	1.992	1482.18	-510.191	0.5	**	[151]
	B	D	0	0	-75.966	332.460	0.3	*	[153]
	C	D	-0.991	0.725	110.275	69.232	0.3	*	[147]
4.6	A	B	-2.885	2.191	1123.950	-863.731	0.3	*	[133]
	A	C	0	0	122.685	-136.481	0.3	*	[134]
	B	C	0	0	-91.146	75.898	0.3	*	[135, 136]
	A	D	0	0	54.480	-44.669	0.3	*	[155]
	B	D	0	0	-171.642	196.143	0.3	***	N/A
	C	D	0	0	-130.024	102.357	0.3	*	[156]

The vapor pressure $p_i^{*,l}$ is calculated with the extended Antoine equation (Aspen Plus internal name PLXANT) which is shown in equation A.2. The corresponding parameters are shown in Table A.3.

$$\ln p_i^{*,l} = A_{1,i} + \frac{A_{2,i}}{T + A_{3,i}} + A_{4,i}T + A_{5,i}\ln T + A_{6,i}T^{A_{7,i}} \tag{A.2}$$

The critical temperature (TC) and pressure (PC) are required to calculate the liquid

Table A.3: Parameters for Antoine equation ($[p]$ = bar, $[T]$ = K).

Comp. i	$A_{1,i}$	$A_{2,i}$	$A_{3,i}$	$A_{4,i}$	$A_{5,i}$	$A_{6,i}$	$A_{7,i}$	T_{LB} [K]	T_{UB} [K]
2-Methylbutane	59.8	-4976	0	0	-7.7	0	2	113.3	460.4
Benzene	71.6	-6486.2	0	0	-9.2	0	2	278.7	562.1
Butanal	40.1	-5301.4	0	0	-4.3	0	6	176.8	537.2
Cumene	91.3	-8674.6	0	0	-11.9	0	2	177.1	631
Ethanol	61.8	-7122.3	0	0	-7.1	0	2	159.1	514
Isobutanol	110.3	-10504	0	0	-13.9	0	6	165.2	547.8
Methanol	71.2	-6904.5	0	0	-8.9	0	2	175.5	512.5
Methylacetat	49.8	-5618.6	0	0	-5.6	0	6	175.2	506.6
n-Butane	54.8	-4363.2	0	0	-7	0	2	134.9	425.1
n-Butanol	94.8	-9866.4	0	0	-11.7	0	6	183.9	563.1
n-Pentane	67.2	-5420.3	0	0	-8.8	0	2	143.4	469.7
p-Xylene	77.2	-7741.2	0	0	-9.9	0	2	286.4	616.2
Propanol	73.2	-8307.2	0	0	-8.6	0	6	147	536.8
Toluene	65.4	-6729.8	0	0	-8.2	0	2	178.2	591.8

molar volume according to the Rackett model. In the case of supercritical fluids, also the critical volume (VC) is required. The critical parameters of all used components are summarized in Table A.4.

The enthalpy of vaporization (Aspen Plus internal name DHVLDP) is calculated with DIPPR equation 106 (shown in equation A.3).

$$\text{DHVLDP} = B_{1,i}\left(1 - T_{r,i}\right)^{B_{2,i}+B_{3,i}T_{r,i}+B_{4,i}T_{r,i}^2+B_{5,i}T_{r,i}^3} \tag{A.3}$$

$$T_{r,i} = \frac{T}{TC_i}$$

Table A.4: Critical parameter and heat of formation of an ideal gas of all components.

Comp. i	TC [K]	PC [bar]	VC $\left[\mathrm{m^3 \cdot kmol^{-1}}\right]$	DHFORM $\left[\mathrm{kJ \cdot mol^{-1}}\right]$
2-Methylbutane	460.4	33.8	0.31	-14.1
Benzene	562.1	49	0.26	129.6
Butanal	537.2	44.1	0.26	-114.8
Cumene	631	32.1	0.43	137.9
Ethanol	514	61.4	0.17	-167.9
Isobutanol	547.8	43	0.27	-154.9
Methanol	512.5	80.8	0.12	-162.3
Methylacetat	506.6	47.5	0.23	-324.2
n-Butane	425.1	38	0.26	-16.7
n-Butanol	563.1	44.1	0.27	-150.7
n-Pentane	469.7	33.7	0.31	-8.8
p-Xylene	616.2	35.1	0.38	121.4
Propanol	536.8	51.7	0.22	-159.9
Toluene	591.8	41.1	0.32	122.2

The corresponding DIPPR parameters of all components are shown in Table A.5. For the calculation of the enthalpy of a vapor (HVMX) and liquid mixtures (HLMX), equation A.4 and A.5 are used, respectively. The liquid enthalpy is calculated with another method for supercritical fluids, however here it is assumed that no supercritical fluids are present and thus it is not shown here.

$$\mathrm{HVMX} = \sum_{i=1}^{n} \left[x_i^v \cdot \left(\mathrm{DHFORM} + \int_{298.15\,\mathrm{K}}^{T} \mathrm{CPIG}\, dT \right) \right] \tag{A.4}$$

$$\begin{aligned} \mathrm{HLMX} = & \sum_{i=1}^{n} \left[x_i^v \cdot \left(\mathrm{DHFORM} + \int_{298.15\,\mathrm{K}}^{T} \mathrm{CPIG}\, dT \right) \right] \\ & - \sum_{i=1}^{n} \left[x_i^l \cdot \mathrm{DHVLDP} \right] \\ & - R \cdot T^2 \cdot \sum_{i=1}^{n} \left[x_j^l \cdot \frac{\partial \ln(\mathrm{GAMMA})}{\partial T} \right] \end{aligned} \tag{A.5}$$

Table A.5: Parameters for calculation of heat of vaporization DHVLDP ([DHVLDP] = $\mathrm{kJ \cdot mol^{-1}}$).

Comp. i	$B_{1,i}$	$B_{2,i}$	$B_{3,i}$	$B_{4,i}$	$B_{5,i}$	T_{LB} [K]	T_{UB} [K]
2-Methylbutane	42.3	0.95	-0.98	0.46	0	113.3	460.4
Benzene	50	0.65	-0.28	0.03	0	278.7	562.1
Butanal	41.7	0.23	0.02	0.09	0	176.8	537.2
Cumene	75.3	1.37	-1.5	0.6	0	177.1	631
Ethanol	65.8	1.19	-1.77	1	0	159.1	514
Isobutanol	90	0.81	-0.11	-0.18	0	165.2	547.8
Methanol	32.6	-1.04	1.87	-0.61	0	175.5	512.5
Methylacetat	43.3	0.19	0.34	-0.17	0	175.2	506.6
n-Butane	36.2	0.83	-0.82	0.4	0	134.9	425.1
n-Butanol	71.3	0.05	0.9	-0.51	0	183.9	563.1
n-Pentane	45.1	0.96	-0.92	0.39	0	143.4	469.7
p-Xylene	66.5	1.17	-1.28	0.54	0	286.4	616.2
Propanol	69	0.65	-0.54	0.33	0	147	536.8
Toluene	54.6	0.77	-0.62	0.26	0	178.2	591.8

x is the molar fraction of a component, the superscription v indicates the vapor phase and l the liquid phase, i and j are the two components. DHFORM is the ideal gas heat of formation at 298.15 K which is summarized in Table A.4, CPIG is the heat capacity of an ideal gas, which is calculated according to DIPPR equation 107 (see equation A.6).

$$\mathrm{CPIG} = C_{1,i} + C_{2,i}\left(\frac{C_{3,i}/T}{\sinh\left(C_{3,i}/T\right)}\right)^2 + C_{4,i}\left(\frac{C_{5,i}/T}{\cosh\left(C_{5,i}/T\right)}\right)^2 \tag{A.6}$$

The input parameters are summarized in Table A.6.

Table A.6: Parameters for CPIG equation ([CPIG] = $\mathrm{J} \cdot (\mathrm{mol} \cdot \mathrm{K})^{-1}$).

Comp. i	$C_{1,i}$	$C_{2,i}$	$C_{3,i}$	$C_{4,i}$	$C_{5,i}$	T_{LB} [K]	T_{UB} [K]
2-Methylbutane	74.6	326.5	1545	192.3	666.7	200	1500
Benzene	55.2	173.4	764.3	72.5	2445.7	298.2	1500
Butanal	89.2	156.8	901.9	109.8	2566	298.2	1500
Cumene	108.1	379.3	1750.5	300.3	794.8	200	1500
Ethanol	49.2	145.8	1662.8	93.9	744.7	273.2	1500
Isobutanol	87.9	241.6	1718	165.4	798.7	298.2	1200
Methanol	39.3	87.9	1916.5	53.7	896.7	273.2	1500
Methylacetat	55.5	178.2	1260	85.3	562	298	1500
n-Butane	80.2	162.4	841.5	105.8	2476.1	298.2	1500
n-Butanol	74.5	259.1	1607.3	173.2	712.4	298.2	1500
n-Pentane	88.1	301.1	1650.2	189.2	747.6	200	1500
p-Xylene	75.1	339.7	1492.8	224.7	675.1	200	1500
Propanol	61.9	202.1	1629.3	129.6	727.4	298.2	1500
Toluene	58.1	286.3	1440.6	189.8	650.4	200	1500

A.2.2 Flow sheet implementation options for dividing wall columns

Figure A.2 shows the implementation options of a dividing wall column in Aspen Plus which are evaluated according to their calculation time and number of errors in Section 3.1.

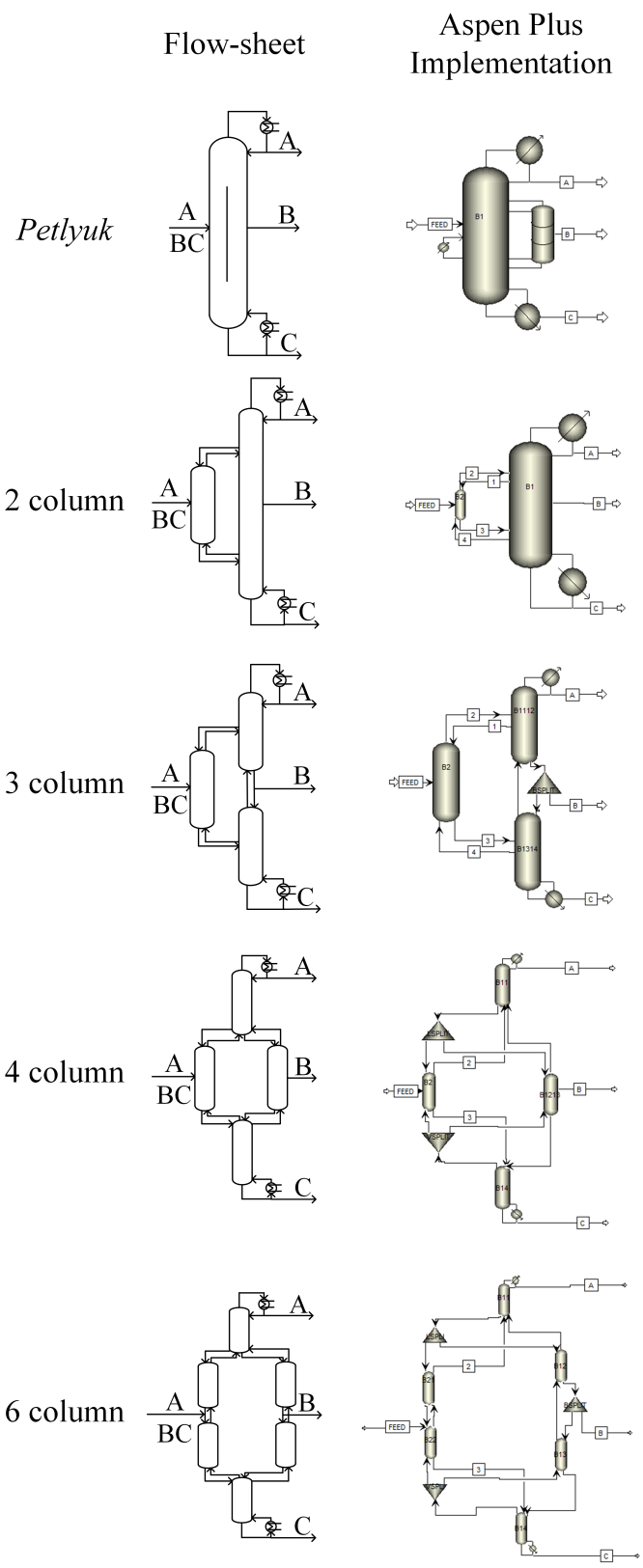

Figure A.2: Tested implementation options of the dividing wall column.

A.3 Supplements to Interface Aspen Plus - MS Excel

Figure A.3 shows schematically how the interface works. The corresponding code can be found in the supporting material [62].

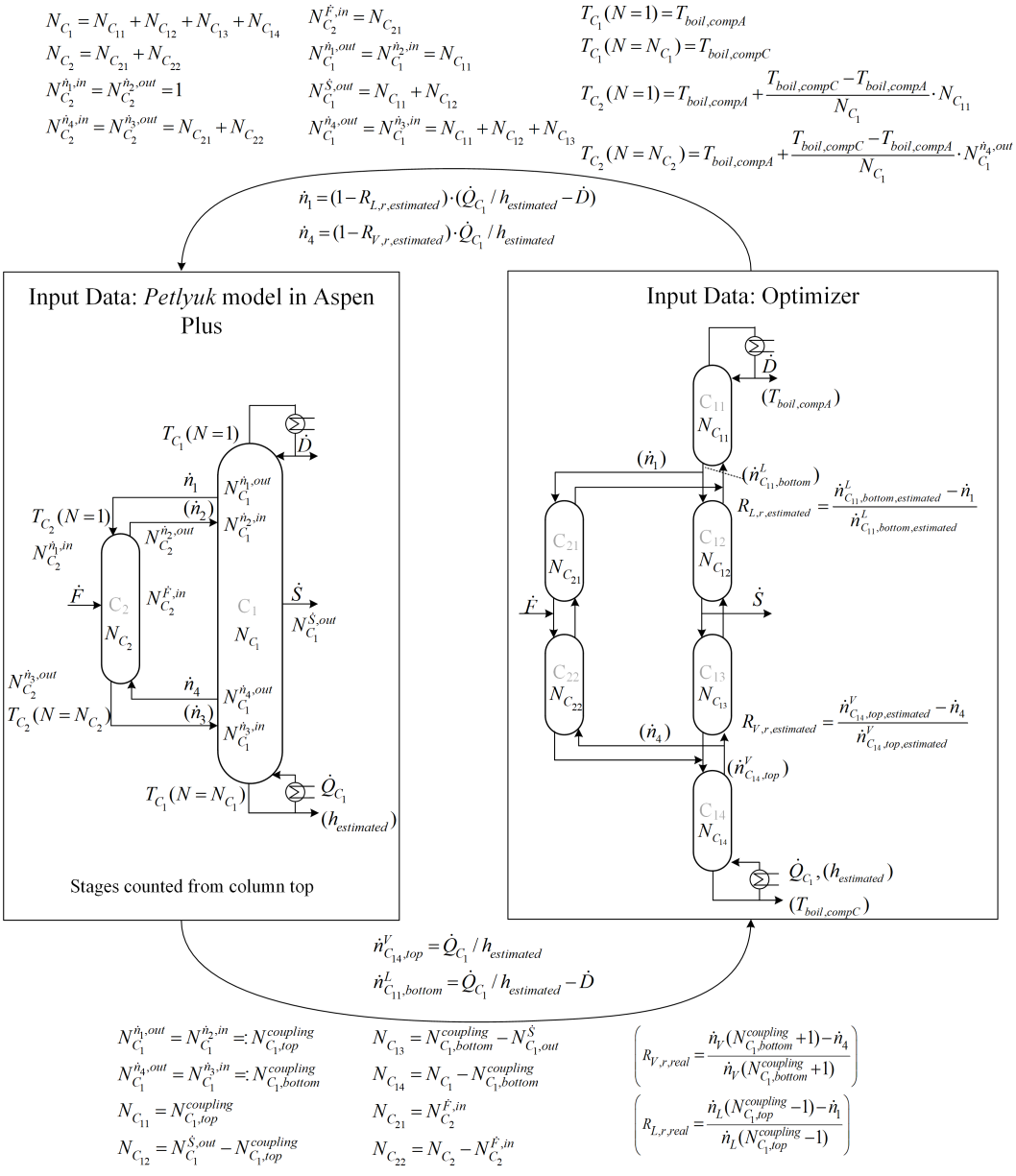

Figure A.3: Data exchange between Aspen Plus and Excel programmed in VBA. [107]

Table A.7: Overview over optimization problem definitions in simple distillation columns.

Opt	System	Objectives		Variables		Constraints	
		ΣN_{Ci}	$\dot{Q}$	m_{Ci}	$\frac{\dot{D}}{\dot{F}}$	Equation	Condition
2x1	Variation of 4.1	min	min	var	1	$x_A^{\dot{D}}$	≥ 0.95
2x2	Variation of 4.1	min	min	var	var	$-\frac{\dot{B}_A}{\dot{F}_A}$	$- \geq 0.05$
						$-\frac{\dot{D}_B}{\dot{F}_B}$	$- \geq 0.05$
2x3	Variation of 4.1	min	min	var	2	$-\frac{\dot{D}_B}{\dot{F}_B}$	$- \geq 0.05$

A.4 Supplements to Optimizations

In this section supporting information for performed optimizations is provided. Note that more extensive information for all optimizations is provided in the supporting material [62].

The following Tables briefly summarize the most important information of all optimizations performed. In Table A.7 the optimization runs of in a simple two-product distillation column are shown, followed by the results for ternary systems in a simple dividing wall column (Table A.8) or direct split sequence (Table A.9). The optimization setups for quaternary systems can be found in Table A.10 for the simplified multiple dividing wall column in combination with Table A.12 and Table A.11 for the quaternary direct split sequence.

Table A.8: Overview over optimization problem definitions for ternary cases in simple dividing wall column. If a value is given for a variable, it was set to this during the optimization and if "var" is filled, it was varied as optimization variable.

Opt	System	Objectives			Variables					Constraints		
		ΣN_{Ci}	$\dot{Q}$	$x_A^{\dot{D}}$, $x_B^{\dot{S}}$, $x_C^{\dot{B}}$	m_{Ci}	$\frac{\dot{D}}{\dot{F}_A}$	$\frac{\dot{S}}{\dot{F}_B}$	R_V	R_L	$x_A^{\dot{D}}$	$x_B^{\dot{S}_1}$	$x_C^{\dot{S}_2}$
531	3.1	min	min	max	var	var	var	var	var	no	no	no
231	3.1	min	min	no	var	1	1	var	var	≥ 0.95	no	no
232	3.1	min	min	no	var	1	1	var	var	no	≥ 0.95	no
233	3.1	min	min	no	var	1	1	var	var	no	no	≥ 0.95
234	3.1	min	min	no	var	1	1	var	var	≥ 0.95	≥ 0.95	≥ 0.95
235	3.1	min	min	no	var	var	var	var	var	≥ 0.95	≥ 0.95	≥ 0.95
236	3.1	min	min	no	var	1	1	var	var	no	≥ 0.98	no
237	3.1	min	min	no	var	1	1	var	var	no	≥ 0.99	no
238	3.1	min	min	no	var	1	0.95	var	var	no	≥ 0.95	no
239	3.1	min	min	no	var	1	1.05	var	var	no	≥ 0.95	no
2312	3.2	min	min	no	var	var	var	var	var	≥ 0.95	≥ 0.95	≥ 0.95
2314	3.3	min	min	no	var	var	var	var	var	≥ 0.95	≥ 0.95	≥ 0.95
2316	3.4	min	min	no	var	var	var	var	var	≥ 0.95	≥ 0.95	≥ 0.95

Table A.9: Overview over optimization problem definitions of ternary direct split sequences.

Opt	System	Objectives		Variables			Constraints
		ΣN_{Ci}	$\Sigma\dot{Q}$	m_{Ci}	$\frac{\dot{D}_{C1}}{\dot{F}}$	$\frac{\dot{D}_{C2}}{\dot{F}}$	$x_A^{\dot{D}_{C1}} = x_B^{\dot{D}_{C2}} = x_C^{\dot{B}_{C2}}$
2310	3.1	min	min	var	var	var	≥ 0.95
2311	3.2	min	min	var	var	var	≥ 0.95
2313	3.3	min	min	var	var	var	≥ 0.95
2314	3.4	min	min	var	var	var	≥ 0.95

Table A.10: Overview over optimization problem definitions for quaternary cases. * stage allocation of pilot plant (Section 2.1.2 or Table A.12), ** see Table A.12, *** estimated vapor split.

Opt	System	Objectives			Variables						Constraints
		ΣN_{Ci}	$\dot{Q}$	$x_A^{\dot{D}}$, $x_B^{\dot{S}_1}$, $x_C^{\dot{S}_2}$, $x_D^{\dot{B}}$	m_{Ci}	$\frac{\dot{D}}{\dot{F}_A}$	$\frac{\dot{S}_1}{\dot{F}_B}$	$\frac{\dot{S}_2}{\dot{F}_C}$	$R_{V,i}$	$R_{L,i}$	$x_A^{\dot{D}} = x_B^{\dot{S}_1} = x_C^{\dot{S}_2} = x_D^{\dot{S}_2}$
541	4.1	no	min	max	set*	var	var	var	var	var	no
241	4.1	min	min	no	var	1	1	1	var	var	≥ 0.98
242	4.1	min	min	no	var	1.008	0.992	0.992	var	var	≥ 0.98
243	4.1	min	min	no	var	1.02	0.98	0.98	var	var	≥ 0.98
244	4.1	min	min	no	var	var	var	var	0.5***	var	≥ 0.98
245	4.1	min	min	no	var	var	var	var	var	var	≥ 0.98
246	4.1	min	min	no	set*	var	var	var	var	var	≥ 0.98
247	4.1	min	min	no	set**	var	var	var	var	var	≥ 0.98
248	4.1	min	min	no	set**	var	var	var	var	var	≥ 0.98
249	4.1	min	min	no	set**	var	var	var	var	var	≥ 0.98
2412	4.1	min	min	no	set*	var	var	var	var	var	≥ 0.99
2414	4.1	min	min	no	set*	var	var	var	var	var	≥ 0.998
2416	4.2	min	min	no	set*	var	var	var	var	var	≥ 0.98
2418	4.3	min	min	no	set*	var	var	var	var	var	≥ 0.98
2420	4.4	min	min	no	set*	var	var	var	var	var	≥ 0.98
2422	4.5	min	min	no	set*	var	var	var	var	var	≥ 0.98
2424	4.6	min	min	no	set*	var	var	var	var	var	≥ 0.98

Table A.11: Overview over optimization problem definitions of quaternary direct split sequences.

Opt	System	Objectives		Variables				Constraints
		ΣN_{Ci}	$\Sigma\dot{Q}$	m_{Ci}	$\frac{\dot{D}_{C1}}{\dot{F}}$	$\frac{\dot{D}_{C2}}{\dot{F}}$	$\frac{\dot{D}_{C3}}{\dot{F}}$	$x_A^{\dot{D}_{C1}} = x_B^{\dot{D}_{C2}} = x_C^{\dot{D}_{C3}} = x_D^{\dot{B}_{C3}}$
2410	4.1	min	min	var	var	var	var	≥ 0.98
2411	4.1	min	min	var	var	var	var	≥ 0.99
2413	4.1	min	min	var	var	var	var	≥ 0.998
2415	4.2	min	min	var	var	var	var	≥ 0.98
2417	4.3	min	min	var	var	var	var	≥ 0.98
2419	4.4	min	min	var	var	var	var	≥ 0.98
2421	4.5	min	min	var	var	var	var	≥ 0.98
2423	4.6	min	min	var	var	var	var	≥ 0.98

Table A.12: Stage allocations used in Section 4.2.2 (Figure 4.10) and for the pilot plant (Section 2.1.2).* stage allocation of pilot plant, applied for Opt541, 246, 2412, 2414, 2416, 2418, 2420, 2422, 2424 and screenings. Given as reference: ** m_i at N_{min} resulting from optimization.

Opt	m_{C11}	m_{C12}	m_{C13}	m_{C14}	m_{C15}	m_{C16}	m_{C21}	m_{C22}	m_{C31}	m_{C32}
PP*	$0.\overline{09}$	$0.\overline{09}$	$0.\overline{09}$	$0.\overline{09}$	$0.\overline{09}$	$0.\overline{09}$	$0.\overline{09}$	$0.\overline{09}$	$0.\overline{09}$	$0.\overline{18}$
245**	0.109	0.040	0.109	0.178	0.158	0.099	0.119	0.020	0.089	0.079
247	0.100	0.100	0.100	0.100	0.100	0.100	0.100	0.100	0.100	0.100
248	0.051	0.071	0.131	0.111	0.141	0.081	0.071	0.101	0.121	0.121
249	0.061	0.061	0.121	0.121	0.111	0.111	0.091	0.081	0.121	0.121

A.5 Supplements to Approximations

In this section supporting information for the approximation approach to calculate $N\dot{Q}$ optima is presented. Section A.5.1 presents the integration of the approximation equation for the calculation of the Decision Number. Afterwards, Section A.5.2 summarizes the inputs used for approximations in this work.

A.5.1 Integration for Decision Number

This section summarizes the integration procedure to calculate the Decision Number that is based on the approximation of $N\dot{Q}$ curves presented in Section 4.3.1. To calculate the area between the two curves, the integral of the lower curve has to be subtracted from the one of the upper curve (either i or j). Since the overall equation is quite extensive, the calculation of the integrals A_1 and A_2 is split according to equation A.7.

$$\begin{aligned} A_1 &= A_{1a}^i + A_{1b}^i - A_1^j \\ A_2 &= A_2^i + A_2^j \end{aligned} \tag{A.7}$$

Note that the asymptote of option i is located in the integration range of A_1, thus the integral is split again in two parts. The first part is calculated according to equation A.8.

$$A_{1a}^i = \int 5 \cdot \dot{Q}_{min}^j \, \mathrm{d}N \tag{A.8}$$

Table A.13: Integrals calculated for the Decision Number.

Area	Lower bound	Upper bound	Method
A^i_{1a}	$N^j\left(\dot{Q} = 5 \cdot \dot{Q}^j_{min}\right)$	$N^i\left(\dot{Q} = 5 \cdot \dot{Q}^j_{min}\right)$	A.8
A^i_{1b}	$N^i\left(\dot{Q} = 5 \cdot \dot{Q}^j_{min}\right)$	N_{is}	A.9
A^j_1	$N^j\left(\dot{Q} = 5 \cdot \dot{Q}^j_{min}\right)$	N_{is}	A.9
$A^i_2 = A^j_2$	N_{is}	$4 \cdot N^i_{min}$	A.9

All other integrals are solved according to equation A.9. The integral below an approximated $N\dot{Q}$ curve of the system k is calculated based on equation 4.3 in Section 4.3.

$$\begin{aligned} A^k_l &= \int \dot{Q}^k_{min} \left(1 + \frac{0.27}{\left(\frac{N}{0.97 \cdot N^k_{min}}\right)^2 - 1}\right) \mathrm{d}N \\ &= 0.135 \cdot \dot{Q}^k_{min} \cdot 0.97 \cdot N_{min} \cdot \ln\left(1 - \frac{N}{0.97 \cdot N^k_{min}}\right) \\ &- 0.135 \cdot \dot{Q}^k_{min} \cdot 0.97 \cdot N_{min} \cdot \ln\left(1 + \frac{N}{0.97 \cdot N^k_{min}}\right) \\ &+ \dot{Q}^k_{min} \cdot N + const \end{aligned} \tag{A.9}$$

Note that the complex logarithm is required. However, the imaginary parts cancel out when subtracting the upper and lower border of the integration range. Accordingly, as simplification the absolute values can be used inside the logarithm brackets.
The integration ranges of all required integrals is shown in Table A.13.

A.5.2 Inputs used for approximations

The following Table A.14 summarizes the input data used for the approximations of $N\dot{Q}$ optima.

Table A.14: Inputs for used for approximation of $N\dot{Q}$ curves.

Approx	z_A $\left[\frac{\text{mol}}{\text{mol}}\right]$	z_B $\left[\frac{\text{mol}}{\text{mol}}\right]$	z_C $\left[\frac{\text{mol}}{\text{mol}}\right]$	α_{AC}	α_{BC}	Pur. [mol %]	N_{min} DWC	N_{min} DSS	N_{min} ISS	$\frac{\dot{V}_{min}}{\dot{F}}$ DWC	$\frac{\dot{V}_{min}}{\dot{F}}$ DSS	$\frac{\dot{V}_{min}}{\dot{F}}$ ISS
1	0.33	0.33	0.34	8.36	4.63	95.00	22	21	17	1.12	1.62	1.95
2	0.33	0.33	0.34	5.20	2.52	95.00	24	21	20	1.07	1.69	2.01
3	0.33	0.33	0.34	5.77	2.31	95.00	22	19	19	1.12	1.61	1.88

Continued on next page

Table A.14: Inputs for used for approximation of $N\dot{Q}$ curves.

Continued from previous page

App-rox	z_A $\left[\frac{\text{mol}}{\text{mol}}\right]$	z_B $\left[\frac{\text{mol}}{\text{mol}}\right]$	z_C $\left[\frac{\text{mol}}{\text{mol}}\right]$	α_{AC}	α_{BC}	Pur. [mol %]	N_{min} DWC	N_{min} DSS	N_{min} ISS	$\frac{\dot{V}_{min}}{\dot{F}}$ DWC	$\frac{\dot{V}_{min}}{\dot{F}}$ DSS	$\frac{\dot{V}_{min}}{\dot{F}}$ ISS
4	0.33	0.33	0.34	4.00	1.70	95.00	28	24	26	1.54	2.08	2.35
5	0.33	0.33	0.34	4.00	1.50	95.00	31	26	32	1.88	2.36	2.60
6	0.33	0.33	0.34	3.71	1.31	95.00	39	32	43	2.61	3.23	3.29
7	0.33	0.33	0.34	2.50	2.00	98.00	73	69	42	3.06	4.04	4.43
8	0.33	0.33	0.34	3.00	2.00	98.00	52	43	30	1.73	2.71	3.05
9	0.33	0.33	0.34	4.00	2.00	98.00	40	31	24	1.34	2.03	2.33
10	0.33	0.33	0.34	4.00	1.80	98.00	40	30	26	1.48	2.08	2.35
11	0.33	0.33	0.34	4.00	1.50	98.00	44	33	32	1.94	2.43	2.67
12	0.33	0.33	0.34	5.79	2.31	90.00	17	14	N/A	1.06	1.49	N/A
13	0.33	0.33	0.34	5.79	2.31	95.00	22	19	N/A	1.12	1.58	N/A
14	0.33	0.33	0.34	5.79	2.31	96.50	26	21	N/A	1.13	1.60	N/A
15	0.33	0.33	0.34	5.79	2.31	98.00	32	24	N/A	1.15	1.63	N/A
16	0.33	0.33	0.34	5.79	2.31	99.90	36	26	N/A	1.16	1.64	N/A
17	0.20	0.40	0.40	5.43	2.25	95.00	23	20	20	1.17	1.65	1.78
18	0.40	0.20	0.40	5.81	2.30	95.00	22	19	20	0.98	1.38	1.75
19	0.40	0.40	0.20	6.06	2.38	95.00	21	18	19	1.21	1.69	2.11
20	0.20	0.60	0.20	5.55	2.36	95.00	22	19	19	1.34	1.91	2.11
21	0.10	0.80	0.10	5.50	2.36	95.00	22	19	19	1.50	2.14	2.24
22	0.45	0.10	0.45	5.63	2.31	95.00	22	20	19	0.85	1.32	1.68
23	0.60	0.20	0.20	6.23	2.50	95.00	21	18	18	1.09	1.54	2.18
24	0.80	0.10	0.10	6.65	2.63	95.00	20	18	17	1.32	1.53	2.44
25	0.20	0.20	0.60	5.00	2.17	95.00	23	20	21	0.98	1.42	1.48
26	0.10	0.10	0.80	4.60	2.06	95.00	25	22	22	0.94	1.33	1.20
27	0.10	0.45	0.45	4.97	2.21	95.00	24	21	21	1.23	1.74	1.75
28	0.45	0.45	0.10	6.18	2.51	95.00	21	19	18	1.27	1.80	2.30
29	0.20	0.40	0.40	7.96	4.77	95.00	23	24	19	1.08	1.66	1.84
30	0.40	0.20	0.40	8.54	5.00	95.00	23	23	19	1.21	1.54	1.95
31	0.40	0.40	0.20	8.60	4.90	95.00	22	22	18	1.40	1.93	2.35
32	0.20	0.60	0.20	8.09	4.73	95.00	23	23	18	1.28	2.05	2.26

Continued on next page

Table A.14: Inputs for used for approximation of $N\dot{Q}$ curves.

Continued from previous page

Approx	z_A $\left[\frac{\text{mol}}{\text{mol}}\right]$	z_B $\left[\frac{\text{mol}}{\text{mol}}\right]$	z_C $\left[\frac{\text{mol}}{\text{mol}}\right]$	α_{AC}	α_{BC}	Pur. [mol %]	N_{min} DWC	N_{min} DSS	N_{min} ISS	$\frac{\dot{V}_{min}}{\dot{F}}$ DWC	$\frac{\dot{V}_{min}}{\dot{F}}$ DSS	$\frac{\dot{V}_{min}}{\dot{F}}$ ISS
33	0.10	0.80	0.10	7.85	4.65	95.00	23	24	19	1.35	2.35	2.45
34	0.45	0.10	0.45	8.62	5.10	95.00	23	24	19	1.20	1.42	1.88
35	0.60	0.20	0.20	8.89	5.08	95.00	22	22	18	1.59	1.88	2.53
36	0.80	0.10	0.10	8.76	5.16	95.00	23	23	17	1.99	2.13	3.02
37	0.20	0.20	0.60	7.73	4.80	95.00	24	26	20	0.86	1.25	1.41
38	0.10	0.10	0.80	6.96	4.63	95.00	27	29	22	0.55	0.88	0.89
39	0.10	0.45	0.45	7.58	4.66	95.00	24	25	20	0.99	1.65	1.70
40	0.45	0.45	0.10	8.70	4.90	95.00	24	22	18	1.54	2.10	2.59

A.6 Supplements to Screenings

For more information considering the screenings please consider the supporting material [62].

B Supervised thesis

B.1 Main project

1.) B. H.: *Methodenentwicklung zur Parameterauswahl aus Ergebnissen einer mehrkriteriellen Optimierung ternärer Destillationen.* Forschungsarbeit, Universität Ulm, Ulm, 08.04.2020

B.2 Industrial side project

1.) L. K.: *Experimentelle Untersuchung eines industriellen Prozesses zur Herstellung von Fleischersatzprodukten.* Bachelorarbeit, Universität Ulm, Ulm, 18.11.2019

2.) L. S.: *Entwicklung einer neuen Methode zur industriellen Herstellung von Fleischersatzprodukten.* Bachelorarbeit, Universität Ulm, Ulm, 04.09.2020

C Publications

During the period of the dissertation, the following publications were made.

C.1 Scientific papers

1.) Lena-Marie Ränger, Ulrich Preissinger and Thomas Grützner: *Robust Initialization of Rigorous Process Simulations of Multiple Dividing Wall Columns via Vmin Diagrams.* ChemEngineering, 2(2), 2018 (10.3390/chemengineering2020025) [1]

2.) Lena-Marie Ränger, Ulrich Preissinger and Thomas Grützner: *Multiple Dividing-Wall Columns - Current Status and Future Prospects.* Chemie Ingenieur Technik, 91(4), 2019 (10.1002/cite.201800080) [1]

3.) Ulrich Preissinger, Lena-Marie Ränger and Thomas Grützner: *Design Considerations of a Simplified Multiple Dividing Wall Column Pilot Plant.* ChemEngineering, 3(2), 2019 (10.3390/chemengineering3020034) [1]

4.) Lena-Marie Ränger, Martin von Kurnatowski, Michael Bortz and Thomas Grützner: *Multi-Objective Optimization of Dividing Wall Columns and Visualization of the High-Dimensional Results.* Computers & Chemical Engineering, 142, 2020 (10.1016/j.compchemeng.2020.107059) [1]

5.) Imke Preibisch, Lena-Marie Ränger, Pavel Gurikov and Irina Smirnova: *In Situ Measurement Methods for the CO2-Induced Gelation of Biopolymer Systems.* Gels (Basel, Switzerland), 6(3), 2020 (10.3390/gels6030028) [2]

6.) Lena-Marie Ränger, Lea Trescher, Martin von Kurnatowski, Michael Bortz and Thomas Grützner: *Vapor and liquid split flexibility in dividing wall columns in relation to the theoretical stage allocation.* Chemical Engineering and Processing: Process Intensification, 163, 2021 (10.1016/j.cep.2021.108365) [1]

7.) Lena-Marie Ränger and Thomas Grützner: *Shortcut Method for Initialization of Dividing Wall Columns and Estimating Pareto-Optimal NQ-curves.* Chemical Engineering and Technology, 44(10), 2021 (10.1002/ceat.202100256) [1]

8.) Tobias Seidel, Lena-Marie Ränger, Thomas Grützner and Michael Bortz: *Simultaneous simulation and optimization of multiple dividing wall columns.* Computers & Chemical Engineering, 107607, 2021 (10.1016/j.compchemeng.2021.107607) [1]

[1] Main project
[2] Based on Master Thesis at TUHH

C.2 Presentations

1.) Thomas Grützner, Ulrich Preissinger and Lena-Marie Ränger:*Multiple Trennwandkolonnen Quo Vadis: Stand der Technik und Ausblick auf die Aktivitäten an der Uni Ulm:* Presentation at Jahrestreffen der ProcessNet-Fachgruppen Fluidverfahrenstechnik, Membrantechnik und Mischvorgänge, 27. - 28. Februrary 2018 [1]

2.) Ulrich Preissinger, Lena-Marie Ränger and Thomas Grützner: *Multiple Dividing Wall Columns - Quo Vadis? State of the art and outlook on the activities at Ulm University*: Presentation at 23rd International Congress of Chemical and Process Engineering, 25. - 29. August 2018 [1]

3.) Lena-Marie Ränger, Martin von Kurnatowski, Michael Bortz and Thomas Grützner: *Mehrkriterielle Optimierung von ternären Destillationen*: Presentation at Jahrestreffen der ProcessNet-Fachgruppen Fluidverfahrenstechnik und Membrantechnik, 27. - 29. March 2019 [1]

4.) Lena-Marie Ränger, Martin von Kurnatowski, Michael Bortz and Thomas Grützner: *Multi-Objective Optimization of Dividing Wall Columns*: Presentation at 23rd Polish Conference of Chemical and Process Engineering, 02. - 05. June 2019 [1]

5.) Ulrich Preissinger, Lena-Marie Ränger and Thomas Grützner: *Considerations on the Design of a Pilot-Plant-Scale Simplified Multiple Dividing Wall Column*: Presentation at 23rd Polish Conference of Chemical and Process Engineering, 02. - 05. June 2019 [1]

6.) Lena-Marie Ränger, Martin von Kurnatowski, Michael Bortz and Thomas Grützner: *Mehrkriterielle Optimierung von Trennwandkolonnen: Darstellung in self organizing patch plots*: Presentation at Jahrestreffen der ProcessNet-Fachgemeinschaften "Prozess-, Apparate- und Anlagentechnik" unterstützt durch Sustainable Production, Energy and Resources", 04. - 05. November 2019 [1]

7.) Lena-Marie Ränger, Martin von Kurnatowski, Michael Bortz and Thomas Grützner: *Multi-objective optimization of dividing wall columns*: Presentation at 2020 Virtual Spring Meeting and 16th GCPS, 17. - 21. August 2020 [1]

8.) Lena-Marie Ränger, Martin von Kurnatowski, Michael Bortz and Thomas Grützner: *Flexibler Betrieb von Trennwandkolonnen am energetischen Optimum: Auf die Verteilung der Stufen kommt es an*: Presentation at Jahrestreffen der ProcessNet-Fachgruppen Fluidverfahrenstechnik und Wärme- und Stoffübertragung, 24. - 26. Februrary 2021 [1]

9.) Tobias Seidel, Lena-Marie Ränger, Michael Bortz and Thomas Grützner: *Robuste Simulation und Optimierung von multiplen Trennwandkolonnen*: Presentation at Jahrestreffen der ProcessNet-Fachgruppen Fluidverfahrenstechnik und Wärme- und Stoffübertragung, 24. - 26. Februrary 2021 [1]

10.) Lena-Marie Ränger, Martin von Kurnatowski, Michael Bortz and Thomas Grützner: *Operational flexibility of simple and multiple dividing wall columns close to Pareto-optimal solutions*: Accepted Presentation at 13th European Congress of Chemical Engineering and 6th European Congress of Applied Biotechnology, 20. - 23. September 2021 [1]

C.3 Poster

1.) Lena-Marie Ränger, Martin von Kurnatowski, Michael Bortz and Thomas Grützner: *Mehrkriterielle Optimierung ternärer Destillationen: Gesamter Lösungsraum*: Poster at Jahrestreffen der ProcessNet-Fachgruppen Fluidverfahrenstechnik, Adsorption und Extraktion, 26. - 28. Februrary 2020 [3]

C.4 Patents

1.) Wolfgang Schneider, Alexander Graber, Andreas Heyl, Radovan Sporka, Lena-Marie Ränger and Thomas Grützner: *A prosess for preparing an edible product from non-animal proteins*: Filed Patent [4]

[3] Main project, Poster price winner
[4] Industrial side project

D Curriculum Vitae

Lena-Marie Ränger

M.Sc. Process Engineering

Education	
since 02.2018	Ulm University Institute of Chemical Engineering Research assistant with PhD project Optimization of distillation processes and food process engineering
2015 – 2018	Hamburg University of Technology M.Sc. Process Engineering
2011 – 2015	Hamburg University of Technology B.Sc. Bioprocess Engineering
2011	Gymnasium am Kattenberge, Buchholz General matriculation standard

Work Experience	
11.2016 – 04.2017	Industrial Internship Lonza AG Visp (Switzerland)
05.2015 – 10.2016 & 06.2017 – 11.2017	Assistant researcher Hamburg University of Technology Institute of Thermal Separation Processes
03.2015 – 05.2015	Basic Internship Lühmann Stahlbau Buchholz i.d.N.

Teaching Experience	
2018	Exercise *Thermische Prozesstechnik* (Bachelor)
2018	Exercise *Thermal Process Engineering II* (Master)
2019	Exercise *Technische Thermodynamik* (Bachelor)
2021	Exercise *Thermal Process Engineering III* (Master)